International Scientific-Technical and Production Journal

The Paton WELDING JOURNAL

October 2009 # 10

English translation of the monthly «Avtomaticheskaya Svarka» (Automatic Welding) journal published in Russian since 1948

Founders: E.O. Paton Electric Welding Institute of the NAS of Ukraine
International Association «Welding»

Publisher: International Association «Welding»

Address:
E.O. Paton Electric Welding Institute,
International Association «Welding»,
11, Bozhenko str., 03680, Kyiv, Ukraine
Tel.: (38044) 287 67 57
Fax: (38044) 528 04 86
E-mail: journal@paton.kiev.ua
http://www.nas.gov.ua/pwj

State Registration Certificate
KV 4790 of 09.01.2001

Subscriptions:
$324, 12 issues per year,
postage and packaging included.
Back issues available.

CONTENTS

75th ANNIVERSARY OF THE E.O. PATON ELECTRIC WELDING INSTITUTE

On October 2, 2009 a gala meeting devoted to the 75th anniversary of the E.O. Paton Electric Welding Institute was held at the Institute, which is the world-renowned research center in the field of welding, electrometallurgy and protective coating deposition. The meeting was attended by the Institute staff, as well as numerous guests ---- heads of departments, enterprises, leading academic and research institutions and higher educational establishments of Ukraine.

The meeting was opened by academician B.E. Paton, President of the National Academy of Sciences of Ukraine, Director of the E.O. Paton Electric Welding Institute, who delivered a report on the main stages of the Institute activity in different periods. He noted that «the Institute has a powerful scientific potential and is developing, its structure and management system are being improved ---- all the efforts are focused on further advance of welding and related processes, on solving the basic problems of production».

Boris E. Paton expressed his sincere gratitude to all those who had congratulated the Institute's staff with the jubilee, his high appreciation of the staff activity and his hope for further development of the Institute and achievement of new high results by young scientists in the theory and practice of welding fabrication.

Among those who congratulated the Institute are tens of research establishments, enterprises and organizations, colleagues and friends from Ukraine, Russia, Belarus, Bulgaria, Armenia, Georgia, Kazakhstan, Germany, Slovakia and Uzbekistan.

Then Yu.P. Bogutsky, Deputy Head of the Secretariat of the President of Ukraine, read the greetings from V.A. Yushchenko to the Institute staff, expressing a firm belief that «with its highly professional and inspired activities the Institute's staff will continue making a substantial contribution to development of the national and world science and strengthening of the economy of the Ukrainian state». Yu.P. Bogutsky read the Decree of the President of Ukraine on decorating the Institute staff with the state awards of Ukraine.

V.B. Yalovoj read the greetings on behalf of V.M. Litvin, Chairman of Verkhovna Rada of Ukraine. In them it was noted that the indefatigable creative activity of the representatives of the known Paton school promoted transformation of welding into the leading technology in many branches of the national economy, which is applied in different environments, in particular deep under the water and high up in space. To-day significant results have already been achieved also in the medical field, namely making reliable welded joints of soft live tissues. Scientific achievements and developments of patonovites, and technologies developed by them are milestones in the progress of world science and engineering. The Institute scientists have convincingly proved their ability to solve scientific and engineering problems of any complexity.

A.N. Gurzhy read the address of Yu.V. Timoshenko, Prime Minister of Ukraine. It expressed sincere gratitude to the Institute's staff for their self-sacrificing work and recognized scientific-engineering achievements, which make our economy competitive and enhance the scientific authority of Ukraine in the world.

Short speeches of V.S. Romanyuk, Director of PWI Experimental Design-Technological Bureau, and V.I. Stepakhno, Director of Pilot Plant of Welding Equipment, were followed by greetings and warm congratulations for the Institute staff from the Presidium of the NAS of Ukraine (A.G. Shpak), Department of Physical and Technical Problems of Materials Science of the NAS of Ukraine (I.K. Pokhodnya), NTUU «Kiev Polytechnic Institute» (Yu.I. Yakimenko), Ministry of Industrial Policy (S.G. Grishchenko) and Chairman of Kiev Goloseevo District Administration (A.G. Neznal).

In conclusion a gala concert of merited performers and ensembles of Ukraine was held.

DECREE
OF THE PRESIDENT OF UKRAINE # 779/2009

On Decoration with the State Awards of Ukraine of Employees of the E.O. Paton Electric Welding Institute of the NAS of Ukraine, Kyiv

For a weighty contribution to advance of the national science, engineering and technologies in the field of welding of materials and structures, many years of fruitful scientific activity and on the occasion of the 75th anniversary of the E.O. Paton Electric Welding Institute I hereby decree:

To decorate with the Order of Yaroslav the Wise of the V degree

YUSHCHENKO Kostyantyn Andrijovych — Deputy Director, Dr. of Sci. (Eng.), academician of the NAS of Ukraine

To decorate with the Order «For Merit» of the II degree

KOSENKO Petro Oleksijovych — Director of State Enterprise «Pilot Plant of Welding Consumables of the E.O. Paton Electric Welding Institute of the NAS of Ukraine»
LOBANOV Leonid Mykhajlovych — Deputy Director, Dr. of Sci. (Eng.), academician of the NAS of Ukraine

To decorate with the Order «For Merit» of the III degree

STRELNIKOV Mykhajlo Oleksijovych — Chief Technologist of Joint-Stock Company «Pilot Plant of Welding Equipment of the E.O. Paton Electric Welding Institute of the NAS of Ukraine»

To decorate with the Order «For Bravery» of the III degree

KOTSYUBA Sergij Mykolajovych — diver

To award the honorary titles

«HONORED SCIENCE AND TECHNOLOGY WORKER OF UKRAINE»
KYRIAN Valerij Ivanovych — Department Head, Dr. of Sci. (Eng.), Corresponding Member of the NAS of Ukraine
NEDOSEKA Anatolij Ivanovych — Department Head, Dr. of Sci. (Eng.), Professor
STEPAKHNA Volodymyr Ivanovych — Head of Administation of Joint-Stock Company «Pilot Plant of Welding Equipment of the E.O. Paton Electric Welding Institute of the NAS of Ukraine», Dr. of Sci. (Phys.-Math.), Professor

«HONORED INDUSTRY WORKER OF UKRAINE»
BUBLYK Volodymyr Petrovych — gas welder
VARIVODA Mykola Oleksijovych — electric welder
GERASHCHENKO Viktor Borysovych — foreman of stamper team of Joint-Stock Company «Pilot Plant of Welding Equipment of the E.O. Paton Electric Welding Institute of the NAS of Ukraine»

«HONORED MECHANIC OF UKRAINE»
SAKHARNOV Vasyl Oleksijovych — senior staff scientist
STESIN Viktor Volodymyrovych — Chief Designer of the State Enterprise «Experimental Design Technological Bureau of the E.O. Paton Electric Welding Institute of the NAS of Ukraine».

President of Ukraine
Viktor YUSHCHENKO

September 29, 2009
Kyiv

NUMERICAL ANALYSIS OF CHARACTERISTICS OF THE ARC PLASMA IN AIR-VAPOUR PLASMATRONS WITH REFRACTORY CATHODE

I.V. KRIVTSUN[1], **M.Yu. KHARLAMOV**[2], **S.V. PETROV**[1], **G.S. MARINSKY**[1], **V.N. KORZHIK**[1] and **A.V. CHERNETS**[1]
[1]E.O. Paton Electric Welding Institute, NASU, Kiev, Ukraine
[2]V. Dal East-Ukrainian National University, Lugansk, Ukraine

The mathematical model is presented, describing a turbulent flow of the electric arc plasma in air-vapour plasmatrons with a refractory cathode. The effect of operating parameters of a plasmatron and kind of the employed plasma gas on electric and energy characteristics of the arc, as well as on thermal and gas-dynamic characteristics of the plasma flow generated by such a plasmatron, is numerically studied.

Keywords: *arc, electric and energy characteristics, numerical analysis, arc plasma, refractory cathode, vapour plasmatron*

Plasma energy sources are finding an increasingly wider application to meet the needs of the most diverse industrial sectors.

Plasma-arc processes are now used to advantage in metallurgy and welding production for melting of metals and alloys, deposition of different types of coatings, cutting, in chemical engineering, etc.

Lately, plasma has received acceptance for the processes of recycling of particularly dangerous wastes, where traditional methods cannot meet the state-of-the-art requirements for environmental safety [1–8].

One of the promising areas in modern plasma engineering, in particular in the field making of new plasma generators (plasmatrons), is application of the so-called vapour plasmatrons, which use water vapour as a plasma gas, the unique properties of which provide the absolutely new capabilities of the plasmatrons.

Vapour plasmatrons with a high degree of efficiency can be applied to deposit different types of refractory coatings. They can be employed in plasma chemistry, in waste disposal processes, cutting, etc.

The efficiency of operation of vapour plasmatrons directly depends upon the proper selection of their design parameters and operational conditions. This is determined, to a substantial degree, by understanding of the physical processes occurring in a plasmatron, as well as by a proper evaluation of key characteristics of the plasma flow they generate.

The corresponding mathematical model described in this study was developed in order to optimise design of a vapour plasmatron and select the optimal modes for its operation.

Statement of problem. Consider the main conditions used to conduct numerical analysis of characteristics of the arc plasma in a plasmatron (plasma generator). Diagram of the plasmatron under investigation is shown in Figure 1. This diagram corresponds to design of a real plasmatron employed, e.g. in a unit for vapour-plasma processing of organic materials. It was assumed that direct current arc I burns at refractory cathode W and is short-circuited at the plasmatron anode at some distance Z_A from the initial section ($z = 0$) located near the cathode tip. In the initial region the discharge is stabilised by a wall of the cylindrical channel of the cathode nozzle with length Z_C and radius R_C (see Figure 1). The plasma gas, i.e. argon, is fed via this nozzle at low flow rate G_1, which is required to protect the cathode tip from oxidation and maintain a stable burning of the electric arc. This gas is heated and accelerated by the arc, and is fed to a wider channel with radius R_1, whereto the main plasma gas, e.g. air or water vapour, is fed via a coaxial annular channel with $R_C \le r \le R_1$, located immediately after the cathode channel (at $z = Z_C$). The main plasma gas is fed to the channel in a relatively cold state at mass flow rate G_2, which is much higher than the flow rate of the gas fed via the cathode nozzle. This makes it possible to ignore mixing of these plasma gases in analysis of the further flow of plasma, and to assume that only the main plasma gas with

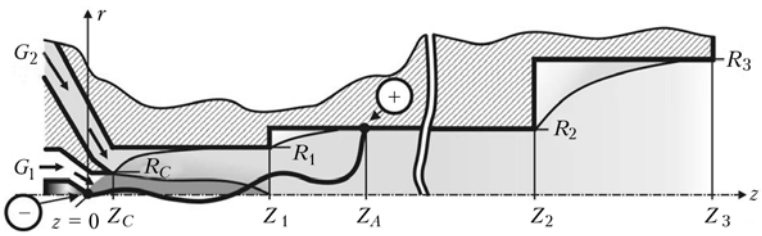

Figure 1. Plasmatron design diagram

total mass flow rate $G_1 + G_2$ flows via the plasmatron channel. Also, it is assumed that the arc current gradually decreases in a region of anode fixation, and that further (at $Z > Z_A$) on the inertial motion of the no-current plasma takes place in the plasmatron channel, while after section Z_3 the plasma jet flows into the environment with a pressure close to the atmospheric one.

It should be noted that the plasmatron channel has a very complicated geometry and comprises several broadening regions (at $z = Z_C, Z_1, Z_2$), with substantial restructuring of characteristics of the flow and corresponding broadening of the plasma flow occurring in each of them. The complex gas-dynamic phenomena, including formation of an area of backflow of the plasma jet behind the shoulder, etc., take place in a zone of each broadening region. It is necessary to use the complete system of the Navier–Stokes equations to correctly describe such phenomena. However, because the cylindrical regions of the channel are rather long, disturbances introduced into the plasma flow by the channel broadening regions have no marked effect on parameters of the arc plasma near the exit from the corresponding channel region, and characteristics of the flow here approach the asymptotic ones. This allows using a simplified system of magnetic gas-dynamic (MGD) equations written down in a boundary layer approximation to describe the thermal and gas-dynamic processes occurring in the plasmatron under consideration [9–11].

Given that a big amount of the plasma gases flows through the plasmatron, it features, as a rule, a turbulent mode of the plasma flow realised in it. In this case, parameters of the plasma flow change with time in a random way about their average values. The turbulent plasma flow is described by using the Boissinesq hypothesis (model of turbulent viscosity), proceeding from the fact that turbulence is hydrodynamic (i.e. pulsations of electromagnetic values being neglected), and considering pressure pulsations to be low.

The following assumptions were used for mathematical description of the plasma flow in channel of the considered plasma generator [10–12]:

- the plasma system is characterised by a cylindrical symmetry, while the processes occurring are assumed to be stationary;
- the main plasma gas is fed in an axisymmetric flow via the annular channel coaxially to the plasma gas fed via the cathode nozzle;
- mixing of the gas flows is ignored, and it is assumed that, after they begin interacting (at exit from the cathode channel), further on the plasma gas that is identical in composition to that fed via the annular channel flows through the plasmatron, the mass flow rate being common for both flows;
- it is assumed that disturbances introduced into the flow passing over the shoulders in planes of broadening of the channel have no substantial effect on thermal and gas-dynamic characteristics of the jet;
- plasma is in a state of local thermodynamic equilibrium, self-radiation of the plasma is volumetric;
- the main mechanism of heating of the plasma is a Joulean heat release (energy of pressure forces and viscous dissipation can be ignored), and energy transfer in the plasma flow occurs due to heat conduction and convection (natural convection is neglected);
- the plasma flow is viscous and subsonic, while the mode of the flow is turbulent;
- there are no external magnetic fields.

Input equations. Allowing for the above assumptions, gas-dynamic and thermal characteristics of the plasma flow can be described by the following system of MGD equations in an approximation of the turbulent boundary layer for time averaged values of temperature and velocity of the plasma [10, 11]:

$$\frac{\partial}{\partial z}(\rho u) + \frac{1}{r}\frac{\partial}{\partial r}(r\rho\bar{v}) = 0; \quad (1)$$

$$\rho\left(u\frac{\partial u}{\partial z} + \bar{v}\frac{\partial u}{\partial r}\right) = \frac{1}{r}\frac{\partial}{\partial r}\left(r\bar{\eta}\frac{\partial u}{\partial r}\right) - \frac{\partial}{\partial z}\left(p + \mu_0\frac{H^2}{2}\right); \quad (2)$$

$$\rho C_p\left(u\frac{\partial T}{\partial z} + \bar{v}\frac{\partial T}{\partial r}\right) = \frac{1}{r}\frac{\partial}{\partial r}\left(r\bar{\chi}\frac{\partial T}{\partial r}\right) + \sigma E^2 - \psi, \quad (3)$$

where T is the averaged temperature of the plasma; $\bar{v} = (\rho v + \rho' v')/\rho$; v is the averaged radial velocity; ρ is the averaged density of the plasma; ρ' and v' are the pulsations of the density and radial velocity; u is the averaged axial velocity of the plasma; p is the pressure; C_p is the specific heat of the plasma under a constant pressure; σ is the specific electric conductivity of the plasma; ψ is the volume self-radiation power density; $\bar{\eta}$ and $\bar{\chi}$ are the total coefficients of dynamic viscosity and thermal conductivity of the plasma, which are the sums, respectively, of molecular and turbulent viscosity and thermal conductivity; E is the axial component of intensity of the electric field; μ_0 is the universal permeability of vacuum; and H is the azimuthal component of the magnetic field of the arc:

$$H = \frac{1}{r}E\int_0^r \sigma r dr. \quad (4)$$

Within the limits of the boundary layer approximation used, the axial component of intensity of the electric field of the arc is practically constant across the channel [10], and can be determined from the condition of conservation of the total current:

$$I = 2\pi E\int_0^{R_\sigma(z)} \sigma r dr, \quad (5)$$

where $R_\sigma(z)$ is the radius of the current-conducting region. Considering that outside this region the conductivity of the plasma is practically equal to zero, it is possible to use radius of the calculation region as an upper limit of integration in formula (5), i.e. it can be assumed that $R_\sigma(z) = R_C$ at $0 \le z \le Z_C$; $R_\sigma(z) =$

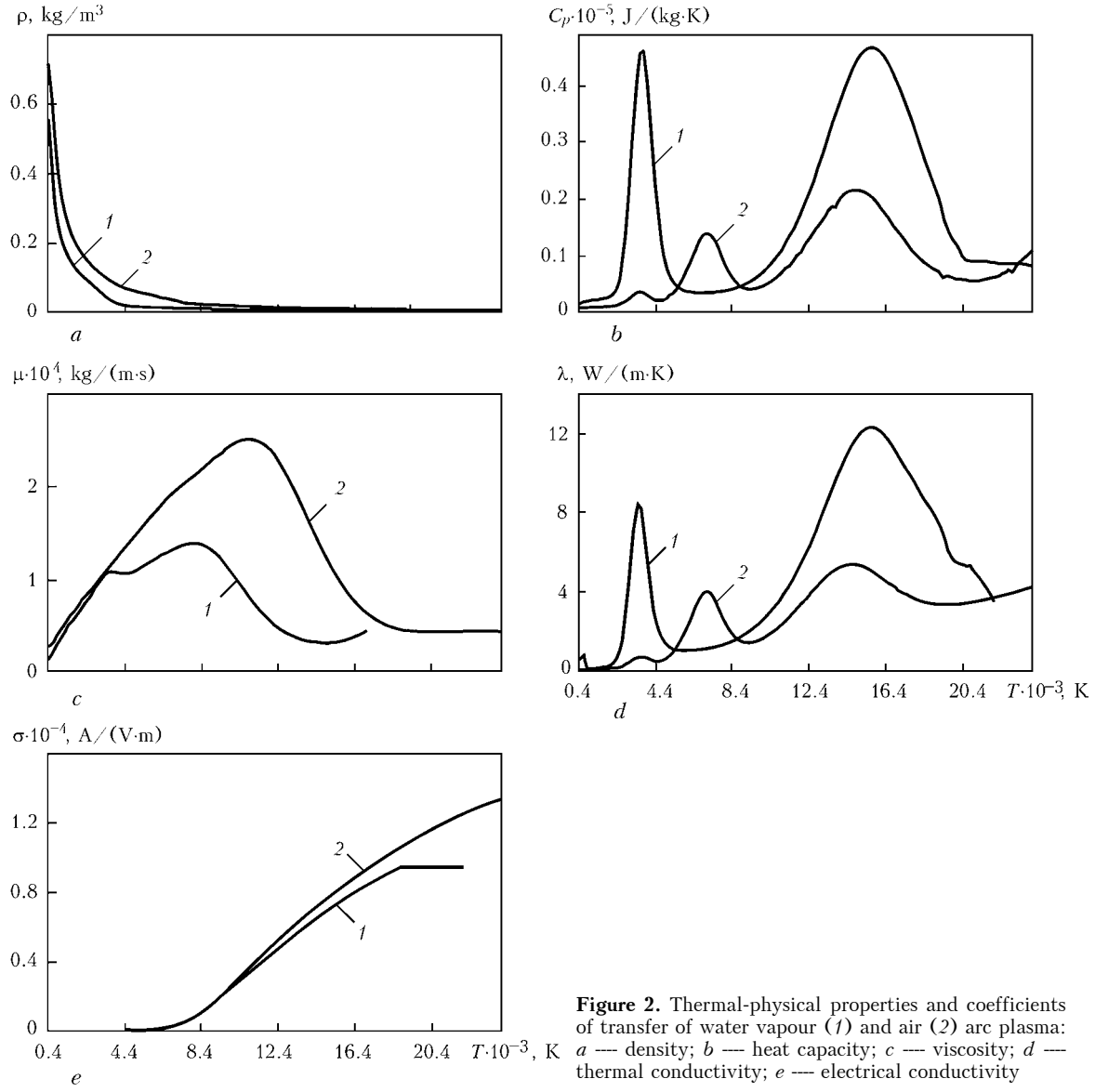

Figure 2. Thermal-physical properties and coefficients of transfer of water vapour (*1*) and air (*2*) arc plasma: *a* ---- density; *b* ---- heat capacity; *c* ---- viscosity; *d* ---- thermal conductivity; *e* ---- electrical conductivity

$= R_1$ at $Z_C < z \le Z_1$; $R_\sigma(z) = R_2$ at $Z_1 < z \le Z_2$, and $R_\sigma(z) = R_3$ at $Z_2 < z \le Z_3$ (see Figure 1).

The distribution of pressure within the plasma-shaping channel is determined with allowance for the magnetic component of pressure:

$$p = p_{ext} - \int_{Z}^{Z_3} \frac{dp_C}{dz} + \mu_0 E \int_{r}^{R_C} \sigma H dr, \qquad (6)$$

where p_{ext} is the pressure in the external environment. The gradient of gas-static pressure, dp_C/dz, in the boundary layer approximation is also constant across the channel [9], and can be determined from the condition of conservation of the total rate of the gas flowing through the plasmatron:

- in flow region of the cathode channel ($z \le Z_C$)

$$G_1 = 2\pi \int_0^{R_C} \rho u r dr; \qquad (7)$$

- in flow region $Z_C < z \le Z_3$

$$G_1 + G_2 = 2\pi \int_0^{R_w(z)} \rho u r dr, \qquad (8)$$

where $R_w(z)$ is the radius of the plasmatron channel equal to R_1 at $Z_C < z \le Z_1$; $R_w(z) = R_2$ at $Z_1 < z \le Z_2$, and $R_w(z) = R_3$ at $Z_2 < z \le Z_3$.

The system of equations (1) through (8) is supplemented with the following relationships:

$$\begin{aligned} &\rho = \rho(T, p); \quad C_p = C_p(T, p); \quad \chi = \chi(T, p); \\ &\eta = \eta(T, p); \quad \sigma = \sigma(T, p); \quad \psi = \psi(T, p), \end{aligned} \qquad (9)$$

which determine dependence of the thermodynamic characteristics, molecular coefficients of transfer and optical properties of the plasma upon the temperature and pressure. Some values of the parameters used in the calculations of plasma gases, e.g. argon and air, are given in [10, 13]. As to the thermodynamic properties and molecular coefficients of transfer of the water vapour plasma, these data were taken from [14, 15]. Corresponding properties of the air and water

vapour plasma in a range of 400 to 24,000 K (under atmospheric pressure) are shown in Figure 2.

Modelling of turbulence. The coefficients of dynamic viscosity and thermal conductivity of the plasma used in the above equations have the following form:

$$\bar{\eta} = \eta + \eta_t; \quad \bar{\chi} = \chi + \chi_t, \tag{10}$$

where η and χ are the coefficients of molecular viscosity determined according to (9), and η_t and χ_t are the coefficients of turbulent viscosity and thermal conductivity.

To determine the turbulent coefficients of transfer, we used model k–ε [16], which has recently received wide acceptance in practice of modelling of turbulent flows. Its characteristic features include allowance for the prehistory of a flow, as well as commonness of the model for different flow conditions.

Within the limits of the given model, the coefficients of turbulent viscosity and thermal conductivity can be determined from the following expressions:

$$\eta_t = \frac{C_\mu \rho (\bar{k})^2}{\varepsilon}; \tag{11}$$

$$\chi_t = \eta_t \frac{C_p}{\mathrm{Pr}_t}, \tag{12}$$

where C_μ is the empirical constant equal to 0.09; $\bar{k}$ is the kinetic energy of turbulence; ε is the rate of dissipation of turbulence; Pr_t is the Prandtl number of turbulence, which is selected according to the recommendations in [17] or assumed to be equal to one [10]. The equation of turbulent viscosity is closed with the equations of transfer for the kinetic energy of turbulence and dissipation rate:

$$\rho\left(u\frac{\partial \bar{k}}{\partial z} + \bar{v}\frac{\partial \bar{k}}{\partial r}\right) = \frac{1}{r}\frac{\partial}{\partial r}\left[r\left(\eta + \frac{\eta_T}{\mathrm{Pr}_k}\right)\frac{\partial \bar{k}}{\partial r}\right] + G - \rho\varepsilon; \tag{13}$$

$$\rho\left(u\frac{\partial \varepsilon}{\partial z} + \bar{v}\frac{\partial \varepsilon}{\partial r}\right) = \frac{1}{r}\frac{\partial}{\partial r}\left[r\left(\eta + \frac{\eta_T}{\mathrm{Pr}_\varepsilon}\right)\frac{\partial \varepsilon}{\partial r}\right] + C_1 G\frac{\varepsilon}{\bar{k}} - C_2\rho\frac{\varepsilon^2}{\bar{k}}. \tag{14}$$

Here $G = \eta_t\left(\frac{\partial u}{\partial r}\right)^2$ is the source term; C_1, C_2, Pr_ε and Pr_k are the constants of turbulence model k–ε equal to 1.44, 1.92, 1.30 and 1.00, respectively.

Expressions for the turbulent coefficients of transfer in an inertial region of the plasma flow at $z > Z_A$ remain the same as in the arc region.

Boundary conditions. To close the above system of equations, it is necessary to set boundary and initial (input) conditions corresponding to the design of the chosen plasmatron (see Figure 1).

The following conditions were assumed to be valid for symmetry axis of the system ($r = 0$):

$$\frac{\partial T}{\partial r} = 0; \quad \frac{\partial u}{\partial r} = 0; \quad \bar{v} = 0; \quad \frac{\partial \bar{k}}{\partial r} = 0; \quad \frac{\partial \varepsilon}{\partial r} = 0. \tag{15}$$

The «adhesion» condition is assumed to take place on the wall of the plasmatron channel (at $r = R_w(z)$), and temperature of the cooled wall, T_w, is set, i.e.

$$u = 0; \; T = T_w. \tag{16}$$

It is necessary to use the wall function to set the values of $\bar{k}$ and ε near the channel wall [16, 18], while the said values can be determined as follows:

$$\bar{k} = \frac{u_*^2}{\sqrt{C_\mu}}; \quad \varepsilon = \frac{u_*^3}{k_0(R_C - r)}, \tag{17}$$

where $k_0 = 0.41$, and u_* is the solution of the transcendental equation (logarithmic law of the wall):

$$\frac{u}{u_*} = \frac{1}{k_0}\ln\left[\frac{\Lambda\rho u_*(R_C - r)}{\eta}\right], \tag{18}$$

where $\Lambda = 9$ is the parameter of the wall roughness.

Expressions (17) and (18) are used to correctly allow for the viscous sub-layer when evaluating $\bar{k}$ and ε in the near-wall region, i.e. at $y^+ = \rho(R_C - r)u_*/\eta < f^+$, where f^+ is chosen from a range of 20 to 100 [18]. Equations (13) and (14) for the fully developed turbulent flow are used to describe the internal region of the flow ($y^+ \le f^+$).

Distributions of flow rate of the plasma gas, values of $\bar{k}$ and ε [16] and current densities in the near-cathode region are set for the inlet section of the cathode channel ($z = 0$) [19]:

$$u(r, 0) = u_0\left[1 - \left(\frac{r}{R_C}\right)^n\right]; \tag{19}$$

$$\bar{k}(r, 0) = i_t(u^2 + \bar{v}^2); \quad \varepsilon(r, 0) = 3\frac{\bar{k}(r, 0)^{3/2}}{R_C}; \tag{20}$$

$$j(r, 0) = j_0 e^{-r/r_C}, \tag{21}$$

where $n = 15$, and a value of u_0 is selected from the condition of conservation of mass rate of the plasma gas flowing via the channel of the plasmatron cathode nozzle (7); $i_t = 0.003$ is the turbulence intensity; j is the electric current density; j_0 is the constant corresponding to a maximal value of the current density in the cathode region; and r_C is the radius of the cathode region of the arc fixation. In particular, at $I = 200$ A it is possible to use a value of $j_{0C} = 1.2\cdot10^8$ A/m^2 [19], and radius of the cathode region can be determined from the condition of conservation of the total current (5) and Ohm's law

$$j = \sigma E. \tag{22}$$

The temperature of the plasma gas in inlet section of the cathode channel is chosen on the basis of an empirical dependence of the current density in the cathode region (21) by using dependence $\sigma = \sigma(T, p)$ and relationship (22). In this case, intensity of the electric field, E, at $z = 0$ is assumed to be independent of coordinate r and corresponding to j_0 and $\sigma(T_C)$, where T_C is the maximal temperature of plasma near

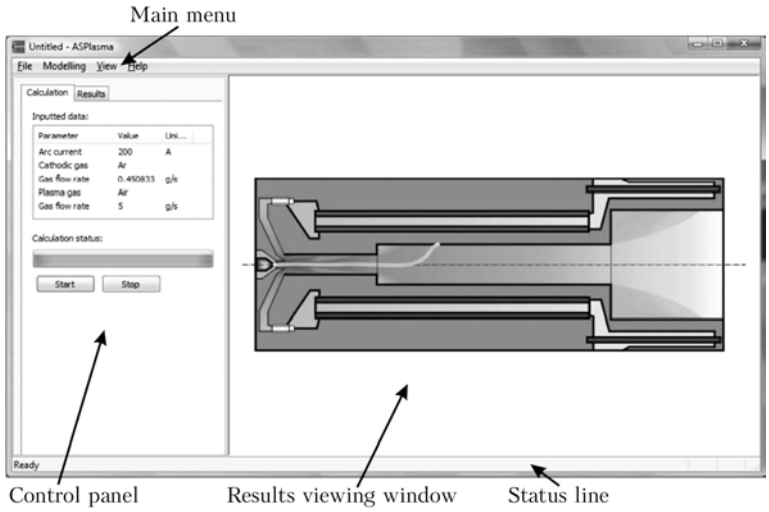

Figure 3. Main window of software package ASPlasma

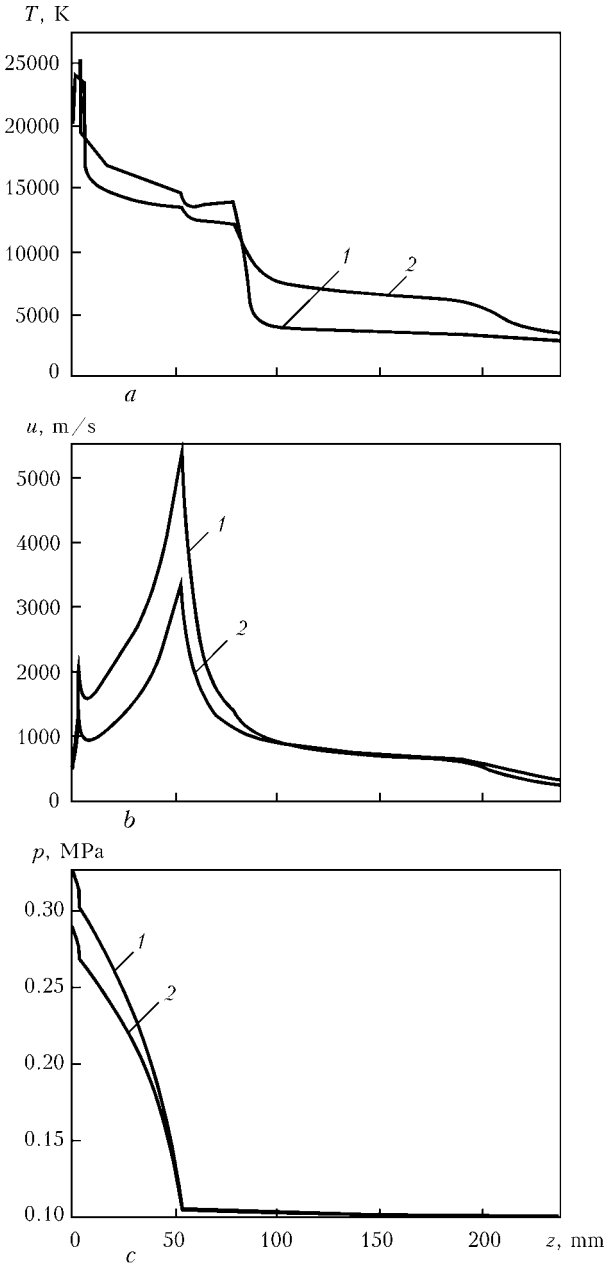

Figure 4. Distribution of axial values of plasma temperature (*a*) and velocity (*b*), and pressure (*c*) along the channel length at I = 200 A and G_2 = 5 g/s: *1* ---- water vapour; *2* ---- air

the cathode surface, which can be determined either from literature data [19] or experimentally.

When determining the distributions of temperature and rate of the main plasma gas flowing to the working channel of the plasmatron via coaxial annular channel $R_C \le r \le R_1$ in section $z = Z_C$, we proceed from the conditions that a homogeneous isothermal flow of gas with a temperature equal to wall temperature T_w is fed to the plasmatron channel. Then, at $R_C \le r \le R_1$ and $z = Z_C$, we will obtain the following:

$$T(r, Z_C) = T_w; \quad u(r, Z_C) = u_2 \equiv \frac{G_2}{\pi\rho_2(R_1^2 - R_C^2)}, \quad (23)$$

where ρ_2 is the density of the main plasma gas fed to the plasma-shaping channel.

The boundary conditions for $\bar{k}$ and ε at exit from the annular channel for feeding the main plasma gas are selected from similar dependencies (20) according to condition (23).

Results of computer modelling. The problem posed was solved numerically by the finite difference method [20, 21]. The main difference scheme was used for integration of systems of equations of the type of the boundary layer ones [22]. Second-order differential equations (2), (3), (12) and (13) were approximated with respect to an implicit two-layer six-point difference scheme, and first-order equation (1) ---- with respect to the four-point scheme. The resulting algebraic system of difference equations was solved by the sweep method using layer-by-layer iterations by z, along with global pressure iterations.

Software ASPlasma (Figure 3) was developed on the basis of the above model, algorithms and methods for numerical solution of the differential equations used. This software can be applied for calculation and visualisation of key characteristics of the occurring processes, including spatial distributions of velocity and temperature of the plasma, electric and energy characteristics of the arc discharge depending upon the operating mode of the plasmatron under investigation.

ASPlasma was used for detailed numerical analysis of thermal, gas-dynamic and electromagnetic charac-

teristics of the plasma in the plasmatron considered (see Figure 1). Calculation of the distributed and integral characteristics of the arc plasma was made by using the following values of geometric parameters of the cathode nozzle channel and plasma-shaping channel of the plasmatron: R_C = 1.5 mm, R_1 = 4 mm, R_2 = = 8 mm, R_3 = 22.5 mm, Z_C = 3 mm, Z_1 = 53 mm, Z_2 = 178 mm, and Z_3 = 238 mm at arc length Z_A = = 78--103 mm. It should be noted that the arc length in the model employed is an external parameter, which can be determined by using experimental data in the form of volt-ampere characteristics of the arc burning in the plasmatron considered.

For the calculations, parameters of the operating mode of the plasmatron were chosen so that they corresponded to real ranges of operating modes of such plasmatrons, e.g. in a unit for high-temperature plasma pyrolysis of wastes: arc current I = 100--400 A; flow rate of the plasma gas (argon) used to protect the cathode G_1 = 0.45 g/s (1 m^3/h); mass flow rate of the main plasma gas (air or water vapour) G_2 = = 2--10 g/s; and atmospheric pressure at exit from the plasmatron channel. Initial temperature of the main plasma gas (air or water vapour) fed to the channel corresponded to temperature of the walls of the plasma-shaping channel of the plasmatron, and was assumed to be equal to 400 K.

Figures 4--7 show distributed and integral characteristics of the air and water vapour arc plasma in channel of the plasmatron under consideration at Z_A = = 78 mm. In particular, Figure 4 shows axial dependencies of the axial values of temperature and velocity of the plasma, as well as the distribution of pressure along the length of the channel at arc current I = = 200 A and main plasma gas flow rate G_2 = 5 g/s. Figure 5 shows radial distributions of temperature and axial component of the velocity of the plasma in characteristic sections of the plasmatron channel at the same values of the arc current and mass flow rate of the plasma gas.

As follows from the calculation data shown in these Figures, a substantial decrease in temperature of the arc plasma from 25,000 K (Figure 4, *a*, and curve *1* in Figure 5, *a*, *b*), which is characteristic of exit section of the cathode channel, to about 14,000 K (Figure 4, *a*, and curve *2* in Figure 5, *a*, *b*) in exit section of the first region of the plasma-shaping channel ($z = Z_1$) occurs in the initial region of the electric arc in the plasmatron considered. This is associated with an intensive extraction of energy from the central high-temperature flow of the argon plasma by a colder main plasma gas (air or water vapour), which, in addition, has a higher heat capacity (see Figure 2). At $z \geq Z_A$, i.e. in transition to the no-current region of the flow, another dramatic decrease in temperature of the plasma takes place at exit from the second (anode) region of the channel ($z = Z_2$) ---- down to about 7000 K for air and 4000 K for water vapour (see Figure 4, *a*, and curve *3* in Figure 5, *a*, *b*), this being related to disappearance here of the main heat source in plasma ---- Joulean heat release.

The velocity of the plasma along the channel axis first falls (see Figure 4, *b*), which is related to deceleration of the axial flow of the argon plasma by a

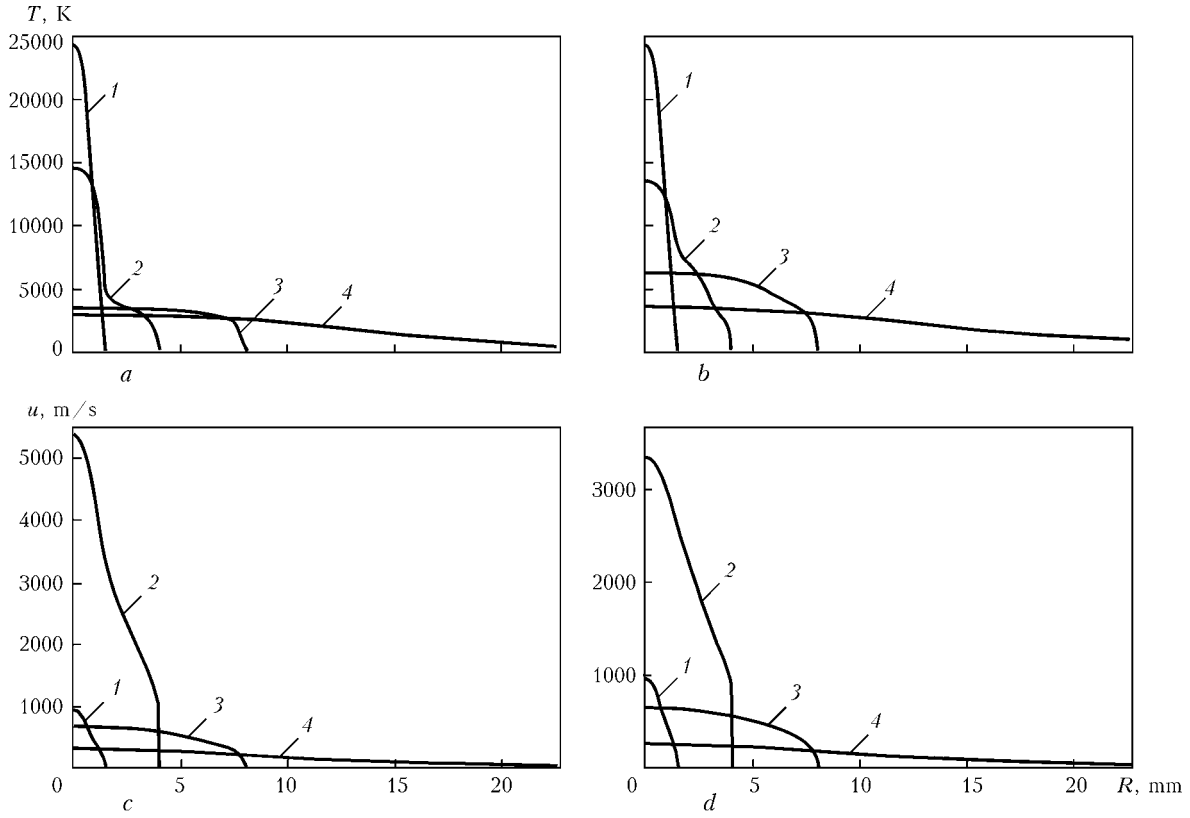

Figure 5. Radial distributions of temperature (*a, b*) and velocity (*c, d*) of water vapour (*a, c*) and air (*b, d*) plasma in different sections of the plasma-shaping channel: *1* ---- $z = Z_C$; *2* ---- $z = Z_1$; *3* ---- $z = Z_2$; *4* ---- $z = Z_3$

slower coaxial flow of the main plasma gas fed to the plasma-shaping channel in this region. Then it grows rather quickly, reaching the values above 3000 m/s for air and 5000 m/s for water vapour (see Figure 4, *b*, and curve *2* in Figure 5, *c*, *d*), which is caused by a higher flow rate of the main plasma gas and its gradual heating with the electric arc. In this case, the near-wall annular flow of a colder plasma gas prevents broadening of the axial plasma flowing from the cathode nozzle [12]. That is why, at the initial stage of their interaction the core of the plasma flow broadens but insignificantly. Therefore, the $Z_C \le z \le Z_1$ region is a complex zone of the flow characterised by gradual involvement of cold gas into the flow of the arc plasma due to the processes of momentum and energy exchange between different zones of the flow.

After the first shoulder of the plasma-shaping channel ($z \ge Z_1$), the arc plasma velocity decreases because of a substantial increase in its cross section area, falling to 600–700 m/s at exit of the anode region of the channel ($z = Z_2$).

The pressure in the plasmatron considered falls markedly only in a region of the cathode nozzle and first region of the plasma-shaping channel, further on remaining at an almost constant level (see Figure 4, *c*). This is associated with a low gas-dynamic drag of the second (anode) region and exit nozzle of the plasmatron.

As can be seen, the spatial distributions of characteristics of the water vapour plasma in the given plasmatron copy qualitatively the corresponding distributions for the air plasma. As to the quantitative differences, it should be noted that, other conditions being equal (I = 200 A, G_2 = 5 g/s), the temperature of the water vapour plasma at exit from the second (anode) region of the plasma-shaping channel is a bit lower than the corresponding temperature of the air plasma. Most likely, this is associated with a higher

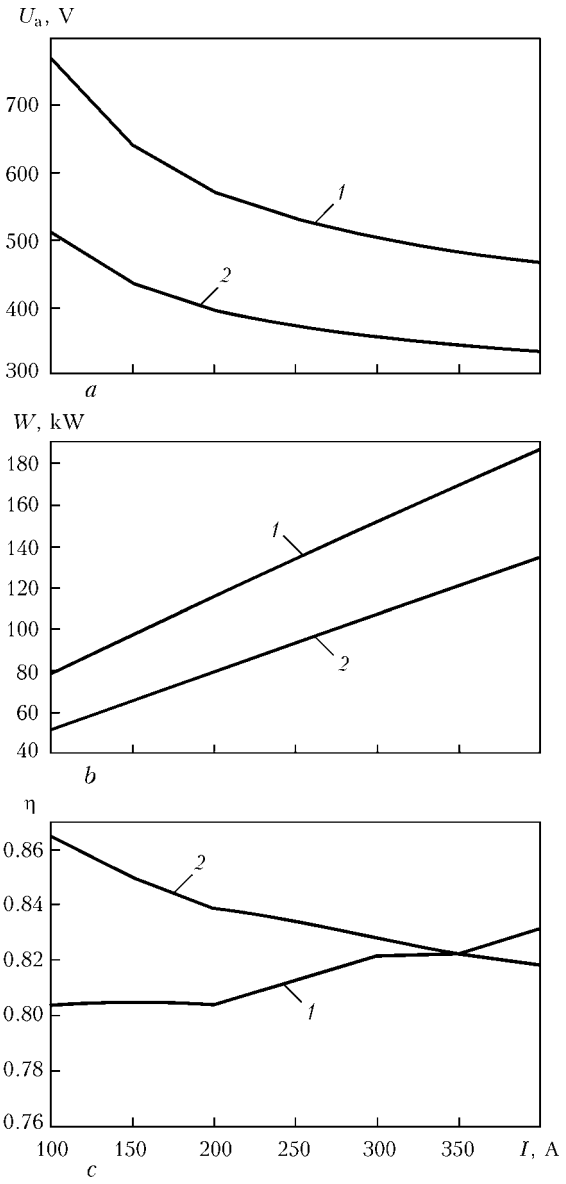

Figure 6. Volt-ampere characteristic (*a*), dependence of electric power of the plasmatron (*b*) and its efficiency (*c*) upon the arc current at G_2 = 5 g/s: *1, 2* ---- see Figure 4

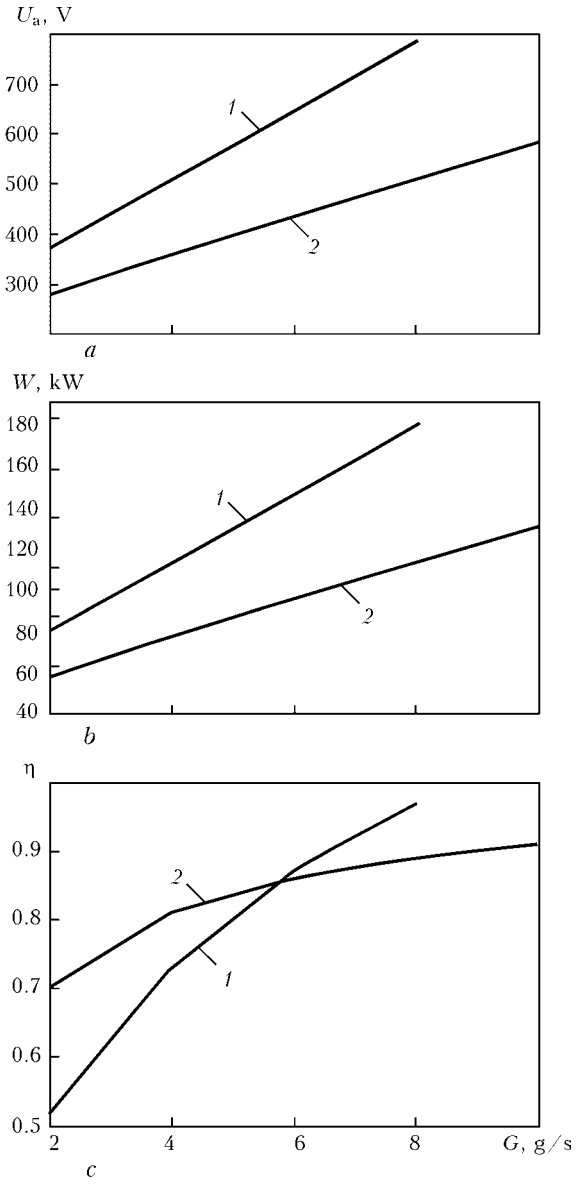

Figure 7. Dependence of the arc voltage (*a*), electric power of the plasmatron (*b*) and its efficiency (*c*) upon the plasma gas flow rate at I = 200 A: *1, 2* ---- see Figure 4

heat capacity of vapour, compared with air. The velocity of the water vapour plasma, on the contrary, is a bit higher, which can be explained by a lower density of vapour. The gradient of pressure along the channel length also turns out to be higher.

Figure 6 shows the calculated dependencies of integral characteristics of the plasmatron upon the arc current and flow rate of the main plasma gas (air or water vapour). As follows from Figure 6, *a*, the calculated volt-ampere characteristic of the arc in the given plasmatron is drooping, whereas dependence of the arc voltage upon the plasma gas flow rate at a constant arc current is of a growing character (Figure 7, *a*). The value of the plasmatron efficiency only slightly depends upon the variations in the arc current (Figure 6, *c*), but it considerably grows with increase in the plasma gas flow rate (Figure 7, *c*). And the calculated electric power of the plasmatron grows almost linearly with increase both in the arc current (Figure 6, *b*) and in the main plasma gas flow rate (Figure 7, *b*).

The resulting calculation data are indicative of a substantial effect of the kind of the main plasma gas (air or water vapour) and operating parameters of the plasmatron (arc current and plasma gas flow rate) on the electric and energy characteristics of the plasmatron, as well as on the thermal and gas-dynamic characteristics of the plasma flow it generates. In particular, in air (G_2 = 5 g/s) the mass-averaged temperature and maximal velocity of the generated plasma flow at exit from the plasmatron change from 4243 K and 416 m/s (I = 100 A) to 6572 K and 985 m/s (I = = 400 A), and, correspondingly, at I = 200 A they change from 6175 K and 398 m/s (G_2 = 2 g/s) to 4823 K and 853 m/s (G_2 = 10 g/s). In water vapour (G_2 = 5 g/s), the values of the above parameters change from 3025 K and 509 m/s (I = 100 A) to 3550 K and 973 m/s (I = 400 A), while at I = 200 A they change from 3195 K and 358 m/s (G_2 = 2 g/s) to 3280 K and 951 m/s (G_2 = 8 g/s).

CONCLUSIONS

1. The developed mathematical model of physical processes occurring in air-vapour plasmatrons with a refractory cathode, which are used, in particular, in units for high-temperature (plasma) pyrolysis of medical and other dangerous wastes, makes it possible to conduct numerical analysis of distributed and integral characteristics of the arc plasma flow generated by a plasmatron over a wide range of variations in the arc current and flow rate of the plasma gas, which can be either air or water vapour. Software with graphical interface was developed for computer implementation of this model. The software can be used to select optimal operating parameters of the plasmatron and further improve its design.

2. Results of numerical analysis of characteristics of the arc plasma in the plasmatron considered showed the substantial effect of the kind of the plasma gas on electric and energy characteristics of the arc, as well as on thermal and gas-dynamic characteristics of the generated plasma flow. In particular, the arc voltage and, hence, power of the plasmatron operating with water vapour turn out to be much higher than those of the air plasmatron, other conditions being equal. In this case, the mass-averaged temperature of the water vapour plasma in exit section of the plasmatron is lower than the corresponding temperature of the air plasma, whereas velocity of the water vapour plasma is higher, this being attributable to peculiarities of thermal-physical properties and coefficients of transfer of the above plasma gases.

1. (2001) Non-incineration medical waste treatment technologies. A resource for hospital administrators, facility managers, health care professionals, environmental advocates and community members. *Health care without harm*. August. www.noharm.org
2. Springer, M.D., Barkley, T., Burns, W.C. *Apparatus and method for treating hazardous waste*. Pat. 5534659 USA. Int. Cl. A 62 D 3/00. Publ. 09.07.96.
3. *PEAT International*. http://www.peat.com
4. *Startech Enronmental Corp*. http://www.startech.net
5. Paton, B.E., Chernets, A.V., Marinsky, G.S. et al. (2005) Prospects of using plasma technologies for disposal and recycling of medical and other hazardous waste. *Advances in Electrometallurgy*, **3**, Pt 1, 49–57; **4**, Pt 2, 46–53.
6. Petrov, S.V., Marinsky, G.S., Chernets, A.V. et al. (2006) Application of steam-plasma process for pyrolysis of organic wastes including medical and other hazardous ones. *Ibid*., **2**, 55–59.
7. Petrov, S.V., Korzhik, V.N., Marinsky, G.S. et al. (2007) Steam plasma technology for recycling of hazardous wastes. In: *Abstr. of 7th Int. Sci.-Techn. Conf. on Energy- and Material-Saving Environmental Technologies* (Grodno, Belarus, 27–28 Sept. 2007), 20–22.
8. Petrov, S.V., Korzhik, V.N., Marinsky, G.C. et al. (2008) Electric arc steam plasma conversion of medicine wastes and carbon containing materials. In: *Proc. of 17th Int. Conf. on Gas Discharges and Their Applications* (Cardiff, Wales, Sept. 7–12, 2008), 465–468.
9. Lojtsyansky, L.G. (1973) *Mechanics of fluids and gases*. Moscow: Nauka.
10. (1990) *Theory of electric arc column*. Ed. by M.F. Zhukov. Novosibirsk: Nauka.
11. Borisov, Yu.S., Chernyshov, A.V., Krivtsun, I.V. et al. (1994) Computer-aided simulation and experimental study of dusted plasma jets emitting into limited space. In: *Proc. of the Nat. Thermal Spray Conf*. (Boston, USA, 20–24 June, 1994), 361–366.
12. Kharlamov, M.Yu., Krivtsun, I.V., Korzhik, V.N. et al. (2007) Mathematical model of arc plasma generated by plasmatron with anode wire. *The Paton Welding J*., **12**, 9–14.
13. Boulos, M.I., Fauchais, P., Pfender, E. (1994) *Thermal plasmas. Fundamentals and applications*. Vol. 1. New York; London: Plenum Press.
14. Coufal, O. (2007) Composition and thermodynamic properties of thermal plasma up to 50 kK. *J. Phys. D: Appl. Phys.*, **40**, 3371–3385.
15. Starchyk, P.D., Porytsky, P.V. (2008) On the properties of the nonideal plasma of electrical pulse discharges in water. *Problems of Atomic Sci. and Techn.*, **6**, 207–209.
16. Launder, B.E., Spalding, D.B. (1990) The numerical computation of turbulent flows. *Computer Methods in Applied Mechanics and Eng*., **8**, 269–289.
17. Ievlev, V.M. (1975) *Turbulent motion of high-temperature continua*. Moscow: Nauka.
18. Wilcox, D.C. (1994) *Turbulence modeling for CFD*. Clendale, California: Griffin Print.
19. Zhukov, M.F., Kozlov, N.P., Pustogarov, A.V. et al. (1982) *Near-electrode processes in arc discharges*. Novosibirsk: Nauka.
20. Samarsky, A.A. (1971) *Introduction to the theory of difference schemes*. Moscow: Nauka.
21. Anderson, D., Tannehill, J., Pletcher, R. (1990) *Computational hydromechanics and heat exchange*. Vol. 1. Moscow: Mir.
22. Paskonov, V.M., Polezhaev, V.I., Chudov, L.A. (1984) *Numerical modelling of heat and mass exchange processes*. Moscow: Nauka.

MECHANICAL IMPACT OF GAS FLOW ON THE SURFACE OF PENETRATION CHANNEL WALLS IN GAS-LASER CUTTING

I.V. SHUBA
E.O. Paton Electric Welding Institute, NASU, Kiev, Ukraine

The paper deals with the features of assist gas flow in gas-laser cutting of 10 mm steel plates. It is established that distribution of tangential stresses on the melt surface depends on the position of the gas jet axis relative to the entrance face of the penetration channel. The possibility of ensuring a uniform distribution of tangential stresses on the melt surface in a broad range of working gas excess pressure is shown.

Keywords: *gas-laser cutting, steel, gas jet, excess pressure, penetration channel, melt surface, tangential stresses*

Technological processes, which use laser radiation, in particular, in the processes of gas-laser cutting (GLC) and laser welding are now widely accepted in industry. GLC does not always permit making products, which can be used for subsequent welding in structures without additional edge treatment. In this connection there is the need to minimize or completely eliminate the factors, which lead to formation of roughness on the edge surface or deviation of product edge geometry from the specified dimensions. During GLC a gas jet is used to remove the melt from the processing zone, the jet being guided by a nozzle inside the penetration channel (PCh) ---- a region, within which the metal is in the liquid state. Mechanical action of the gas flow generates a force on the melt surface, which overcomes the surface tension and viscous friction forces. Here the melt mass is accelerated and moves in the direction of the gas flow. Thus, the process of metal removal from the processing zone and formation of the product side face is realized.

Based on the data given in [1--3], it is possible to single out three groups of factors, determining the nature of running of GLC process and the final quality of products made with this technological process. The first group of factors is related to the physical properties of the processed material and their influence on its behaviour under the impact of thermal or mechanical loads, as well as the nature of running of chemical reactions with its participation. The second group is related to the properties of laser radiation, as well as the conditions of radiation absorption in the processing zone. The third group is related to the working gas properties, nature of its chemical interaction with the processed material and its destruction products, as well as gas dynamic parameters in the processing zone. At present, there is no common theory, which would unambigously determine the interrelation between the above factors and final product quality. Therefore, it is rational to study the individual aspects of the influence of various technological factors on running of GLC process.

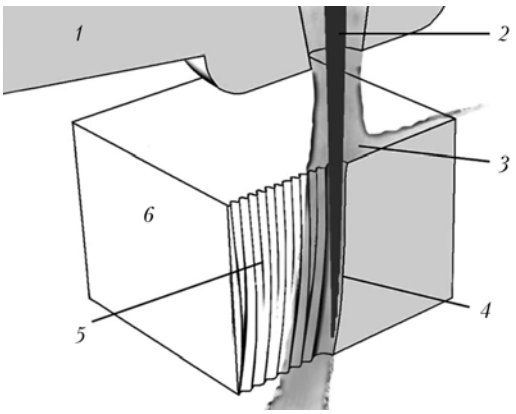

Figure 1. Schematic of GLC process: *1* ---- nozzle; *2* ---- beam; *3* ---- gas jet; *4* ---- penetration channel front wall; *5* ---- penetration channel side wall; *6* ---- plate

The purpose of this work is establishing the gas-dynamic conditions and factors, which adversely affect the effectiveness of melt removal from the processing zone, as well as finding the methods of their elimination.

In the considered technological process, in the region where intensive interaction of the gas flow, laser radiation and material occurs, the gas moves inside a narrow long channel, the front wall of which is covered by a layer of liquid melt (Figure 1). This work deals only with mechanical interaction between the gas and melt, normal pressure on the interface is determined by static pressure of gas, and tangential pressure is determined by dynamic pressure of the flow, which depends on gas velocity. Simultaneous motion of gas and liquid creates mechanical interaction on the interphase, which leads to a change of the interface shape, as well as formation and evolution of dynamic structures ---- stationary or moving waves on the melt surface [2]. Assuming that phase transformations are absent, according to [4] it may be taken that under such conditions the tangential and normal components of the stress vectors and phase velocity vectors coincide on the interphase. Therefore, if the distribution of tangential and normal stresses on the boundary surfaces of the calculation region is known from gas dy-

namic calculations, then for those boundary surfaces of the calculation region, which are in contact with the surface of the solid or liquid body, the obtained data can be regarded as values of the tangential and normal stresses on this body surface, i.e. in our case on the surface of PCh walls.

In order to study the gas-dynamic aspects of GLC process using Rhinoceros geometrical simulation package [5] two calculation regions were established, the shape of which corresponds to location of the gas-laser cutter nozzle at 1 mm distance from the surface of 10 mm thick plate, which has a through-thickness flat slit channel 0.4 mm wide with parallel walls (Figure 2). The length of the channel nozzle region is 30 mm. Nozzle section profile is conical with cylindrical outlet section 1 mm long, the angle between the walls being 30°. Diameter of the nozzle outlet opening is 1.2 mm, PCh length (plate thickness) being 10 mm. Boundary surface, which was PCh front wall, was modeled as the cylinder side surface, bisected along the axis. It was assumed that the position of this boundary surface relative to the nozzle axis corresponds to effective radius of the laser beam, which was equal to 0.2 mm in both the cases.

The first calculation region corresponds to a typical method of positioning the nozzle axis relative to laser beam axis, at which they are placed along one line to ensure equal conditions of coming of the thermal energy of radiation into the material volume at the change of the movement direction during processing (position *A*). For such a layout the distance between the PCh front wall and nozzle axis was equal to 0.2 mm.

The second calculation region corresponds to positioning of the laser beam axis with 0.15 mm shifting relative to nozzle axis in the direction of laser cutter movement (position *B*), so that the distance between the PCh front wall and nozzle axis was equal to 0.35 mm. For all the boundary surfaces of the calculation region, which were solid walls, zero gas velocity in all the nodes of the calculation region, belonging to these surfaces, was assigned (Figure 2, pos. *3–5, 7*).

Division of the calculation region into finite elements, assigning the boundary conditions and calculation of gas-dynamic parameter distribution were conducted using a commercial package of finite-element simulation ANSYS CFX. This was followed by numerical computations of gas flow parameter distribution for both the schematics of working gas feeding into the processing zone: without shifting of the nozzle axis relative to beam axis and with shifting. For each schematic a series of five calculations was conducted at values of flow velocity at the inlet (Figure 2, pos. *2*) of the calculation region from 1 to 5 m/s.

In both the calculations just the gas-dynamic effects were taken into account, not the thermal effects. Melt behaviour as an elastic structure under the thermal flow impact was not taken into account, so that its properties and characteristics were not assigned or determined during the calculation. Nature of gas flow

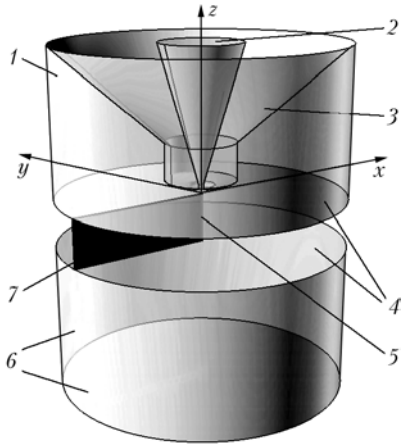

Figure 2. Schematic of the calculation region; *1, 6* ---- surfaces, through which gas evolves to the ambient atmosphere; *2* ---- entrance to cutter nozzle channel; *3* ---- nozzle channel outer surface; *4* ---- cut plate upper and lower surfaces; *5* ---- front wall of slit channel in the plate; *7* ---- side walls of a flat slit channel in a plate

impact on the melt surface was determined indirectly by the value of such parameters, as tangential stresses on the PCh wall surface and gas velocity at 0.05 mm distance from PCh wall surface. Properties of the calculation region material corresponded to those of air under the normal conditions.

In order to obtain the data allowing an indirect assessment of the effectiveness of the jet utilization as the factor which acts on the melt surface in both the variants of the jet axis positioning relative the PCh entrance face, a line running along the surface of the PCh front wall, was plotted (Figure 3, pos. *3*). Then the values of tangential stresses and values of gas velocity in the boundary layer at 0.05 mm distance from the wall were obtained for the points of this line. As an example, Figure 4 gives the isolines of velocity distribution inside the calculation region for both the positions and the respective graphs of tangential stress distribution along the PCh front wall for the value of gas velocity at the nozzle channel entrance of 5 m/s (corresponds to the pressure of 7.2 atm of working gas in the receiver).

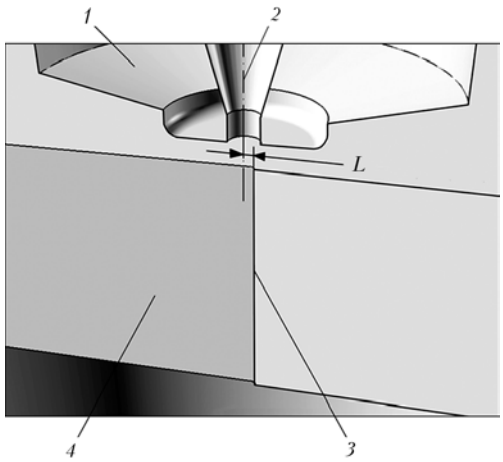

Figure 3. Cross-section of the calculated region: *1* ---- nozzle; *2* ---- nozzle axis of symmetry; *3, 4* ---- PCh front and side wall, respectively; *L* ---- distance between the nozzle axis of symmetry and PCh front wall

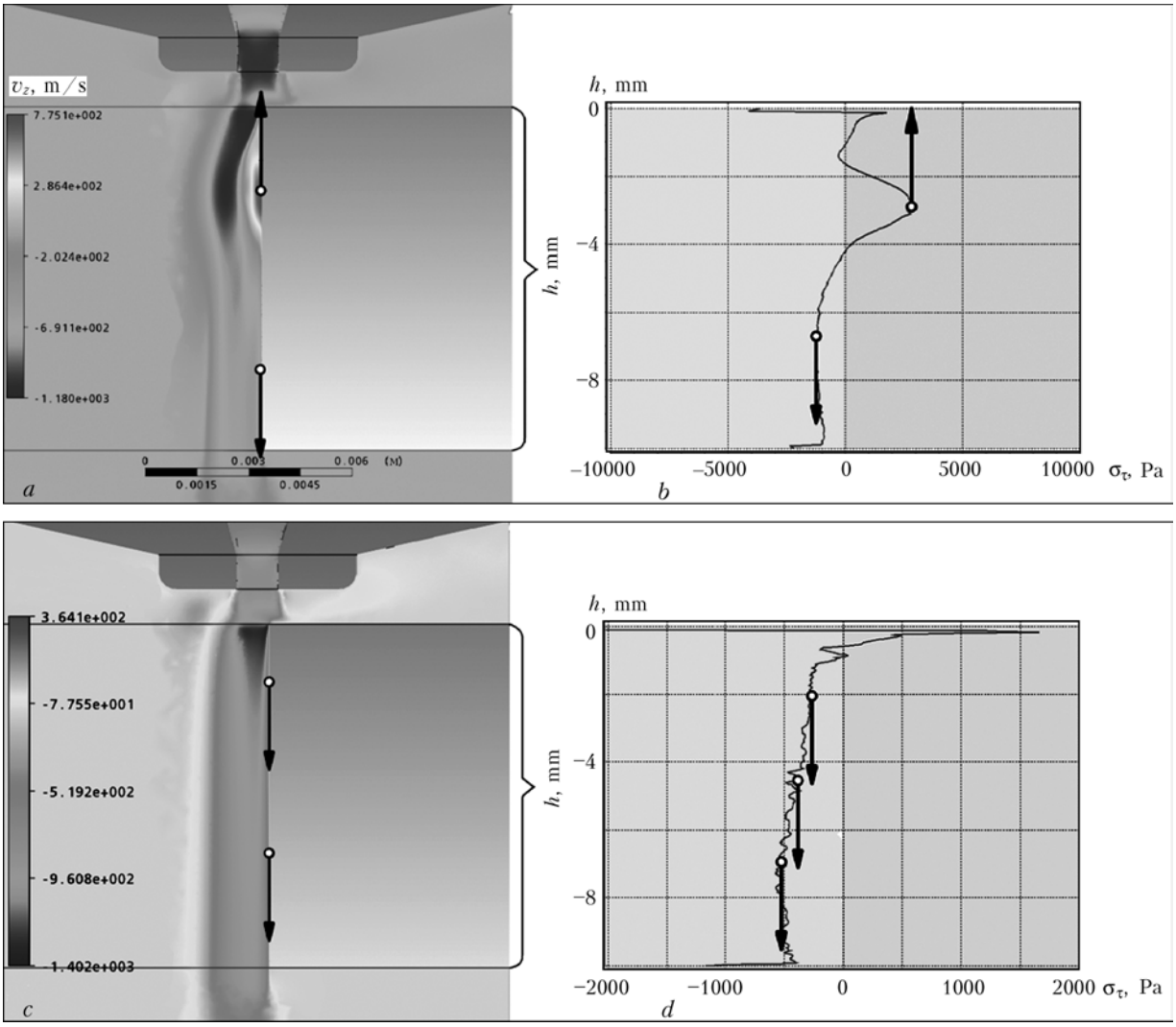

Figure 4. Distribution of flow velocity inside the PCh at gas velocity at nozzle channel inlet of 5 m/s for positions *A* (without shifting) (*a*) and *B* (with displacement) (*c*), and tangential stress distribution on PCh front wall corresponding to these conditions (*b*, *d*)

This was followed by plotting the graphs of tangential stress distribution over the surface of the PCh front wall and velocity distribution in the boundary layer along the entire channel for each calculated value of velocity at the nozzle channel inlet (Figures 5 and 6). From the viewpoint of a technologist or operator of the laser system, excess pressure inside the nozzle channel is a more informative parameter of the technological process, than the velocity at the nozzle inlet, as this parameter of the process can be readily controlled (measured) and adjusted (changed), so that in the graphs (see Figures 5 and 6) the numbers of curves of distribution of the tangential stresses and velocity along the PCh correspond to the calculated values of pressure inside the nozzle channel (Table).

Calculation results allowed revealing the main difference between gas flows inside the channel in the plate in position *A* and position *B*. Deviation of the jet at flowing over the PCh entrance face leads to boundary layer separation from PCh front wall and formation of a stagnation region, in which the eddy flow develops. Comparing the patterns of velocity distribution inside the PCh (see Figure 6) and the respective graphs of tangential stress distribution on PCh front wall along the channel (see Figure 5), one can see that in position *A*, when the jet flow deviates considerably at the channel entrance, tangential stresses on the channel front wall change their sign several times. In position *B*, contrarily, the value of tangential stresses, on the whole, rises downstream and does not change its sign at all the values of excess pressure in the nozzle channel.

The cause for such differences in parameter distribution for each of the positions is the fact that, in the first case, part of the gas flow penetrating inside the channel, greatly deviates from the rectilinear motion at interaction with PCh entrance face. As a result of formation of an eddy region, a considerable part of the gas flow inside the channel does not contact the channel front wall, and does not provide the mechanical impact on the wall surface in the direction of exit from the channel for melt removal from the processing zone. This supposition is confirmed by patterns of current lines, which are plotted for both the positions of the nozzle axis relative to the PCh front wall at excess pressure of the nozzle flow in the nozzle channel

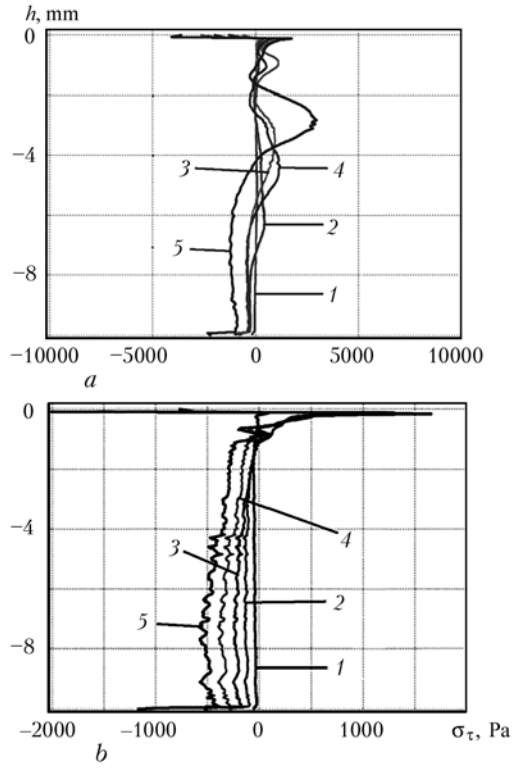

Figure 5. Distribution of z-component of tangential stresses on the PCh front wall at different values of excess pressure in the receiver for position A (*a*) and B (*b*) : *1* ---- 30; *2* ---- 117 (*a*), 116 (*b*); *3* ---- 260; *4* ---- 460; *5* ---- 725 (*a*), 714 (*b*) kPa

of 260 kPa, and are shown in Figure 7. It is seen that in position A (Figure 7, *a*) the eddy region takes up a considerable volume inside the channel and prevents the impact of the main flow on the surface of PCh

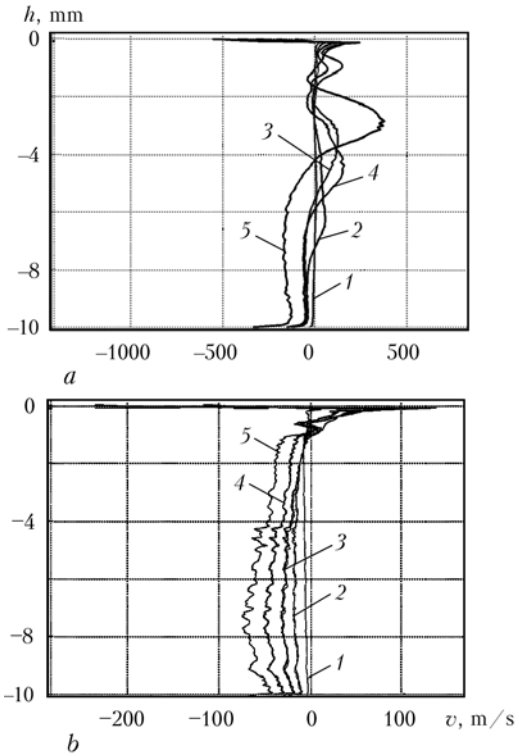

Figure 6. Distribution of z-component on the PCh front wall at different values of excess pressure in the receiver for position A (*a*) and B (*b*): *1* ---- 30; *2* ---- 117 (*a*), 116 (*b*); *3* ---- 260; *4* ---- 460; *5* ---- 725 kPa

Calculated values of excess pressure inside the nozzle channel at different values of gas velocity at the entrance to nozzle channel

Calculation number	Velocity at the entrance to nozzle channel v_e, m/s	Pressure in the nozzle channel P_{rec}, Pa
Position A (L = 0.1 m)		
1	1	30,000
2	2	117,500
3	3	260,000
4	4	460,000
5	5	725,000
Position B (L = 0.35 mm)		
6	1	30,000
7	2	116,000
8	3	260,000
9	4	460,000
10	5	714,000

front wall, unlike position B (Figure 7, *b*). Comparing the graphs of distribution of the tangential stress and velocity near the wall for all the initial conditions (see Figures 5 and 6), it is seen that for the calculation region in position A the tendency to appearance of the effect of flow separation from the channel surface with formation of eddy current near the wall is manifested for all, even the lowest, values of excess pressure inside the nozzle channel, while for the calculation region

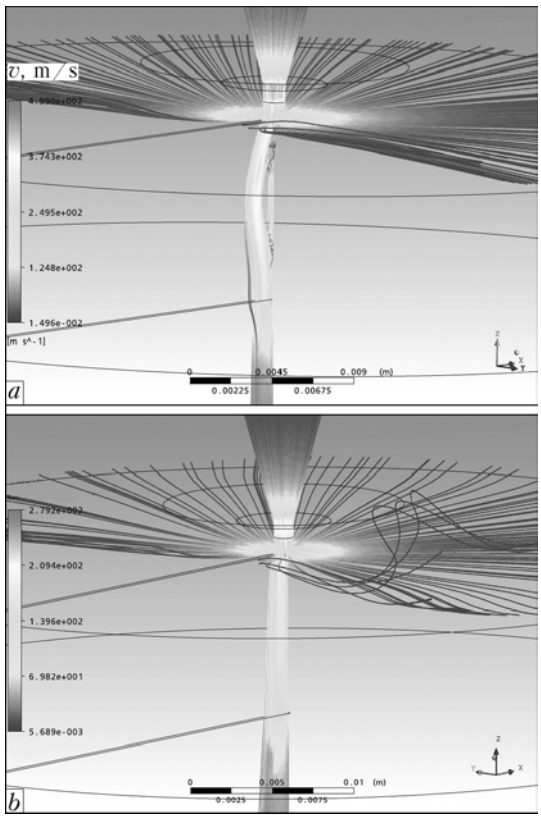

Figure 7. Current lines for the position of nozzle axis without shifting ---- position A (*a*) and with shifting ---- B (*b*) relative to the PCh front wall at 260 kPa excess pressure of working gas inside the cutter

in position B just the local jumps in distribution of the obtained gas-dynamic parameters along the entire surface of the PCh front wall are observed.

Thus, for a typical schematic of the nozzle axis location relative to laser beam axis, conditions are in place, at which the forces, applied to the surface of the penetration channel walls act in opposite directions in some sections of the channel, which is indicative of the destabilizing impact of the gas flow on the melt flow. Comparing the graphs of distribution of tangential stresses and velocities for the two systems of gas feeding into the processing zone at the same initial conditions, one can see that there exists the possibility of such a distribution of the tangential stresses along the channel, which provides a unidirectional action of the mechanical forces from the gas flow side on the melt surface. For this purpose, for instance, it is possible to shift the axis of symmetry of the nozzle relative to the PCh front wall so that the gas jet at penetration inside the channel deviated as little as possible from the rectilinear direction of the flow. This lowers the probability of stagnation section formation inside the channel and of the conditions of eddy flow formation, which adversely affects the uniformity of tangential stress distribution on the melt surface. In our opinion, in practice this should have a positive effect on melt flow stabilization and should improve the geometrical characteristics of the side edge of products made by GLC.

Thus, the relative location of the nozzle axis and laser beam axis, determining the position of the PCh front wall, has a significant influence on the distribution of tangential stresses on the PCh wall surface during cutting, and can be used as a technological parameter, controlling the melt flow during GLC to improve the quality of the cut-out product.

1. Steen, W.M., Kamalu, J.N. (1983) *Laser cutting*. London Imperial College of Science and Technology.
2. Golubev, V.S. (2005) Analysis of dynamic models of deep penetration of materials by laser beam. In: RAN IPLIT Transact. Ed. by V.Ya. Panchenko, V.S. Golubev. Moscow: Interkontakt Nauka.
3. Grigoriants, A.G., Sokolov, A.A. (1988) Laser cutting of metals. Series: Laser technique and technology. Book 7. Moscow: Vysshaya Shkola.
4. Kutateladze, S.S., Nakoryakov, V.E. (1984) *Heat and mass exchange and waves in gas-liquid systems*. Novosibirsk: Nauka.
5. http:www.rhino3d.com

BEAM CURRENT CONTROL SYSTEM IN ELECTRON BEAM WELDING GUN WITH DIRECTLY HEATED CATHODE

Yu.N. LANKIN, L.F. SUSHY and **V.F. SHULYM**
E.O. Paton Electric Welding Institute, NASU, Kiev, Ukraine

The system for automatic control of beam current of electron beam welding gun with directly heated cathode is described.

Keywords: *electron beam welding, directly heated cathode gun, automatic adjustment, beam current*

Diode electron beam guns (EBG) with directly heated cathodes are widely used in machines for electron beam welding, melting and coating. Adjustment and stabilization of electron beam current in them is performed by adjustment of cathode filament current. In EBG with indirect heating of the cathode by electron bombardment, the assembly for generation of bombardment electron beam actually is a built-in low-power EBG with directly heated cathode.

Publications lack the data on static and dynamic characteristics of EBG with directly heated cathodes with and without automatic adjustment of electron beam current. Described below is a system of automatic control of beam current in a low-amperage EBG with directly heated cathode, which partially fills this gap.

The electron beam current of diode EBG is usually regulated by changing the cathode temperature. For a tungsten cathode the emission current density is related to the cathode temperature by the following dependence:

$$j_e = 37T^2 \exp [-47825T^{-1}].$$

Thus, beam current can be adjusted in a broad range, by varying the heating power of the cathode, which operates in the saturation mode, i.e. all the electrons, emitted by the cathode, reach the anode. At a high density of cathode current, beam current is limited by the spatial charge in the interelectrode gap and is equal to

$$I_b = kE_{acc}^{3/2},$$

where k is the coefficient dependent on electrode shape and their spacing; E_{acc} is the accelerating voltage.

Static characteristic of EBG with directly heated cathode is given in Figure 1. As is seen from the Figure, for this EBG at $I_b < 25$ mA the cathode operates in the saturation mode, and beam current dependence on heating power is of an exponential nature. Slight (6 %) changes of filament power lead to significant (25 %) changes of beam current values. In this connection, automatic stabilization of beam current by adjustment of cathode heating power is required. At

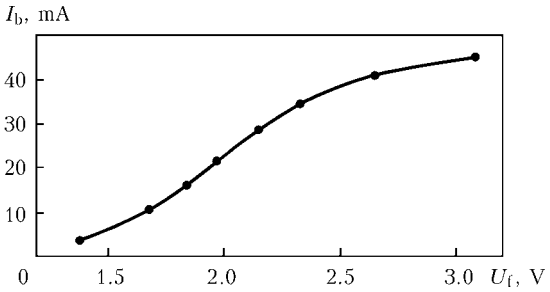

Figure 1. Static characteristic of EBG with directly heated cathode: U_f — filament voltage

I_b > 25 mA the cathode gradually goes into the mode of current limiting by the spatial charge. The width of the intermediate region depends on non-uniformity of cathode temperature distribution over the emitting surface.

It is seen from Figure 2 that directly heated EBG is an aperiodic link of the first order with time constants 1.3 s at the drop and 0.94 s at the rise of beam current. A very high inertia of the gun makes program control of the electron beam extremely difficult, which is required, for instance, in welding up of the crater at the end of the welding process. This is another reason for application of automatic adjustment, as negative feedback considerably reduces the time of beam current adjustment realization.

Figure 3 gives the block diagram of the system of automatic program adjustment of beam current in diode EBG with directly heated cathode.

The regulator performs automatic stabilization of the assigned value of EBG beam current by smooth regulation of gun filament current. At crater welding up at the end of the welding process a smooth decrease of current at a specified rate is performed.

Feedback voltage proportional to beam current I_b is taken from throttle $R8$, connected between the «ground» and positive pole of accelerating voltage

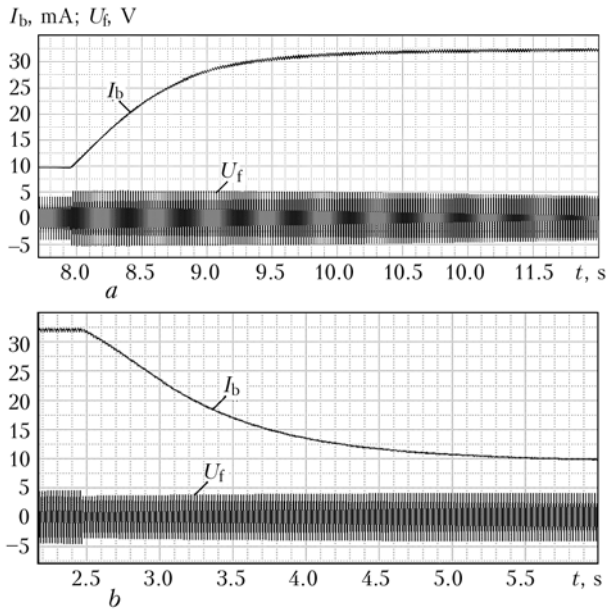

Figure 2. Transition functions of EBG with directly heated cathode: *a* — current rise at jump-like increase of filament voltage; *b* — current drop at jump-like decrease of filament voltage

source PS. This voltage through resistor $R5$ is applied to inverter input of error amplifier $DA2$. Discharger $FV1$, filter $R7$–$C6$ and stabilitron $VD3$ protect regulator input circuits from noise at high-voltage breakdowns in the welding machine. Beam current setting voltage U_{pr}, changing according to a program, which is taken from potentiometer R_3, is applied to inverter input of amplifier $DA2$ through resistor $R4$. Amplified difference of the set and measured voltage at the output of operational amplifier $DA2$ is applied to capacitance integrator $R6$–$C3$. As a result, capacitor $C3$ voltage rises linearly. Capacitor $C3$ is connected to emitter of unijunction transistor $VT2$. After the voltage of unblanking of transistor $VT2$ has been reached on the emitter, capacitor $C3$ quickly discharges in the

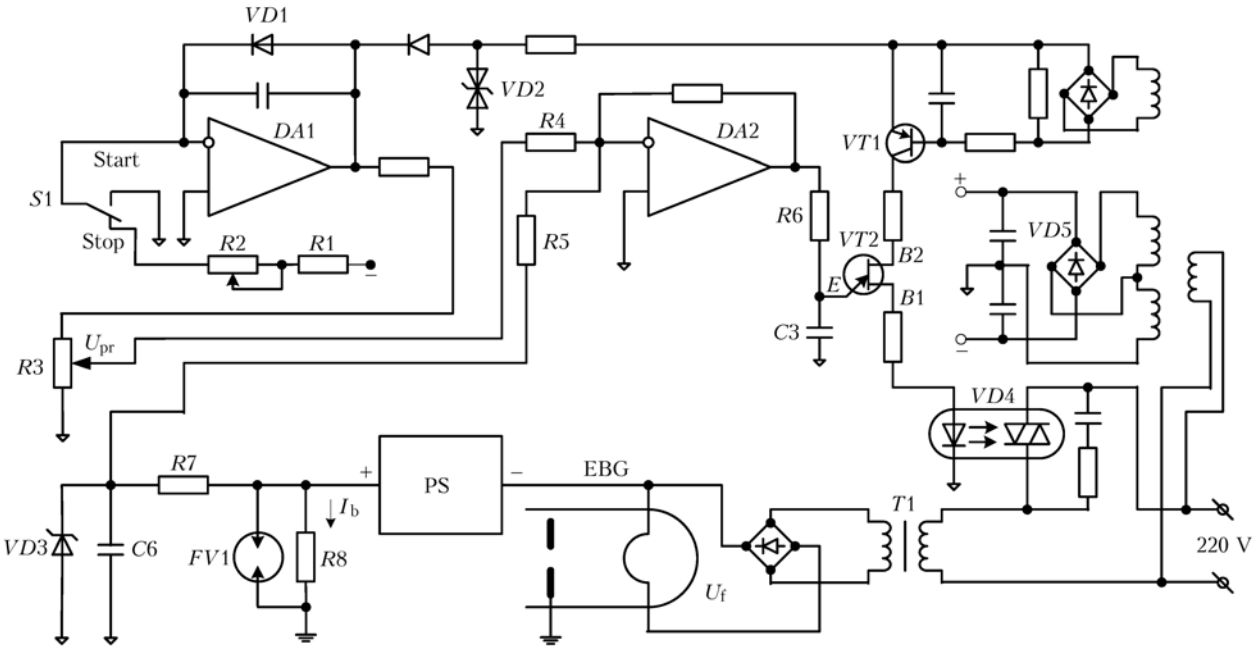

Figure 3. Block-diagram of program regulator of diode welding EBG with directly heated cathode

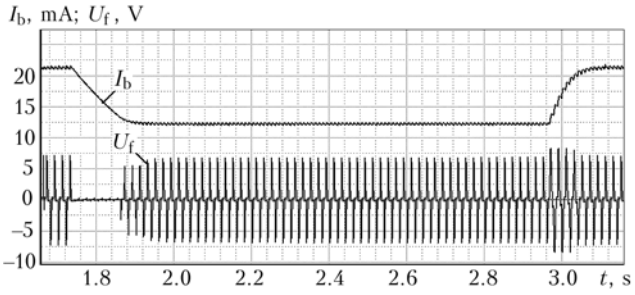

Figure 4. Regulator performing a step-like change of beam current setting

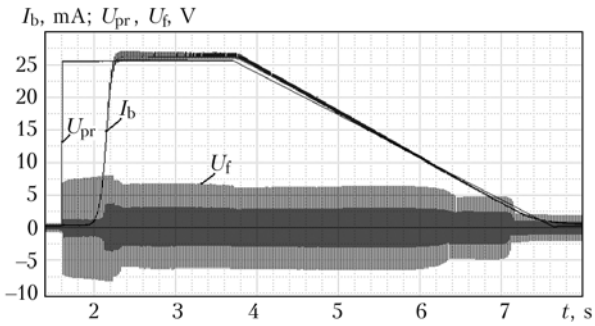

Figure 5. Operating cycle of beam current control block

circuit of emitter E–base $B1$–emitting diode of optosimistor $VD4$, resulting in switching on of the latter. After that capacitor $C3$ is charged again. For synchronizing the simistor switching on with the mains voltage, transistor $VT2$ is forcedly switched on by transistor $VT1$ every time the mains voltage goes through zero.

EBG cathode is powered by rectified voltage of high-potential step-down transformer $T1$. Transformer primary winding is connected to the mains through optosimistor $VD4$. Owing to phase regulation of optosimistor switching on, EBG cathode filament current changes in proportion to the set voltage.

Owing to negative beam current feedback, EBG current value is always equal to the set value, irrespective of any disturbances, acting on it, namely change of cathode emitting capability, mains voltage fluctuations, etc. Moreover, due to the forcing properties of negative feedback, system dynamic characteristics are essentially improved. As an example, Figure 4 gives transient process oscillograms during the system performing a step-like change of beam current setting.

As is seen from Figure 4, the time of beam current lowering from 22 to 12 mA is equal to 0.140 s, and the time of its increase is 0.075 s, which is, approximately, by an order of magnitude faster than without the feedback (see Figure 2). This is accounted for by the fact that limit values of control actions, namely filament voltage is zero or maximum, are set automatically for almost the entire duration of the transient processes. As a result, the system features the properties, close to those of an optimum system with limit possible response.

Beam current programmer for crater welding up is assembled on operational amplifier $DA1$. In the initial position of switch $S1$ maximum voltage, determined by the voltage of high-precision stabilitron $VD2$, is set on $DA1$ output. At $S1$ switching negative voltage is applied at «Crater welding up» command to amplifier input through resistor $R1$ and rheostat $R2$. The amplifier goes into the integrator mode and voltage at its output drops linearly to zero. As amplifier output voltage feeds setting potentiometer $R3$, beam current setting voltage drops to zero, respectively. Time of lowering of beam current setting voltage is adjusted by rheostat $R2$ and is independent on setting voltage, determined by potentiometer $R3$. Range of setting the current drop time is equal from 0.5 up to 5.0 s. Figure 5 gives oscillograms of setting voltage U_{pr}, beam current and filament voltage of EBG cathode.

In the initial «Stop» position of switch $S1$, negative voltage is applied to inverter input of amplifier $DA1$. Amplifier output voltage is limited by diode $VD1$ at approximately zero level. At $S1$ switching into «Start» position, zero is applied to amplifier input, and limit negative voltage is set almost immediately at its output, owing to small inner positive bias. Beam current setting is taken from the slide of potentiometer $R3$. Beam current I_b at cathode maximum filament voltage U_f starts rising with approximately 0.5 s delay, required for cathode heating up to the temperature of the start of electron emission. If desired, this time can be essentially reduced, if initial cathode filament current, at which electron emission is still absent, is set in the «Stop» mode. When beam current has reached the set value, filament voltage decreases to the necessary level and the regulator runs in the mode of stabilization of the set current value. After switching $S1$ into «Stop» position setting voltage U_{pr} decreases by a linear law and regulator goes into the following mode, in which beam current accurately follows the setting voltage.

CONCLUSIONS

1. Cathode time constant in low-power EBG with directly heated cathode is more than 1 s.

2. Automatic adjustment of beam current by regulation of cathode filament current shortens the time for implementing the change of beam current setting by an order of magnitude.

3. Value of limit modulation frequency of beam current by cathode filament current regulation is equal to not more than several hertz.

4. Data obtained for low-amperage EBG are readily extrapolated to guns with a high beam current, i.e. with a more massive and, therefore, higher inertia cathode.

STRUCTURE AND WEAR RESISTANCE OF DEPOSITED METAL 20Kh5M2FS ALLOYED WITH SULPHUR AND PHOSPHORUS

I.A. RYABTSEV, Ya.P. CHERNYAK, I.I. RYABTSEV, V.A. ZHDANOV and **I.L. BOGAJCHUK**
E.O. Paton Electric Welding Institute, NASU, Kiev, Ukraine

The effect of alloying with sulphur and phosphorus on structure and wear resistance of deposited metal 20Kh5M2FS was investigated. It was proved that phosphorus dissolves to harden the martensitic component of structure of the deposited metal, whereas sulphur forms sulphides and oxy-sulphides with other alloying elements. It is shown that the most favourable combination of wear resistance of friction pair components is provided by deposited metal 20Kh5M2FS alloyed with 0.21 wt.% S and 0.56 wt.% P.

Keywords: *arc cladding, medium-alloyed deposited metal, microstructure, phosphorus and sulphur in steel, wear resistance, sulphides, phosphides*

Phosphorus and sulphur can be used to advantage as alloying elements in different-application cladding consumables [1–5]. In this case, phosphorus has a positive effect on wear resistance of the deposited metal as a result of hardening of the matrix and formation of inclusions of phosphides of some alloying elements [6]. Unlike phosphorus, sulphur does not dissolve in iron [7], but forms sulphides and oxy-sulphides in the deposited metal, which may act as «solid lubricants» and prevent its wear caused by adhesion of friction surfaces [5].

This study is dedicated to investigation of the effect of combined alloying with sulphur and phosphorus on structure and wear resistance of deposited metal 20Kh5M2FS. Eight experimental flux-cored wires PP-Np-20Kh5M2FS-op, having a diameter of 2 mm and containing different amounts of sulphur and phosphorus, were made for the experiments. To determine chemical composition and hardness of the deposited metal (Table 1), as well as its structure (Figure 1) and wear resistance, the samples were clad under the same conditions (current 250–270 A, voltage 24–26 V, cladding speed 28 m/h) by the submerged-arc method using flux AN-26P. The contents of sulphur and phosphorus in the deposited metal were varied from 0.02 to 1.40 and 0.06 to 0.97 wt.%, respectively.

The structure of deposited metal 20Kh5M2FS, which was not alloyed with sulphur and phosphorus (sample 1, Table 1), consists of martensite, retained austenite and carbides. Also, it contains a small volume fraction of non-metallic inclusions identified as oxides and silicates (Figure 1, *a*). Microhardness of martensite is *HV*0.5 3860–3620 MPa, and that of retained austenite is *HV*0.5 2320–2460 MPa.

Increase of the weight content of sulphur to 0.24 wt.% (sample 2, Table 1; Figure 1, *b*) and then to 1.40 wt.% (sample 3, Table 1; Figure 1, *c*) has almost no effect on structure of the deposited metal. However, it causes a considerable increase of the content of non-metallic inclusions in it, due to formation of sulphides and oxy-sulphides.

Alloying deposited metal 20Kh5M2FS with phosphorus (0.50 wt.%) in sample 4 (Table 1) leads to growth of the content of retained austenite in the deposited metal structure (Figure 1, *d*). Microhardness of martensite increases to *HV*0.5 4120–5490 MPa, most probably, due to dissolution of phosphorus in it, whereas microhardness of austenite remains at the same level ---- *HV*0.5 2320–2570 MPa. Non-metallic inclusions, i.e. oxides and silicates, are also detected.

Adding 0.21 wt.% S (sample 5, Table 1) to deposited metal 20Kh5M2FS at its phosphorus content of 0.56 wt.% leads to increase in the volume content of non-metallic inclusions, among which there are sulphides and oxy-sulphides. The main structural components of the deposited metal are martensite and retained austenite (Figure 1, *e*), the microhardness of which remains at a level of that in sample 4.

In a case of increasing the phosphorus content to 0.97 wt.% at a standard sulphur content of 0.04 wt.% (sample 6, Table 1), many light regions appear in

Table 1. Chemical composition (wt.%) and hardness *HRC* of deposited metal of the 20Kh5M2FS type alloyed with sulphur and phosphorus

Sample No.	S	P	Balance	*HRC*
1	0.02	0.06	0.18–0.22 C 4.8–5.2 Cr 1.8–2.2 Mo 0.3–0.5 V	37–38
2	0.24	0.06		34–36
3	1.40	0.06		32–34
4	0.04	0.50		34–36
5	0.21	0.56		32–34
6	0.04	0.97		35–37
7	0.18	0.83		34–36
8	1.30	0.90		34–36

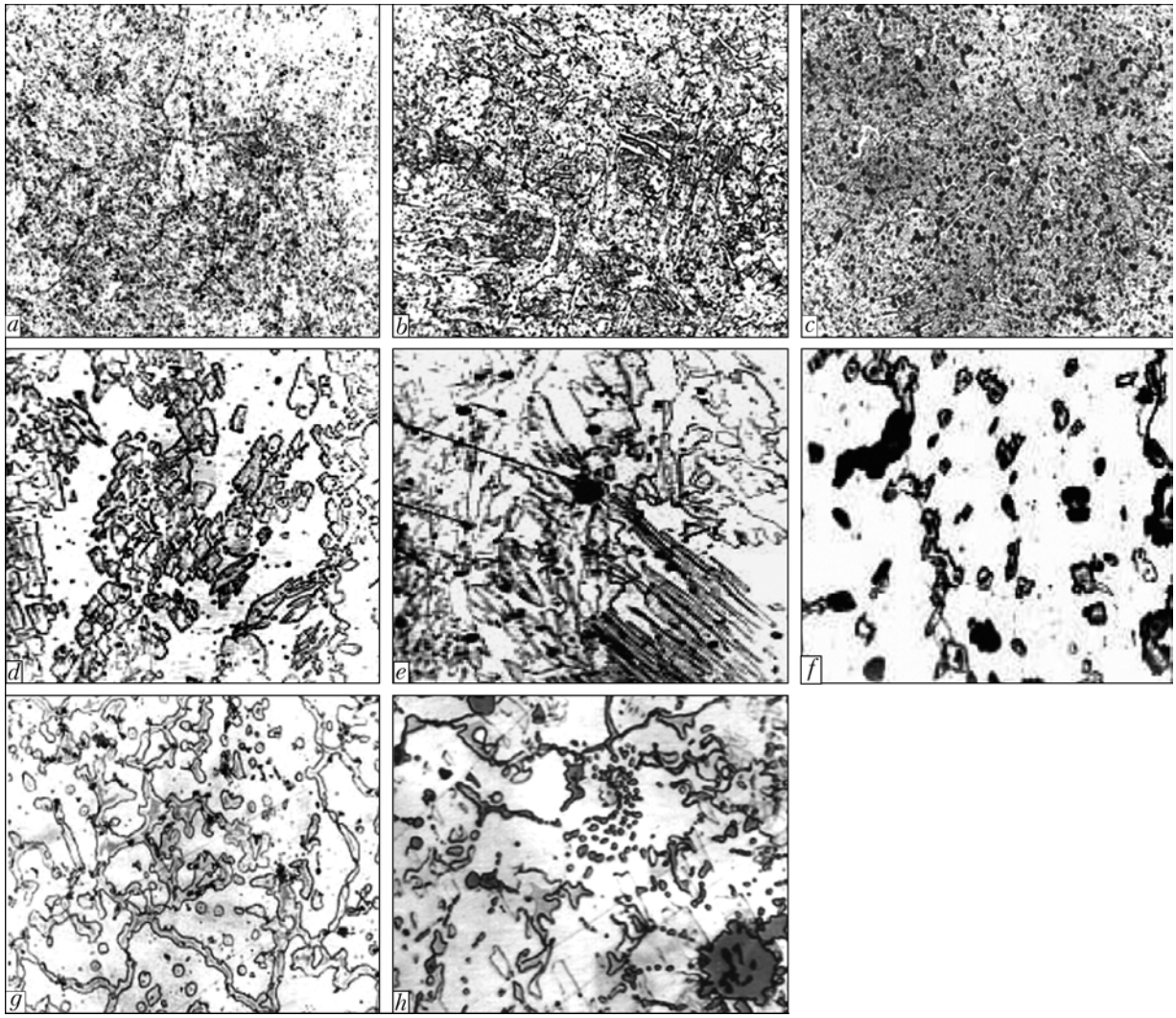

Figure 1. Microstructure (×500) of deposited metal of the 20Kh5M2FS type at different contents of sulphur and phosphorus, wt.%: *a* ---- 0.06 P, 0.02 S; *b* ---- 0.06 P, 0.24 S; *c* ---- 0.06 P, 1.40 S; *d* ---- 0.50 P, 0.04 S; *e* ---- 0.56 P, 0.21 S; *f* ---- 0.97 P, 0.04 S; *g* ---- 0.83 P, 0.18 S; *h* ---- 0.90 P, 1.30 S

structure of the deposited metal, which is indicative of a worse etchability (Figure 1, *f*). This is likely to be associated with increase in corrosion resistance of the deposited metal alloyed with a considerable weight fraction of phosphorus [8]. Microhardness of martensite is *HV*0.5 4730--5490 MPa, and that of retained austenite is *HV*0.5 2570--3050 MPa.

The deposited metal has a cellular structure (Figure 1, *g*) at a phosphorus content of 0.83 wt.% and sulphur content of 0.18 wt.% (sample 7, Table 1). Microhardness of martensite decreases to *HV*0.5 3620--4120 MPa, and that of retained austenite remains at a previous level of *HV*0.5 2830--3060 MPa. The structure of the deposited metal also comprises sulphides and oxy-sulphides.

Increasing the weight content of sulphur to 1.30 wt.% at a practically unchanged content of phosphorus (sample 8, Table 1) causes formation of coarse inclusions of sulphides and oxy-sulphides in the deposited metal structure (Figure 1, *h*).

As it is sulphur that exerts the main effect on formation of non-metallic inclusions, their distribution in the deposited metal was investigated at a different content of this element. Non-etched polished sections were studied with analyser «Omnimet» (×600) by examining 100 view fields (Figures 2 and 3).

As seen from Figure 3, increase of the sulphur content causes a dramatic increase in the quantity and size of non-metallic inclusions. For example, the maximal size of non-metallic inclusions is 2.0 μm at 0.02 wt.% S (Figure 3, *b*), 3.5 μm at 0.24 wt.% S (Figure 3, *d*), and 7.0 μm at 1.40 wt.% S (Figure 3, *f*). The total volume content of non-metallic inclusions of all sizes grows from 0.18 (0.02 wt.% S) to 4.01 % (1.40 wt.% S).

As shown by X-ray microanalysis of deposited metal 20Kh5M2FS, sulphides have complex composition, i.e. they contain an increased weight fraction of chromium, molybdenum and manganese (Table 2).

Wear resistance of samples of deposited metal 20Kh5M2FS was studied at a different content of sulphur and phosphorus under conditions of dry friction of metal on metal at room temperature by the shaft--plane scheme (Figure 4). The 3 × 15 × 25 mm samples were cut from the deposited metal, so that the test plane was in the upper layers of the deposited metal. The shaft mating body 40 mm in diameter was made from steel 45 and hardened to hardness *HRC* 42.

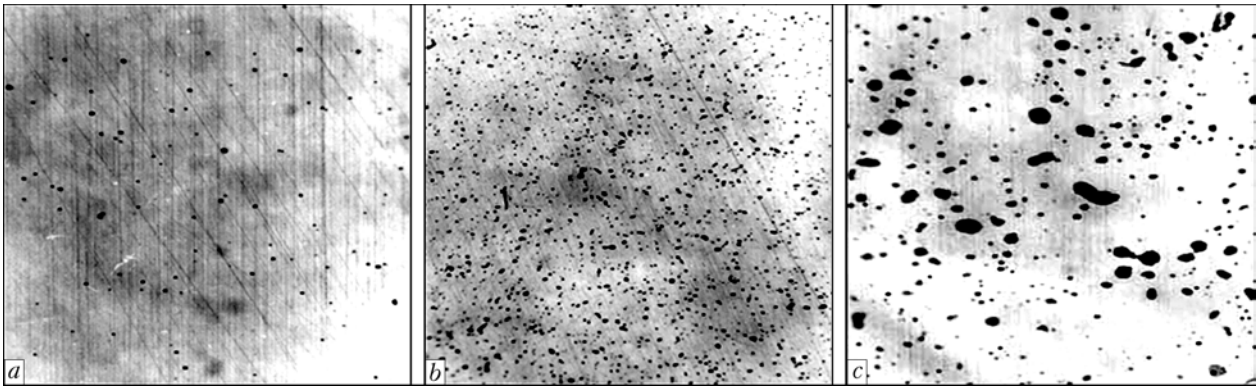

Figure 2. Microstructure (×600) of deposited metal 20Kh5M2FS with sulphur content of 0.02 (*a*), 0.24 (*b*) and 1.4 (*c*) wt.% (non-etched sections)

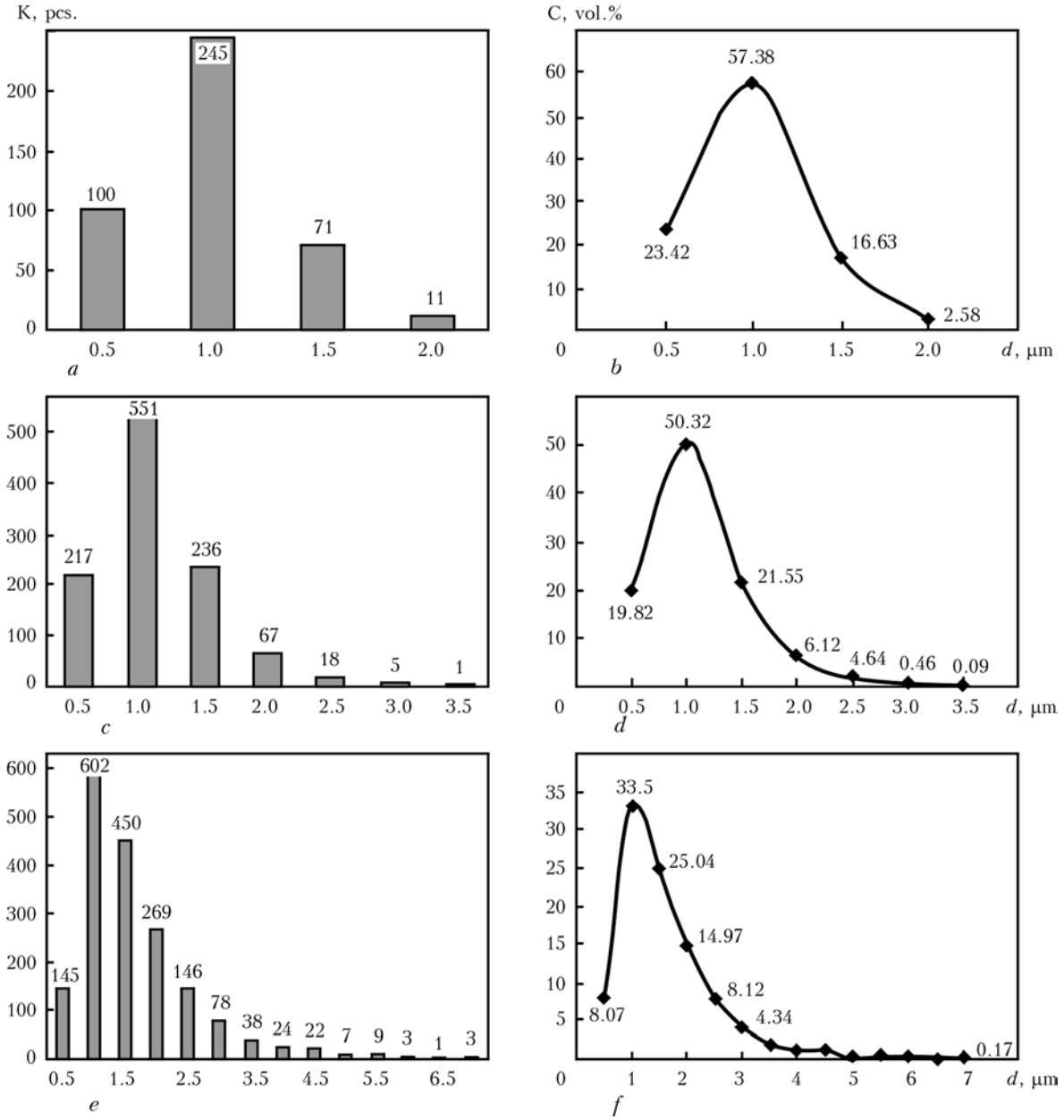

Figure 3. Distribution of non-metallic inclusions *d* by quantity K (*a, c, e*) and volume content C (*b, d, f*) in deposited metal 20Kh5M2FS at sulphur content of 0.02 (*a, b*), 0.24 (*c, d*) and 1.40 (*e, f*) wt.%

Table 2. Chemical composition (wt.%) of structural components of deposited metal 20Kh5M2FS (by X-ray microanalysis results)

Sample No. acc. to Table 1	Point of analysis	Fe	Cr	Mo	V	Mn	Si	S
2	Matrix	89.09	6.38	3.98	0.44	0.04	0.87	--
	Sulphide	22.78	18.69	10.25	1.72	20.96	5.28	20.14
3	Matrix	91.07	6.72	2.01	0.45	0.20	0.68	0.08
	Sulphide	5.58	21.02	14.58	1.58	23.12	4.38	29.47
	Same	5.60	25.36	10.76	2.08	20.85	0.49	34.15

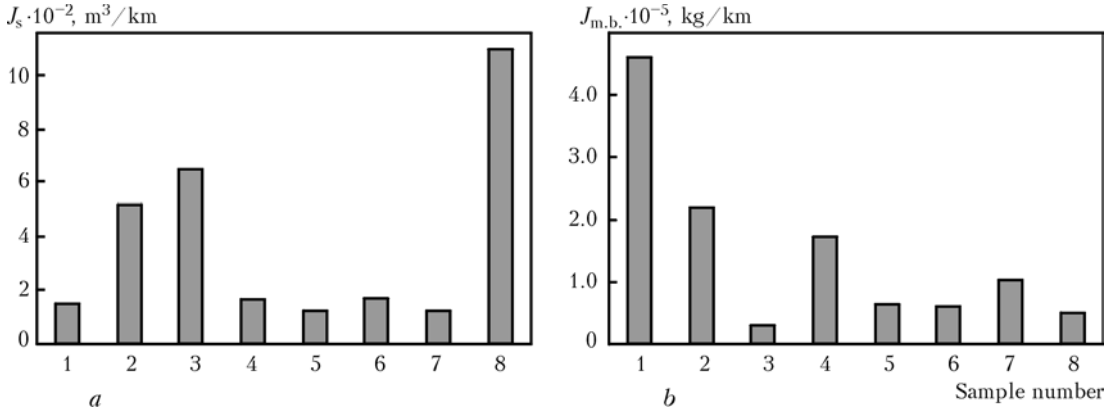

Figure 4. Wear resistance of samples, J_s, of deposited metal 20Kh5M2FS with different contents of sulphur and phosphorus (*a*), and wear resistance of steel 45 mating bodies, $J_{m.b.}$, tested in pair with the above samples (*b*): 1–8 ---- numbers of samples according to Table 1

During the tests, the sample was pressed under a certain load to the mating body with a plane 3 × 25 mm in size. As a result, a hole of a certain depth was formed in the test plane, and a strip was formed on the mating body. The following test conditions were chosen: slip speed 1 m/s, load 30 N, mating body rotation frequency 30 rpm. These conditions provided stabilisation of tribotechnical characteristics of all the samples studied. The use of the positioning system allowed each clad sample to be tested not less than three times in a new region of the friction surface of the sample and in a new friction strip of the mating body.

As seen from the data presented, alloying only with sulphur leads to increase in wear of the deposited metal samples and a simultaneous dramatic decrease in wear of the mating body (Figure 4, samples 1–3). However, total wear of a friction pair remains at a sufficiently high level. It is likely that an increased wear of deposited metal 20Kh5M2FS alloyed with sulphur is explained by the fact that numerous sulphides of relatively big sizes readily break out during wear from the deposited metal matrix. These sulphides act as «solid lubricants» and prevent adhesion of the surfaces of the sample and mating body, thus decreasing its wear.

In alloying the deposited metal with phosphorus (0.50 wt.%) (Figure 4, sample 4), wear of the sample and mating body decreases. Deposited metal 20Kh5M2FS alloyed with sulphur (0.21 wt.%) and phosphorus (0.56 wt.%) has the most favourable combination of properties (Figure 4, sample 5). Wear resistance of the deposited metal at such a content of sulphur and phosphorus is 10–15 % higher compared with standard composition of the deposited metal (Figure 4, *a*, sample 1), wear of the mating body substantially decreasing (8–10 times). Apparently, increase in the wear resistance of the deposited metal is attributable to the fact that phosphorus hardens its matrix. At the same time, alloying the deposited metal with a relatively low weight fraction of sulphur leads to formation of sulphides, which have an optimal shape, quantity and size. Wear of the mating body considerably decreases as a result of the «solid lubrication» effect.

Therefore, it was proved that sulphur, in contrast to phosphorus, does not dissolve in the deposited metal matrix, but forms sulphides and oxy-sulphides in it, their sizes and quantity growing with increase in the sulphur content. Alloying deposited metal 20Kh5M2FS with 0.56 wt.% P and 0.21 wt.% S provides a high wear resistance of the clad samples, whereas a relatively low content of sulphur promotes formation of sulphides, optimal in shape, quantity and size. Wear of the mating body in contact with the clad sample also substantially decreases as a result of the «solid lubrication» effect.

1. Kuskov, Yu.M., Ryabtsev, I.I., Doroshenko, L.K. et al. (2002) Peculiarities of melting and solidification of 20KhGS type deposited metal alloyed with phosphorus. *The Paton Welding J.*, **8**, 21–24.
2. Ryabtsev, I.I., Kuskov, Yu.M., Novikova, D.P. (2006) Effect of phosphorus on crack resistance of low-carbon deposited metal of Fe–Mn–Si–Cr system. *Ibid.*, **5**, 12–15.
3. Ryabtsev, I.I. (2008) Calculation-experimental evaluation of the efficiency of alloying the high-alloy deposited metal with phosphorus. *Ibid.*, **5**, 13–17.
4. Osin, V.V., Ryabtsev, I.A. (2004) Effect of sulphur on properties of iron-base alloys and prospects on its application in surfacing materials. *Ibid.*, **10**, 18–21.
5. Osin, V.V., Ryabtsev, I.A., Kondratiev, I.A. (2006) Study of sulphur effect on properties of deposited metal of Kh5MFS type. *Ibid.*, **12**, 12–15.
6. Ryabtsev, I.I., Kuskov, Yu.M., Grabin, V.F. et al. (2003) Tribological properties of the Fe–Cr–Si–Mn–P system deposited metal. *Ibid.*, **6**, 16–20.
7. Lunev, V.V., Averin, V.V. (1988) *Sulfur and phosphorus in steel*. Moscow: Metallurgiya.
8. Gulyaev, A.P., Tsulkova, V.M. (1974) Effect of phosphorus on corrosion properties of stainless steels. In: *Corrosion-resistant metallic structural materials and their application*. Moscow: Mashinostroenie.

INVESTIGATION OF PHASE TRANSFORMATIONS AND PLASTIC DEFORMATION AT CONTINUOUS HEATING OF Al/Cu MULTILAYER FOIL

A.I. USTINOV[1], **Ya.I. MATVIENKO**[1], **S.S. POLISHCHUK**[2] and **A.E. SHISHKIN**[2]
[1]E.O. Paton Electric Welding Institute, NASU, Kiev, Ukraine
[2]G.V. Kurdyumov Institute for Metal Physics, NASU, Kiev, Ukraine

Pressure welding through an interlayer with a multilayer structure based on intermetallic-forming elements allows solid-state formation of permanent joints in hard-to-weld materials. The role of interlayer structure in formation of permanent joints has been evaluated by an example of Al/Cu multilayer foil. It is shown that such foils subjected to continuous heating to 500 °C, under the conditions of permanent loads are characterized, in addition to phase transformations caused by the reaction diffusion of components, also by plastic deformation, the intensity of which depends upon the foil temperature.

Keywords: *diffusion pressure welding, electron beam deposition, multilayer foil, phase transformation, plastic deformation*

Application of multilayer foils based on intermetallic-forming elements as interlayers in diffusion pressure welding demonstrated their high effectiveness in formation of permanent joints of difficult-to-weld materials [1--4]. Investigation of welded joint microstructure revealed that reaction diffusion occurs between the interlayer layers during welding. It is assumed that this process promotes an increase of diffusion mobility of atoms in material regions which are in direct contact with the interlayer, and provides a «softening» of the conditions required for joint formation.

In order to achieve the optimum parameters in joint formation using multilayer foils as interlayers it is believed to be urgent to establish the processes of phase transformations in such materials under the conditions close to those implemented in diffusion welding.

The sequence of phase transformations in multilayer foils was earlier studied by analyzing the microstructure and X-ray diffraction pattern before and after their heating with soaking at a specified temperature. So, for instance, in the case of Al/Ni and Al/Ti multilayer foils it is established that the processes of phase formation in them are characterized by low activation energy, and their initial stage runs already at 250--350 °C [5, 6].

On the other hand, there exist systems, in which the temperature of the start of solid phase reactions can be even lower. Al--Cu system is one of such systems. As a result of the reaction between a layer of copper and aluminium, formation of intermetallics in this system was observed already at the temperature of about 150 °C [7--9]. Thus, use of Al/Cu multilayer foils as an interlayer in diffusion welding allows lowering the heating temperature and time required for formation of a permanent joint, for instance, of pure aluminium, copper, as well as their alloys, compared to the process of diffusion welding without application of interlayers [10], and in friction welding additional annealing is eliminated [11--13].

Considering also the fact that phase transformations in multilayer foils are largely determined by kinetic factors [5, 6], it is believed to be necessary to study the features of the processes of phase formation in multilayer foils directly during their continuous heating, i.e. under conditions close to those realized in diffusion welding.

A not less important factor, which should be taken into account in selection of the interlayer and diffusion welding modes, is the mechanical behaviour of the interlayer materials at heating under the conditions of constant compressive forces, which are applied to the parts being welded. In this connection it is believed to be necessary to study the deformation behaviour of multilayer foils at their heating under the conditions of constantly applied stresses.

In this work the processes of phase formation and deformation behaviour under the conditions of constantly applied stresses were studied at continuous heating of multilayer Al/Cu foils.

Structural transformations in Al/Cu (84Al--16Cu) multilayer foils with 0.71 μm period of aluminium and copper layer alternation were studied. According to the constitutional diagram of Al--Cu system, 548.2 °C is the minimum temperature of (Al + $CuAl_2$) eutectic (Figure 1). Thus, the composition of multilayer foils after deposition corresponded to the eutectic with the minimum melting temperature for this system.

Al/Cu multilayer foils with a submicron layer thickness were produced by the method of layer-by-layer electron beam deposition of components on a substrate rotating at a constant speed. With this purpose, evaporation by electron beam guns was performed from two sources of aluminium and copper, separated by an impermeable screen [15]. Selection of a certain proportion of the intensity of aluminium and copper vapour flows, as well as the speed of substrate rotation allows widening the range of thick-

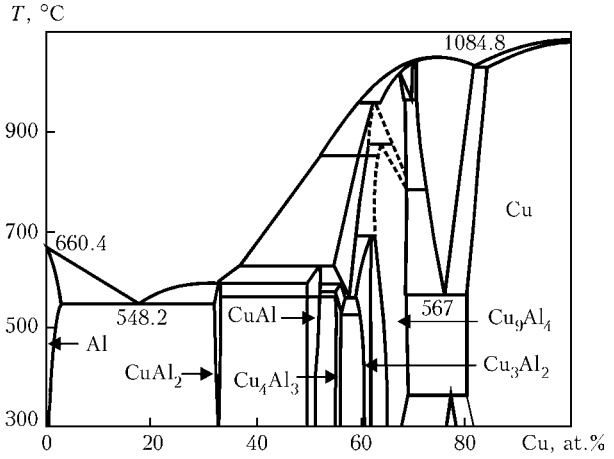

Figure 1. Al–Cu equilibrium phase diagram [14]

nesses (from 10 up to 100 μm) of Al/Cu multilayer foils with different thicknesses of copper and aluminium layers. In order to obtain self-standing condensates, a layer of NaCl salt was first deposited on the substrate, thus allowing easily separating the foil from the substrate later on. Chamber pressure was on the level of $5 \cdot 10^{-3}$ Pa. Evaporation intensity provided the deposition rate of 50 nm/s. Substrate temperature during deposition was equal to about 120 °C.

X-ray diffraction structural investigations of the foil directly after deposition and continuous heating were conducted in standard geometry θ–2θ in DRON-4 diffractometer in Co_{K_α} radiation. Deposited foil microstructure and their composition were studied by the methods of scanning electron microscopy. Condensate composition was controlled in scanning electron microscope CamScan-4 fitted with energy-dispersion spectrometer Energy200. Methods of selective chemical etching were used to reveal the foil structure.

Phase transformations in Al/Cu multilayer foils were studied by the method of high-temperature in situ X-ray diffractometry in cobalt anode radiation at the temperature of 20–520 °C and heating rate of about 20 °C/min, using UVD-2000 attachment in vacuum at the residual pressure of about $1 \cdot 10^{-2}$ Pa. Diffractograms were recorded using a bent linear position-sensitive detector (LPSD) of flow type operating with a xenon-methane gas mixture (Figure 2). LPSD aperture provided simultaneous recording of diffracted radiation in the angular range of up to 40°, radius of detector camera focusing was 200 mm, angular resolution was 0.03°. For determination of the recorded quantum coordinate, LPSD used a time schematic of position data decoding, allowing for the difference in time of the charge movement along the delay line from the acquisition point up to line load resistance.

Information on the coordinate of recording and intensity of diffracted radiation was transmitted through multichannel analyzer to computer input, where it was recorded simultaneously with the data on sample temperature, coming to computer input through analog-digital converter (ADC) directly from the thermocouple. Continuous heating of the sample was ensured using high-precision temperature regulator, which changes the heater power depending on the signal read from the thermocouple.

When studying the deformational behaviour of foils, a sample of Al/Cu microlaminate foil 20 mm long and 8 mm wide was placed into a measuring module, the schematic of which is shown in Figure 3. To determine the level of sample deformation, one end was attached to the platform, which was connected to the base of a stationary block through a stretched steel spring, and the other was connected to a stationary quartz rod, connected to stationary linear displacement sensor. An inductive sensor was used as the latter. Part of the measurement block, containing the sample, was placed between the heaters. In order to monitor the temperature, a thin thermocouple was connected to the foil. Heating was controlled through software, regulating the heater power,

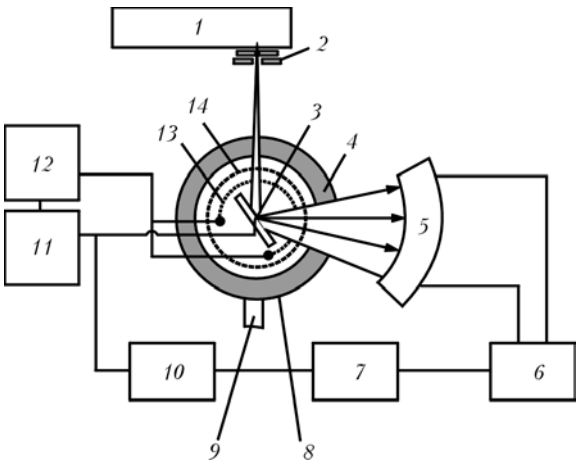

Figure 2. Block diagram of high-temperature diffractometer URVT using diffracted radiation for data recording: *1* ---- X-ray tube; *2* ---- vertical and horizontal slots; *3* ---- thermocouple; *4* ---- camera; *5* ---- LPSD; *6* ---- signal converter; *7* ---- multichannel analyzer; *8* ---- sample; *9* ---- diffusion pump outlet; *10* ---- computer; *11* ---- high-precision temperature regulator; *12* ---- heater power unit; *13* ---- heater; *14* ---- radiator for ensuring uniform heating of the sample

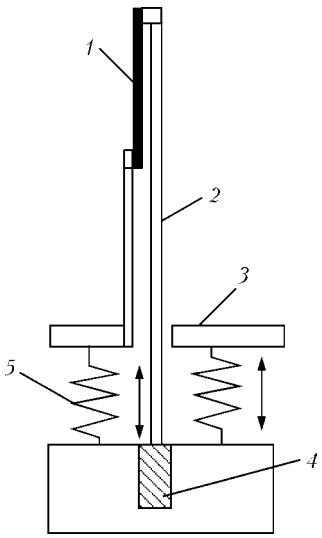

Figure 3. Schematic of the block for measurement of foil deformation under the impact of uniaxial load under the conditions of continuous heating: *1* ---- foil sample; *2, 3* ---- mobile and stationary block parts, respectively; *4* ---- inductive sensor mounted on a mobile platform; *5* ---- spring

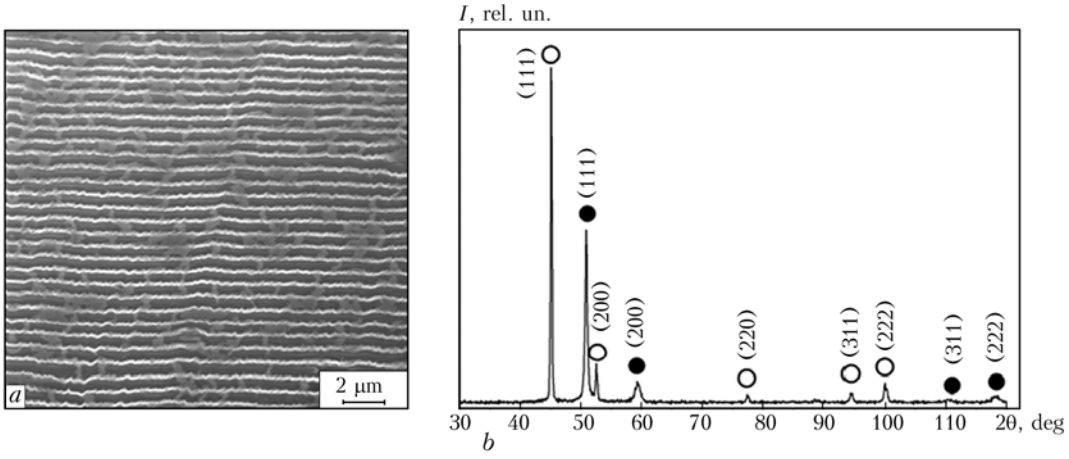

Figure 4. Cross-sectional microstructure of a sample of Al/Cu multilayer foils in the initial condition (*a*), and diffractogram produced after foil deposition (*b*): ● ---- copper phase; ❍ ---- aluminium phase; *I* ---- radiation intensity

depending on the signal read from the thermocouple fastened on the sample.

The essence of the method consisted in measurement of the change of foil length at heating or cooling under the conditions of a constant tensile load (springs providing a tensile load of about 10 N were used for this purpose). Measurement of sample length ΔL at a constant load depending on temperature was conducted using linear displacement sensors, which are connected to the computer through ADC. This allowed recording the data on the change of sample length ΔL and its temperature during heating or cooling. Temperature dependencies of sample deformation $\varepsilon = \Delta L / L_0$ and its change (rate) at heating or cooling $d\varepsilon / \Delta T = (1 / L_0) dL / dT$ in the entire temperature range were calculated, proceeding from the derived data on the change of sample length and initial L_0 values. Unit design and sensitivity of linear displacement sensor allow measuring material deformations with not more than 10 % relative error.

It is seen from Figure 4, *a* that the foil is made of continuous layers, differing by contrast: light layers correspond to copper, dark layers ---- to aluminium. Figure 4, *b* shows X-ray diffraction pattern of the deposited Al/Cu multilayer foil. Presence of only the peaks, corresponding to copper and aluminium in the X-ray diffraction pattern, leads to the conclusion that after deposition Al/Cu multilayer foil consisted of just the copper and aluminium layers.

Figure 5 gives the characteristic X-ray diffraction patterns for some temperatures in the range of angles $2\theta = 42$--$54°$, obtained at continuous heating of Al/Cu multilayer foil up to 520 °C. Such a range of angles was selected as the most representative with the most intensive peaks of aluminium, copper, and of those phases, which may form as a result of the reaction.

From Figure 5 (see curve *2*) it is seen that heating up to 80 °C of a sample of Al/Cu multilayer foils changes the diffraction pattern near the peak $(111)_{Cu}$ compared to the diffraction pattern at a lower heating temperature (Figure 5, curve *1*), identical to that obtained for foils in the initial condition. It is obvious that this is related to the fact that the solid-phase reaction between copper and aluminium runs already at this temperature. Subsequent increase of the heating temperature up to 130--180 °C (Figure 5, curves *3* and *4*), leads to increase of the intensity of the peaks from the formed phases near $(111)_{Cu}$ and enables identifying them as $CuAl_2$ and CuAl phases. Thus, proceeding from the change of the relative peak intensity, one can see that at the temperature of 130 °C the volume fraction of CuAl and $CuAl_2$ phases is greater than the volume fraction of copper, and at 180 °C the copper peaks disappear completely. At temperature increase up to 260 °C and higher (Figure 5, curve *5*) increase of volume fraction of $CuAl_2$ and decrease of volume fraction of CuAl phase is found. Since the diffractograms

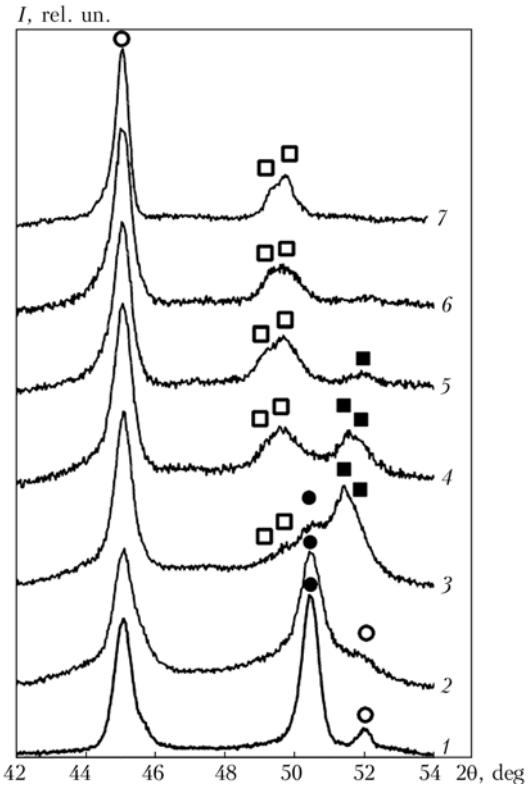

Figure 5. Characteristic fragments of diffractograms of samples of Cu/Al multilayer foils heated up to 40 (*1*), 80 (*2*), 130 (*3*), 180 (*4*), 260 (*5*), 360 (*6*) and 520 (*7*) °C, produced during continuous heating at the rate of 20 °C/min (phases identified in the samples are shown by symbols: ● ---- Cu; ❍ ---- Al; ❒ ---- $CuAl_2$; ■ ---- CuAl)

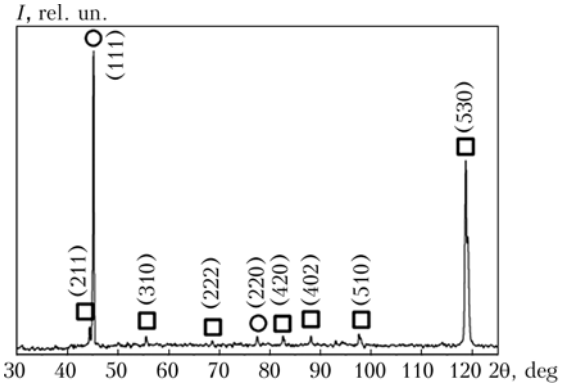

Figure 6. Characteristic fragments of diffractograms of samples of Al/Cu multilayer foils after continuous heating up to 520 °C at the rate of 20 °C/min: ○ ---- aluminium; ❐ ---- $CuAl_2$

have only the peaks of pure aluminium and $CuAl_2$ phase (Figure 5, curves *6* and *7*), and no formation of new phases is found at the temperature of 360 °C and higher, it may be assumed that this results in formation of a two-phase condition of (Al + $CuAl_2$) foil.

X-ray diffraction pattern of a sample of Cu/Al multilayer foils after continuous heating up to 520 °C is shown in Figure 6. It is seen that, indeed, heating results in a heterophase structure of the material, including pure aluminium and $CuAl_2$ phase. Such a structural condition of the foils for the component ratio specified at deposition corresponds to (Al + $CuAl_2$) eutectic with minimum melting temperature of 548.2 °C (see Figure 1).

Thus, at continuous heating up to 520 °C of Al/Cu multilayer foils of a composition close to the eutectic one, the sequence of phase transformations can be presented in the form of the following chain:

$$\text{Al + Cu} \xrightarrow{80\text{--}180\ ^\circ\text{C}} \text{Al + CuAl + CuAl}_2 + \text{Cu} \xrightarrow{80\text{--}180\ ^\circ\text{C}} \rightarrow \text{Al + CuAl + CuAl}_2 \xrightarrow{260\text{--}360\ ^\circ\text{C}} \text{Al + CuAl}_2. \quad (1)$$

It should be noted that the recorded in this work temperature of the start of solid-phase reactions (about 80 °C) is below the temperature of transformations observed for Al--Cu system, which was produced by deposition of a layer of copper and aluminium [7--9, 16] or rolling [17, 18]. Successive phase formation (first $CuAl_2$ phase, and at further increase of temperature or time of heating ---- AlCu and Al_9Cu_4 phases) was found only at heating from 150 up to 500 °C in samples of Al/Cu foils [7--9]. In Al--Cu system produced by rolling after long-term annealing at 250 °C after deposition [16] and at 450 °C [18] simultaneous formation of $CuAl_2$, AlCu and Al_9Cu_4 intermetallics on the layer interface took place. The difference between the temperature of the start of reactions and phase transformations and the published data can be related to the structural features (grain size equal to layer thickness, high defect concentration in the volume and on layer interfaces) of Al/Cu multilayer foils, produced by the method of electron beam deposition, which essentially affects the kinetic factors.

Results of investigation of deformation behaviour of foils at heating under the conditions of a constantly applied uniaxial tension are given in Figure 7. Analysis of these curves shows that temperature dependence of foil deformation can be conditionally divided into three sections: first (from 80 up to 250--260 °C) ---- monotonic increase of deformation occurs; second (from 250--260 up to 350--370 °C) ---- sample length first is somewhat reduced, and then it almost does not change; third (above 350--370 °C) ---- intensive plastic deformation at an increasing rate is found.

Comparison of the obtained data and results of radiographic studies of phase transformations in the foils at heating, leads to the conclusion that intensive plastic deformation of the foils in the first temperature section is chiefly due to the transformations

$$\text{Al + Cu} \rightarrow \text{CuAl + CuAl}_2. \quad (2)$$

At foil heating up to 250--260 °C these reactions are completed, which is due to exhaustion of copper, which results in practically no plastic deformation of the foil. More over, at further temperature rise the foil even shrinks slightly (here the deformation rate becomes negative).

As follows from the data of X-ray structural analysis, further temperature rise is accompanied by phase transformations of metastable (at a given ratio of components in the foil) CuAl phase into stable $CuAl_2$ phase through interaction of CuAl intermetallic with aluminium available in excess amounts:

$$\text{CuAl + Al} \rightarrow \text{CuAl}_2. \quad (3)$$

A slight deformation of the sample in this temperature range occurs chiefly due to foil elongation. This can be assessed by comparing the slopes of temperature curves of sample deformation in this section at heating and cooling. It can be seen from Figure 7 that dependence of sample deformation on temperature at cooling is somewhat greater than at heating. This gives rise to the assumption that reaction (3) runs with a negative bulk effect.

At the temperature above 350--370 °C (third section in the deformation curve) an increase of the sample plastic flow rate is observed. The deformation rate here rises and at the temperature above 450 °C it is similar to an exponential dependence. Considering that when this temperature has been achieved the phase transformations in the foil were over, and a two-phase state from pure aluminium and $CuAl_2$ phase has been formed, such deformation behaviour of the foil can only be related to the mechanical properties of this heterophase system. It is known that in such systems at elevated temperature plastic deformation is mainly determined by the processes of grain-boundary slipping [19, 20]. This is promoted by the heterophase state of the foil, which hampers running of recrystallization processes.

It is known that the compressive forces, which are applied to the joint zone, should provide an increase of the area of contact of the surfaces being joined, promote breaking up of oxide films in them and activate the diffusion mobility of atoms due to plastic

deformation of their surface layers [19]. This allows establishing the physical contact between the surfaces being joined, i.e. eliminates the barriers for the diffusion flows of atoms between the surfaces being joined. Solution of the defined problem is greatly facilitated, if the interlayer is exposed to plastic flow at stresses, which develop in the joint zone at application of external compressive forces.

The obtained data on mechanical behaviour of layered material at continuous heating under the conditions of constant loads showed that there exist two temperature intervals of its intensive plastic deformation. The first can be connected with the superplasticity of layered foil, due to running of solid-phase reactions between its components at heating, the second is related to structural superplasticity, due to deformation behaviour of the heterophase structure, formed during the process of running of the solid-phase reaction. It may be assumed that superplasticity of the multilayer foil will promote lowering of not only the temperature of the joint zone heating, but also the compressive forces required for it. In their totality the processes of both reaction diffusion and increased plasticity of layered materials at heating promote «softening» of the conditions of producing welded joints using such interlayers.

CONCLUSIONS

1. In the case of Al/Cu multilayer foils it is shown that at their continuous heating under the conditions of constantly applied stresses they undergo plastic deformation alongside the phase transformations.

2. It is established that plastic flow of Al/Cu multilayer foils (interlayers) runs in the most intensive manner in two temperature ranges. The first coincides with temperature interval of solid-phase reactions of synthesis of intermetallic compounds (80–240 °C), the second corresponds to plastic flow of the heterophase structure with dispersed components, formed as a result of solid-phase reactions at the temperature of about 450 °C, i.e. by 100 °C lower than the melting temperature of Al + $CuAl_2$ eutectics.

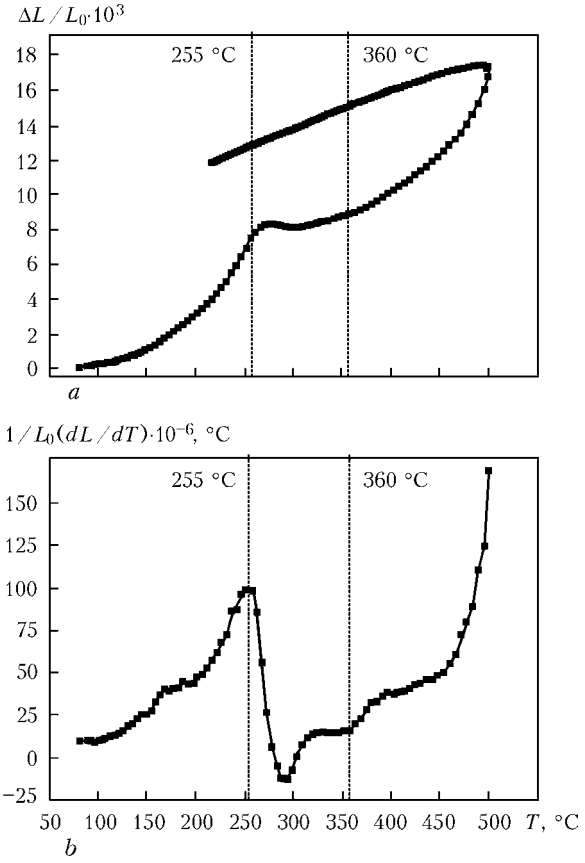

Figure 7. Dependence of deformation $\Delta L/L_0$ (*a*) and its rate $1/L_0(dL/dT)$ (*b*) on the temperature of heating at the rate of 50 °C/min of a sample of Al/Cu multilayer foils (84Al–16Cu) under the conditions of constant tensile stress

1. Cao, J., Feng, J.C., Li, Z.R. (2008) Microstructure and fracture properties of reaction-assisted diffusion bonding of TiAl intermetallic with Al/Ni multilayer foils. *J. Alloys and Compounds*, **466**, 363–367.
2. Ustinov, A.I., Falchenko, Yu.V., Ishchenko, A.Ya. (2008) Diffusion welding of γ-TiAl based alloys through nano-layered foil of Ti/Al system. *Intermetallics*, **16**, 1043–1045.
3. Ramos, A.S., Vieira, M.T., Duarte, L.I. et al. (2006) Nanometric multilayers: A new approach for joining TiAl. *Ibid.*, **14**, 1157–1162.
4. Pascal, C., Marin-Ayral, R.M., Te'denac, J.C. (2002) Joining of nickel monoaluminide to a superalloy substrate by high pressure self-propagating high-temperature synthesis. *J. Alloys and Compounds*, **337**, 221–225.
5. Ustinov, A., Olikhovska, L., Melnichenko, T. et al. (2008) Effect of overall composition on thermally induced solid-state transformations in thick EB PVD Al/Ni multilayers. *Surf. Coat. Techn.*, **202**, 3832–3838.
6. Ustinov, A., Olikhovskaya, L., Melnichenko, T. et al. (2008) Solid-phase reactions in heating of multilayer Al/Ti foils produced by electron beam deposition method. *Advances in Electrometallurgy*, **2**, 19–26.
7. Gershinski, A.E., Fomin, B.I., Cherepov, E.I. et al. (1977) Investigation of diffusion in the Cu–Al thin film system. *Thin Solid Films*, **42**, 269–275.
8. Hentzell, H.T.G., Thomson, R.D., Tu, K.N. (1983) Interdiffusion in copper-aluminium film bilayers. Pt 1: Structure and kinetics of sequential compound formation. *J. Appl. Phys.*, **54**, 6923–6928.
9. Hentzell, H.T.G., Thomson, R.D., Tu, K.N. (1983) Interdiffusion in copper-aluminium film bilayers. Pt 2: Analysis of marker motion during sequential compound formation. *Ibid.*, 6923–6928.
10. Ay, I., Celik, S., Celik, I. (1999) Comparison of properties of friction and diffusion welded joints made between the pure aluminium and copper bars. *BAU fen Bilimleri Enstitusu Dergisi*, **1**, 88–102.
11. Lee, W.-B., Bang, K.-S., Jung, S.-B. (2005) Effects of intermetallic compound on the electrical and mechanical properties of friction welded Cu/Al bimetallic joints during annealing. *J. Alloys and Compounds*, **390**, 212–219.
12. Ouyang, J., Yarrapareddy, E., Kovacevic, R. (2006) Microstructural evolution in the friction stir welded 6061 aluminum alloy (T6-temper condition) to copper. *J. Materials Proc. Techn.*, **172**, 110–122.
13. Abdollah-Zadeh, A., Saeid, T., Sazgari, B. (2008) Microstructural and mechanical properties of friction stir welded aluminum/copper lap joints. *J. Alloys and Compounds*, **460**, 535–538.
14. Massalski, T.B., Okamoto, H., Subramanian, P.R. et al. (1986) *Binary alloy phase diagrams*. Ohio: ASM Int., Materials Park.
15. Ishchenko, A.Ya., Falchenko, Yu.V., Ustinov, A.I. et al. (2007) Diffusion welding of finely-dispersed AMg5/27 % Al_2O_3 composite with application of nanolayered Ni/Al foil. *The Paton Welding J.*, **7**, 2–5.
16. Rajan, K., Wallach, E.R. (1980) A transmission electron microscopy study of intermetallic formation in aluminium-copper thin film couples. *J. Cryst. Growth*, **49**, 297–302.
17. Abbasi, M., Karimi Taherib, A., Salehia, M.T. (2001) Growth rate of intermetallic compounds in Al/Cu bimetal produced by cold roll welding process. *J. Alloys and Compounds*, **319**, 233–241.
18. Heness, G., Wuhrer, R., Yeung, W.Y. (2007) Interfacial strength development of roll-bonded aluminium/copper metal laminates. *Mater. Sci. and Eng. A*, **483/484**, 740–743.
19. Tikhonov, A.S. (1978) *Effect of superplasticity of metallic materials and alloys*. Moscow: Nauka.
20. Pshenichnyuk, A.I., Kajbyshev, O.A., Astanin, V.V. (1998) Model of superplasticity based on notion of cooperative grain-boundary sliding. *Math. Modelirovanie System i Protsessov*, **6**, 99–109.

LASER WELDING OF TITANIUM ALLOYS

B.E. PATON, V.D. SHELYAGIN, S.V. AKHONIN, V.F. TOPOLSKY, V.Yu. KHASKIN, I.K. PETRICHENKO, A.V. BERNATSKY, R.N. MISHCHENKO and **A.V. SIORA**
E.O. Paton Electric Welding Institute, NASU, Kiev, Ukraine

The optimal scheme of gas shielding was chosen for laser welding, allowing production of joints on alloys VT1-0, VT6, SP15, VT22, VT23 and T110. The possibility of using laser welding for low and medium alloys was established. It is shown that further improvement of the laser welding technology is required for high titanium alloys.

Keywords: *laser welding, titanium alloys, gas shielding, process parameters, butt joints, mechanical properties, stress corrosion resistance*

Titanium alloys are widely applied in aircraft and space engineering, ship building, chemical engineering, power generation and many other industries [1]. For example, stringer panels used in aircraft engineering are produced by slot welding of stiffeners to a one-piece panel. Critical long structures of sea-going vessels are manufactured by using titanium alloy welded T-beams. Addressing the above problems is hampered by a large size and small wall thickness of the parts welded. In this connection, thin-sheet structures from titanium alloys are usually made by using electron beam welding (EBW) [2]. However, this welding method is not always applicable for large-size structures because of the need to use vacuum chambers. Traditional arc welding methods often have low productivity and may lead to formation of substantial distortions and buckling of welded structures [3]. Laser welding allows producing narrow welds with a small HAZ using no sophisticated vacuum chambers at a speed that is 2–3 times (or more) higher than that of arc welding [4].

The first attempts to utilise the laser beam for welding titanium alloys were made in the early 1970s, in particular, at the E.O. Paton Electric Welding Institute [5]. It was found out that the process requires reliable shielding with an inert gas because of an active chemical interaction of molten metal of the weld pool with an environment. As follows from [5], the use of helium instead of argon to shield the pool metal allows the penetration depth to be increased by more than 50 %.

The first efforts to commercially apply the laser welding technology for fabrication of titanium parts were made at the beginning of the 1980s. In this respect we have to note the studies by the I.V. Kurchatov Institute of Atomic Energy. The technology for laser welding of a special titanium alloy heat-exchanging module was applied in 1983 at the Company «Baltijsky Zavod». There the laser was used to weld tubes with a wall thickness of up to 2.5 mm into a tube plate [6]. As reported in study [7], the laser beam can also be used for welding titanium parts.

The purpose of this study was to optimise the process of laser welding, based on the criteria of mechanical characteristics of welded joints on titanium alloys, by selecting the welding speed at a focused power of the laser beam. To achieve this purpose, a system was developed for gas shielding of the weld pool and that portion of its tailing part where metal had a temperature above 200 °C, as it is at this temperature that the upper layer of the weld metal and base metal may be saturated with air nitrogen [1]. Commercial titanium VT1-0, medium alloy VT6 stabilised with β-additions, and high alloys SP15, VT22, VT23 and T110 with thickness $b = 5.0$–7.5 mm were chosen as sample materials. Chemical compositions of these alloys are given in Table 1.

Butt joints between plates measuring $300 \times 50 \times b$ mm were welded in the course of the experiments by using the Nd:YAG laser DY 044 («Rofin Sinar», Germany) with a power of up to 4.4 kW and objective

Table 1. Chemical composition (wt. %) of base metal of samples welded

Material	Al	Mo	V	Fe	Cr	Nb	Zr	O_2	N_2	H_2
VT1-0	0.40	–	–	0.15	–	–	–	0.10	0.035	0.008
VT6	6.35	–	4.20	–	–	–	–	0.15	0.050	0.012
SP15	4.50	3.18	3.30	–	–	4.22	1.9	0.16	0.028	0.002
VT22	6.00	4.80	5.10	1.00	1.0	–	–	0.18	0.050	0.015
VT23	4.50	2.00	4.50	0.60	1.0	–	–	0.17	0.004	0.018
T110	4.90	0.90	1.25	1.61	–	4.74	0.5	0.13	0.040	0.002

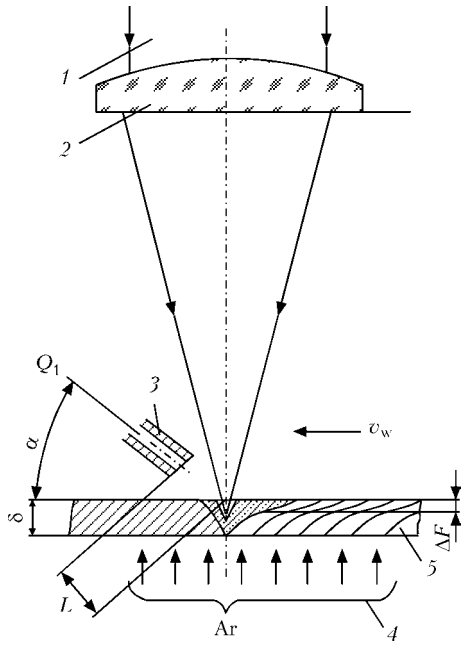

Figure 1. Scheme of laser welding with a shielding gas fed ahead of the welding head: *1* ---- laser beam; *2* ---- focusing objective; *3* ---- nozzle for shielding gas feeding; *4* ---- weld root shielding; *5* ---- sample; Q_1 ---- shielding gas flow rate; v_w ---- welding speed; ΔF ---- focus deepening

with focal distance F = 300 mm, which was part of the welding head. Radiation from the laser to the objective was transmitted via an optical fibre 600 μm in diameter. The welding head with the shielding system was moved during the welding process. In all the cases the lower (root) part of the weld was shielded with argon, the flow rate of which was 7 l/min. It was fed via a tube located in a clamping device. The upper part of the weld (molten pool and its tailing part) was protected with the welding head nozzle.

A series of preliminary experiments was carried out to optimize design of the protective nozzle and

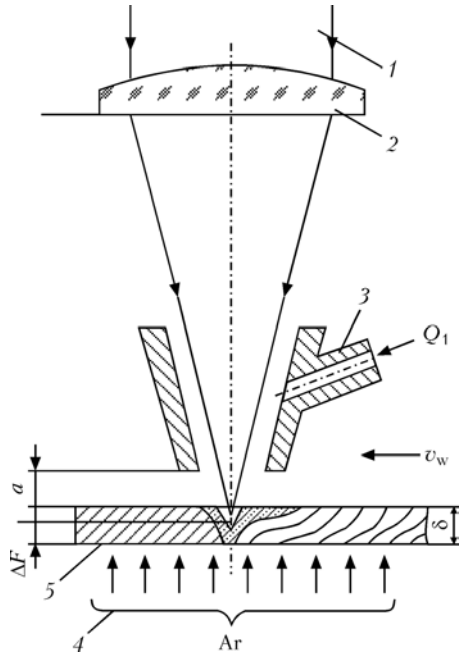

Figure 2. Scheme of laser welding with coaxial shielding gas feeding (see Figure 1 for designations *1–5* here and in Figure 3)

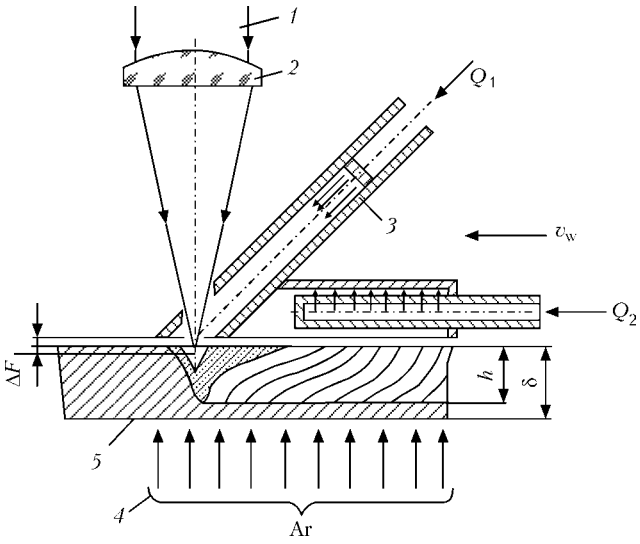

Figure 3. Scheme of laser welding with differentiated shielding of the weld pool and cooling metal by laminar gas flows

select the type of a shielding gas. The early experiments were conducted by using the laser welding scheme shown in Figure 1. It was established that feeding the shielding gas (argon or helium) ahead of the welding head leads to inflow of air to the welding zone, which is intolerable. Then the scheme shown in Figure 2 was tried out. A coaxial gas (argon or helium) feed provided sufficient reliability of shielding of the welding zone. However, this caused a considerable decrease (by up to 50 %) in metal penetration depth, compared with penetrations achieved in welding by the scheme shown in Figure 1. Moreover, it turned out that the welding scheme shown in Figure 2 failed to provide shielding of cooling metal from the surrounding air. As a result, a thin (about 0.1–0.3 mm) surface layer of the weld metal was saturated with nitrogen to form titanium nitride of a goldish colour.

The system for differential feed of laminar gas flows to shield the weld pool and cooling metal of its tailing part from air was developed to eliminate drawbacks of gas shielding of both schemes (Figure 3). The new welding scheme allowed avoidance of disadvantages of the two previous schemes. As found in the course of investigation of its technological capabilities, the use of argon for shielding the weld pool leads to partial screening of the laser beam by a plasma plume forming over the pool, this causing a substantial decrease in the penetration depth. The use of helium allows avoiding this effect. In this connection, the welding scheme shown in Figure 3 was used for further experiments. In this case, helium was used as a shielding gas for the weld pool (flow rate Q_1 = 7 l/min), and argon was used to shield the cooling metal (flow rate Q_2 = 12 l/min). The optimal welding parameters

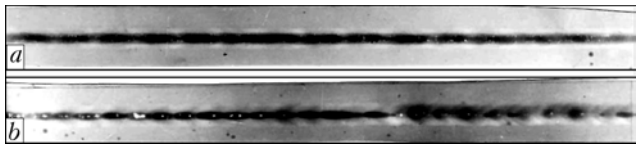

Figure 4. X-ray patterns of laser welded joints on alloy VT6 made under optimal (*a*) and non-optimal (*b*) conditions

Table 2. Laser welding parameters

Material	b, mm	P, kW	v_w, m/h	ΔF, mm
VT1-0	5.0	4.1	48	2.0
VT6	7.5	4.3	36	2.0
SP15	6.5	4.0	42	2.0
VT22	6.5	4.2	30	2.0
VT23	6.0	4.0	42	1.0
T110	7.0	4.0	42	2.0

(Table 2) were chosen by a criterion of through penetration of metal and formation of a narrow (0.5--1.0 mm) weld root (beam power P = 4.0--4.3 kW).

All the samples after welding were subjected to X-ray inspection, which showed that the weld metal resulting from using the optimal scheme and optimal parameters had only isolated pores (Figure 4, *a*). Deviation from the optimal welding technology led to formation of a continuous chain of pores along the weld axis (Figure 4, *b*).

The content of gas impurities was investigated in the laser weld metal (Table 3). As shown by gas analysis, the use of helium and argon as a shielding atmosphere provides the content of oxygen, nitrogen and hydrogen in the weld metal at a level of that in the base metal in compliance with requirements of GOST 19807--91 and ASTM, and for T110 ---- in compliance with TUU 27.4.05416923.071--2005.

To relieve residual welding stresses and stabilise structure, the samples were annealed at a temperature of 650--950 °C (depending upon the alloy grade). Welded joints were subjected to mechanical tensile and impact bend tests in as-welded condition and after annealing. The mechanical test results are given in Table 4.

High values of mechanical properties, meeting specification requirements, were exhibited by the laser welded joints on commercial titanium VT1-0 and alloy

Table 3. Content (wt.%) of gas impurities in laser welds

Material	O_2	N_2	H_2
VT1-0	0.12 / 0.13	0.040 / 0.041	0.012 / 0.011
VT6	0.15 / 0.10	0.050 / 0.045	0.013 / 0.011
VT22	0.18 / 0.17	0.050 / 0.050	0.014 / 0.012
VT23	0.17 / 0.20	0.045 / 0.050	0.017 / 0.016
SP15	0.14 / 0.13	0.043 / 0.041	0.016 / 0.015
T110	0.15 / 0.12	0.060 / 0.045	0.013 / 0.013

Note. Numerator gives the content of gas impurities in the weld, and denominator ---- in HAZ.

Table 4. Mechanical properties of laser welded joints on titanium alloys

Material	Welded joint			Base metal	
	σ_t, MPa	KCV, J/cm^2		σ_t, MPa	KCV, J/cm^2
		Weld	HAZ		
VT1-0	460 / 440	140 / 150	130 / 145	460	150
VT6	1010 / 980	30 / 35	34 / 38	980	45
SP15	1040 / 1030	12 / 19	18 / 30	1030	43
VT23	1050 / 1020	8 / 16	9 / 21	1050	31
T110	1080 / 1050	12 / 13	19 / 20	1100	38
VT22	1070 / 1040	8 / 9	11 / 12	1050	30

Note. Numerator gives data for as-welded condition, and denominator ---- after annealing.

VT6. The β-phase stability coefficient for alloy VT6 was 0.3. The welded joints on alloys with a β-phase stability coefficient equal to 0.6 or higher (SP15, VT23, T110 and VT22) showed high sensitivity to the thermal cycle of laser welding. Both in as-welded condition and after annealing, the weld and HAZ metals on these alloys had a fine structure, which provided strength of the welded joints equal to that of the base metal. However, the level of impact toughness of the weld and HAZ metals on high titanium alloys was unsatisfactory both in as-welded condition and after annealing.

Whereas the weld and HAZ metals of laser welded joints on VT1-0 and VT6 are characterised by a coarse-acicular structure (Figure 5, *a*), the similar zones of welded joints on high alloys have a very fine intragranular structure (Figure 5, *b, c*). These structural differences are one of the causes of a substantial decrease in impact toughness of high alloys, compared with commercial titanium VT1-0 and alloy VT6, in which a crack propagates on a wavy path. The path of propagation of cracks in high alloys with a fine

Table 5. Mechanical properties of welded joints on titanium alloy VT6 made by different welding methods

Welding method	σ_t, MPa	KCV, J/cm^2		Fracture location
		Weld	HAZ	
AAW	940	33	34	Weld
EBW	970	34	31	HAZ
Laser welding	980	35	36	Same

Note. Mechanical properties of base metal: σ_t = 998 MPa; $\sigma_{0.2}$ = = 970 MPa; δ = 12 %; ψ = 24 %; KCV = 42 J/cm^2.

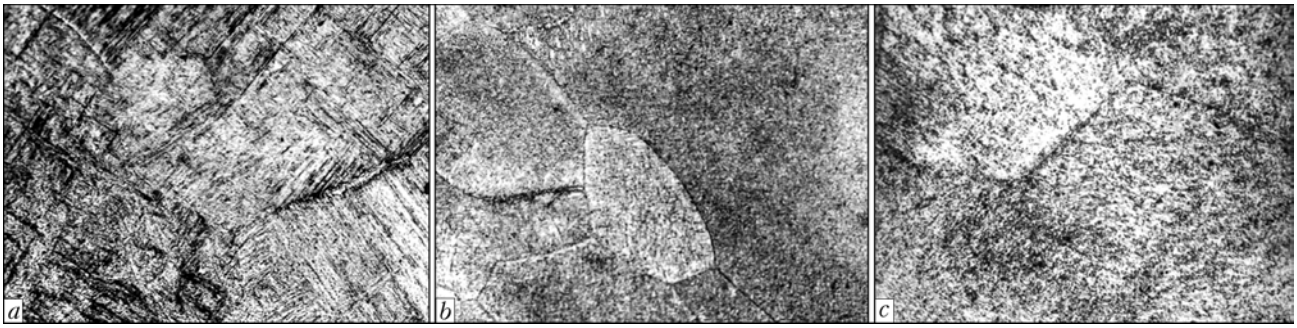

Figure 5. Microstructure of weld metal of laser welded joints on titanium alloys: *a* ---- VT6 (×200); *b* ---- VT23 (×400); *c* ---- T110 (×400)

structure is close to linear, this requiring less energy than in a case of VT1-0 and VT6 [8].

It seems expedient to conduct studies for further improvement of the technology for laser welding of high titanium alloys and finding of optimal parameters for heat treatment of laser welded joints to improve their ductile characteristics.

Of high interest was to compare results of investigations of the VT6 joints made by laser and other welding methods. For this, the laser welded joints on alloy VT6 were studied in parallel with the joints on the same alloy made by argon-arc (AAW) and electron beam (EBW) welding [9, 10].

The butt joints between plates were welded by using the EBW machine UL-144 (power unit ELA 60/60) and commercial equipment for tungsten-electrode AAW of titanium. Flux of the ANT-25A grade was used in the latter case. Helium and argon were used as shielding gases for laser welding, and argon ---- for AAW. In all the cases the welds were made in one pass without groove preparation and without filler wire. Despite the fact that heat input in laser welding was 1.3–2 times lower (2.43 kJ/cm) than in EBW (3.11 kJ/cm) and AAW (4.77 kJ/cm), strength properties of the welded joints differed but very slightly, and were close to those of the base metal (Table 5). Impact toughness of the weld and HAZ metals was 70–80 % of *KCV* of the base metal, which in all the cases met requirements of specifications and technological instructions for titanium alloy VT6. Sensitivity of alloy VT6 and its welded joints to stress corrosion cracking was evaluated in methyl alcohol solution with 0.4 % addition of hydrochloric acid. The tests were conducted at room temperature for 790 h. Each batch consisted of 5 specimens. One of them (reference), No. 1 in each batch (Table 6), was tested in air, and others were tested in an aggressive environment. According to the standard, if all specimens of a batch were in a stress corrosive environment for 100 h and did not crack, an alloy or a welded joint should be considered resistant to stress corrosion cracking. Results of corrosion tests of the joints on alloy VT6 are given in Table 6. Analysis of the results shows that joints on alloy VT6 made by different welding methods using the optimised technologies differ in resistance to stress corrosion cracking.

Table 6. Sensitivity of welded joints on alloy VT6 to stress corrosion cracking

Welding method	Sample No.	Time to formation of corrosion crack, h	Total test time, h	Fracture location
Base metal	1	N/D	790 (air)	No fracture
	2	Same	790	
	3	»	790	
	4	»	790	
	5	»	790	
AAW	1	N/D	790 (air)	Same
	2	107	107	Weld
	3	N/D	790	No fracture
	4	264	264	HAZ
	5	N/D	790	No fracture
EBW	1	Same	790 (air)	Same
	2	»	790	
	3	330	330	HAZ
	4	350	350	
	5	N/D	790	No fracture
Laser welding	1	Same	790 (air)	Same
	2	»	790	
	3	»	790	
	4	504	504	
	5	N/D	790	

CONCLUSIONS

1. Optimal schemes of shielding of the weld metal and composition of a shielding atmosphere for laser welding of titanium alloys, and optimal parameters of laser welding for commercial titanium VT1-0 and alloy VT6 were chosen. It was established that helium should be used to shield the weld metal, and argon ---- to shield the weld root and cooling regions of the base metal in laser welding of commercial titanium VT1-0 and alloy VT6.

2. Strength of laser welded joints on alloy VT6 is at a level of that of the base metal, and impact toughness of the weld and HAZ metals is 70 % of *KCV* of the base metal.

3. The VT6 welded joints made by the improved technologies of AAW over the flux layer, EBW and laser welding meet specification requirements and are resistant to stress corrosion cracking, although their corrosion resistance is inferior to that of the base metal.

4. Further improvement of the laser welding technology and optimisation of parameters of heat treatment of the welded joints on high titanium alloys are required.

The authors are grateful to Dr. S.G. Polyakov and associates of his Department for their consultations and efforts in investigation of stress corrosion resistance of welded joints on titanium alloy VT6.

1. Gurevich, S.M., Zamkov, V.N., Blashchuk, V.E. et al. (1986) *Metallurgy and technology of welding of titanium and its alloys*. Kiev: Naukova Dumka.
2. Nazarenko, O.K., Kajdalov, A.A., Kovbasenko, S.N. et al. (1987) *Electron beam welding*. Ed. by B.E. Paton. Kiev: Naukova Dumka.
3. (1974) *Technology of electric fusion welding of metals and alloys*. Ed. by B.E. Paton. Moscow: Mashinostroenie.
4. Grigoriants, A.G., Shiganov, I.N. (1988) *Laser equipment and technology*: Manual for institutes of higher education. Book 5: Laser welding of metals. Ed. by A.G. Grigoriants. Moscow: Vysshaya Shkola.
5. Velichko, O.A., Garashchuk, V.P., Molchan, I.V. et al. (1974) Laser welds on steel and titanium. *Avtomatich. Svarka*, **10**, 19–21.
6. Zhurov, N.V., Milrud, S.R. (1983) Some technological peculiarities of laser welding of pipe joints. In: *Proc. of Workshop on Application of High Energy Density Sources in Welding Production* (Leningrad, 20–21 Dec. 1983). Leningrad: LDNTP.
7. Zamkov, V.N., Prilutsky, V.P., Novikov, Yu.K. (1993) Achievements in the field of welding technology of titanium. *Avtomatich. Svarka*, **5**, 25–27.
8. Borisova, E.A., Bochvar, G.A., Brun, M.Ya. et al. (1980) *Titanium alloys. Metallography of titanium alloys*. Moscow: Metallurgiya.
9. Zamkov, V.N., Prilutsky, V.P. (1980) Technological capabilities of argon-arc welding of titanium over the flux layer. In: *Proc. of 1st All-Union Conf. on Current Problems of Welding of Non-Ferrous Metals* (Kiev, 21–23 Nov. 1978). Kiev: Naukova Dumka.
10. Zamkov, V.N., Prilutsky, V.P., Petrichenko, I.K. et al. (2001) Effect of the method of fusion welding on properties of welded joints in alloy Ti–6Al–4V. *The Paton Welding J.*, **4**, 2–6.

TIG WELDING OF THICK TITANIUM PLATES BY USING FORMING BACKING

V.Yu. BELOUS
E.O. Paton Electric Welding Institute, NASU, Kiev, Ukraine

The method of fit-up for narrow-gap TIG welding of 20–100 mm thick titanium plates was developed, providing a high quality of welded joints and substantial reduction of cost of the welding process. Fit-up of plates for welding is performed by using a forming backing, which acts as a mould when making the root pass. The use of backings makes it possible to simplify edge preparation and fit-up of the welded joints, and decrease welding deformations.

Keywords: *arc welding, narrow gap, titanium, tungsten electrode, forming backing, control magnetic field*

Narrow-gap welding is a cost-effective and efficient method for joining thick metal. The most important factors in welding of titanium and titanium-base alloys are reduction of consumption of filler wire, inert gas and other welding consumables, and decrease of labour content in preparation of edges of workpieces for welding. Tungsten-electrode narrow-gap welding (NGW) is a known method for welding titanium [1]. The key advantages of this method are small width of the resulting weld, small amount of the deposited metal and simple shape of the weld edges. This technology provides for fit-up of workpieces for welding by using a permanent backing, which is manually welded to a reverse side of a workpiece [1]. This backing acts as a lower wall of the groove when making the first pass. There are cases where the backing should be made from the same titanium alloy as the base metal. Further on the welded permanent backing performs no functions, but its presence hampers the reliable shielding of workpieces from oxidation by air when depositing the next layer. As a rule, the welded backing should be removed after welding. Moreover, an important drawback of this method for fit-up of workpieces for NGW of titanium alloys is that defects are left on the surface after removal of the backing. To remove these defects, it is necessary to partially remove metal from the mating surfaces of the weldments to a depth of 1.0–1.5 mm.

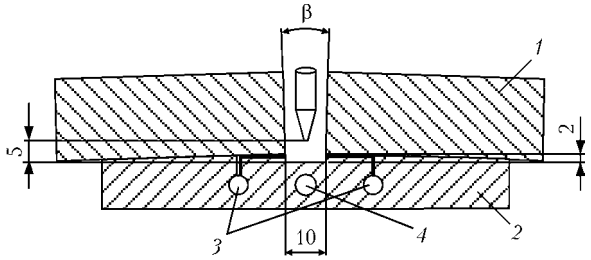

Figure 1. Scheme of fit-up of plates for welding: *1* — plates to be welded; *2* — forming backing; *3, 4* — holes for feed of shielding gas and flow of cooling water, respectively

Known in the art is the method for NGW of titanium by using the U-shaped groove [2]. With this method the root pass is made without a filler wire and without a permanent backing. However, this rules out such an advantage of the NGW process as a simple

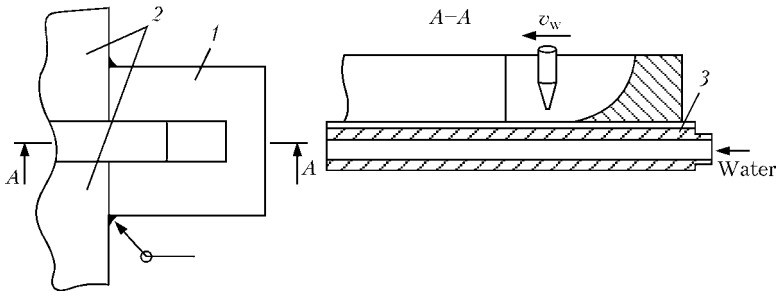

Figure 2. Schematic of welding by using runoff tab: *1* ---- runoff tab; *2* ---- plates to be welded; *3* ---- forming backing

shape of the weld edges. Moreover, in this case the root pass should be made under special conditions, other than those used to make subsequent (filling) passes. At the same time, it is reported [3] that for protection of reverse sides of the welds and adjoining heated regions of the welded joints from oxidation, the process of welding of titanium can be performed by using removable copper backings that comprise forming grooves and a system of holes to feed the inert gas. Also reported [4] is the use of water-cooled straps to decrease welding deformations.

Investigations were carried out to develop the technology for NGW of titanium and titanium alloys using no permanent backings. For practical application of NGW, the technology should provide for making root passes on a special removable forming backing. Along with shielding of a welded joint, such a backing should act as a mould to form the bead of the root pass.

Copper backing of the offered design (Figure 1) has a forming groove and is fitted with water cooling. Cooling makes it possible to maintain stability of thermal conditions when making the entire pass and decrease the HAZ width. The forming backing provides protection of the weld pool, tungsten electrode, molten metal and reverse side of a workpiece from contact with air.

The investigations showed that to make the quality second pass the deposited metal of the first one, i.e. root pass, should meet the following requirements: it should have the concave shape of the surface, and the reverse side of the weld should have no undercuts or lacks of fusion. In addition, after making the root pass, the gap between the side walls of the groove should be not less than 10 mm wide.

Experiments were conducted with welding of 40 mm thick plates of commercial titanium, 30 mm thick plates of titanium alloy PT3V, and 20 mm thick plates of titanium alloy VT23. Welding was performed by feeding a 5 mm diameter tungsten electrode of the EVI-2 grade into the so-called free gap, i.e. without rigid restraining of the workpieces, thus causing reduction of width of the gap during welding due to transverse shrinkage of the weld metal. To decrease the transverse shrinkage, the use was made of a special design of the П-shaped runoff tabs (Figure 2) made from alloy VT1-0 and having thickness equal to that of the base metal, which were welded to the plates welded. The beginning and end of welding were done on the runoff tabs. The welding arc was ignited between the tungsten electrode and the forming backing, and filler wire was fed after ignition of the arc. The arc voltage automatically maintained during welding with the ARND system was 12 V, and welding current was 400–450 A. The rate of the shielding gas flowing via the forming backing was insignificant, i.e. 4–10 l/min.

As shown by the investigations, the offered design of the forming backing provided quality shielding of the welding zone and cooling welded joint. The surface of the reverse bead was shiny, without temper colours.

The content of residual impurity gases, such as oxygen, nitrogen and hydrogen, in weld metal of the root pass made on the forming backing was determined to assess the quality of shielding of the welding zone and this weld metal. Results of the investigations showed that the gas content of the weld metal was at a level of the base metal (Table) and met requirements for the maximum permissible concentration of interstitial impurities in commercial titanium.

To develop the technology for making the root pass, it was necessary to investigate the process of formation of welds on titanium in NGW by using a copper water-cooled forming backing. The investigations showed that in welding by using the forming

Content of impurities (gases) in metal, wt.%

Analysis object	O	N	H
Base metal VT1-0	0.07	0.024	0.0020
Filler wire VT1-00sv	0.06	0.016	0.0023
Root weld metal	0.06	0.020	0.0022

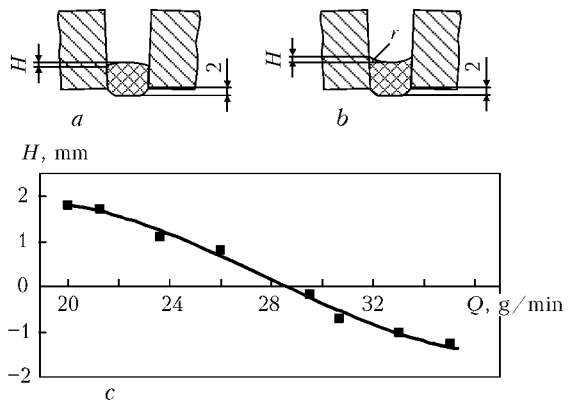

Figure 3. Schematic of formation of the first pass in feed of a specific amount of filler metal equal to less than 30 (*a*) and more than 30 g/min (*b*), and dependence of height of weld reinforcement *H* upon specific amount *Q* of filler metal (*c*)

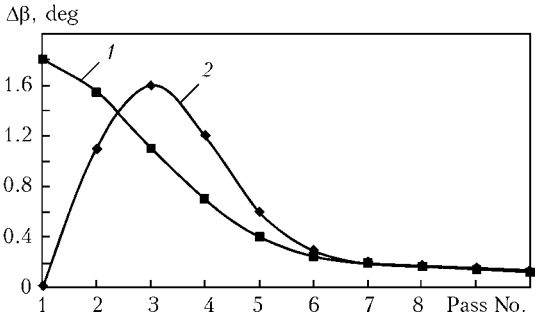

Figure 4. Angular deformation of butt welded joint versus pass number in NGW with the magnetically controlled arc by using permanent (*1*) and forming (*2*) backing

backing it is necessary to control heat input into the vertical opposite walls being welded. Magnetic control of the welding arc was used to provide the dosed heat input [5]. Redistribution of the thermal energy of the arc was achieved due to alternating forced deviations of the arc to the opposite side walls under the effect of the external control magnetic field with a value of the transverse component of magnetic induction equal to 8–12 mT.

The investigations showed that NGW by using the copper water-cooled backing was accompanied by an intensive heat removal from the welding zone. The sound bead of the root pass with a concave surface was formed in the presence of a substantial amount of molten metal, i.e. at a specific feed of filler metal to the welding zone equal to over 30 g/min (Figure 3). At a lower specific feed of the filler metal the formed bead had a convex shape, thus causing lacks of fusion in the groove corners when making the next pass.

Peculiarity of the offered welding method is that angular deformations after the first pass are insignificant (<0.1°). In NGW by using a permanent backing, the angular deformations after making the first pass are maximal and equal to 1.8° (Figure 4). In NGW by using a forming backing the maximal angular deformation of a welded joint is fixed after the third pass, and total value of the angular deformations after welding by using the forming backing is lower than in welding by using the permanent backing. Welded joints made by the developed technology are characterised by small width of HAZ (Figure 5) and uniform melting of the base metal through its thickness.

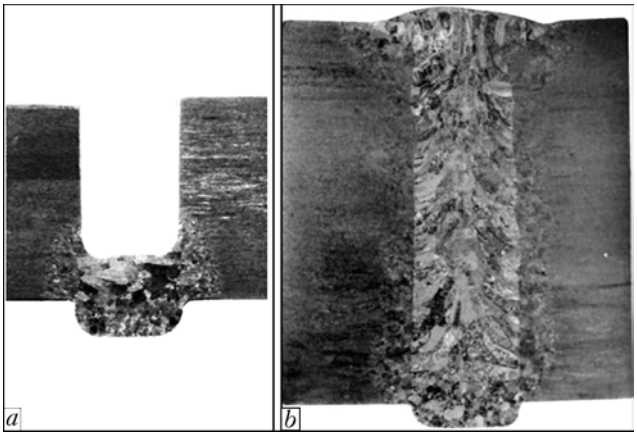

Figure 5. Macrosection of the root pass (*a*) and welded joint on commercial titanium VT1-0 40 mm thick (*b*)

CONCLUSIONS

1. The technology for fit-up and narrow-gap welding of titanium alloy plates by using a forming backing is offered. Compared with the traditional scheme of fit-up (with a permanent backing), the developed technology enabled to avoid the need to remove the welded backing after welding.

2. The use of the water-cooled forming backing makes it possible to avoid machining of reverse sides of the weldments.

3. In welding by using the water-cooled forming backing, there are practically no angular deformations after making the root pass, and total value of the angular deformations after welding is lower than in welding with a permanent backing.

1. Paton, B.E., Zamkov, V.N., Prilutsky, V.P. (1996) Narrow-groove welding proves its worth on thick titanium. *Welding J.*, **4**, 37–41.
2. Matsui, S., Nakayama, S., Sakurai, T. (1988) *Application of narrow gap GTA welding to various products*. Osaka: JWS, 127–134.
3. Gurevich, S.M., Zamkov, V.N., Blashchuk, V.E. et al. (1986) *Metallurgy and technology of welding titanium and its alloys*. Kiev: Naukova Dumka.
4. Kasatkin, B.S., Prokhorenko, V.M., Chertov, I.M. (1987) *Stresses and strains in welding*. Kiev: Vyshcha Shkola.
5. Belous, V.Yu., Akhonin, S.V. (2007) Influence of controlling magnetic field parameters on weld formation in narrow-gap argon-arc welding of titanium alloys. *The Paton Welding J.*, **4**, 2–5.

BIMETAL STEEL-ALUMINIUM JOINTS IN SHIPBUILDING HULL STRUCTURES

A.S. ORYSHCHENKO, E.P. OSOKIN, V.I. PAVLOVA and **S.A. ZYKOV**
Federal State Unitary Enterprise «Central R&D Institute of Structural Materials «Prometej», St.-Petersburg, Russian Federation

The results of works on development of welded steel-aluminium hull structures with application of a bimetal based on shipbuilding steel of D40 type and aluminium alloy of grade 1561 are given. Examples of new engineering solutions on technological design of steel-aluminium joints are shown.

Keywords: *arc welding, steel-aluminium structures, bimetal transition pieces, welded joints, technological design, mechanical properties*

The analysis of development of domestic and foreign shipbuilding showed that to manufacture marine and river vessels the aluminium alloys along with the steel become ever more applicable which provide reduction of total weight of ships, reduction of gravity centre, and also other advantages such as lightness, non-magnetization, corrosion resistance and sufficiently high strength. Both hull structures and superstructures, deckhouses, bridges, chimney casings, partitions, enclosures, etc. are manufactured of aluminium alloys.

The joints of aluminium and steel elements can be riveted and welded. The riveted joints are extremely labour-intensive and not sufficiently reliable and durable judging from the experience of ship service.

The most applicable welding method in the manufacture of steel-aluminium structures is fusion welding for producing the bimetal aluminium-steel joints.

In the foreign shipbuilding and ship repair a bimetal material is used based on low-alloyed steel and aluminium-manganese alloy of 36--40 mm thickness, produced using explosion welding. In particular, such material is used at the «Sumitomo» shipyards (Japan), in the countries of former Yugoslavia, Poland, and also in military shipbuilding of the USA, Great Britain, France and other countries.

In Russia till the end of the last century, when there were no domestic shipbuilding bimetal, the welded joints of steel-aluminium shipbuilding structures were produced using bimetal based on stainless austenite steel 10Kh18N10T and aluminium alloy AMg6 of thickness of 10--12 mm, mastered in the production by OJSC VILS for the demands of aircraft industry [1]. The application of this bimetal in shipbuilding was limited as a rule by minor and low-loaded structures, not participating in providing the total strength of the ship hull, and, therefore, there were no high requirements to technology of fusion welding the bimetal joints, applied at shipbuilding plants, and it was not subjected to improvement during many years. The most popular type of steel-aluminium joint is a variant where steel layer of bimetal was welded overlapped by fillet welds to the steel deck, and sheet structures of aluminium alloys were welded to the aluminium layer of bimetal using T-joints (Figure 1).

When welding the steel layer of bimetal by fillet welds to the deck, which is performed in flat position, the necessary conditions are the inadmissibility of formation of defects on bimetal edges in the form of delamination, fusion of aluminium layer or mixing of molten volumes of dissimilar metals. Judging from practical experience, the performance of mentioned requirement under real conditions of welding of shipbuilding structures is extremely complicated which results in formation of defects mentioned above, which are the potential source of corrosion damages causing the fracture of steel-aluminium joint.

Figure 2 shows the appearance of characteristic fragment of welded joint of aluminium wall of superstructure with aluminium layer of bimetal (alloy 1560--steel 10Kh1810T), and Figure 3 presents the sketch of this joint after the effect of sea environment during service.

As the results of inspection of shipbuilding structures of light superstructures with a deck show, such fractures of welded steel-aluminium joints occur at the decreased corrosion resistance in sea environment of aluminium alloy 1560 (AMg6), especially in its combination with high-alloyed steel due to the formation of essential difference of electrode potentials and result in necessity of full substitution of bimetal joints.

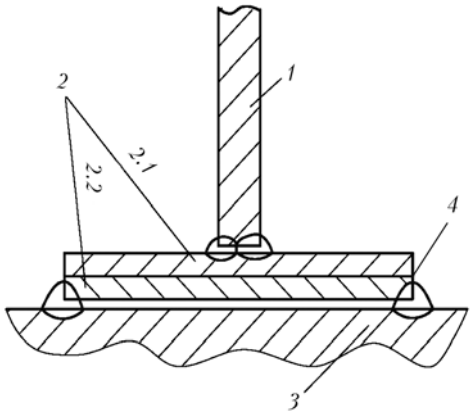

Figure 1. Scheme of performance of joints of aluminium structure with steel one produced using a transition bimetal element: *1* ---- aluminium alloy 1561; *2* ---- bimetal (*2.1* ---- aluminium alloy of 1560 grade, *2.2* ---- austenite chrome-nickel steel 10Kh18N10T); *3* ---- ship hull low-alloyed steel of D40 type; *4* ---- possible source of delamination

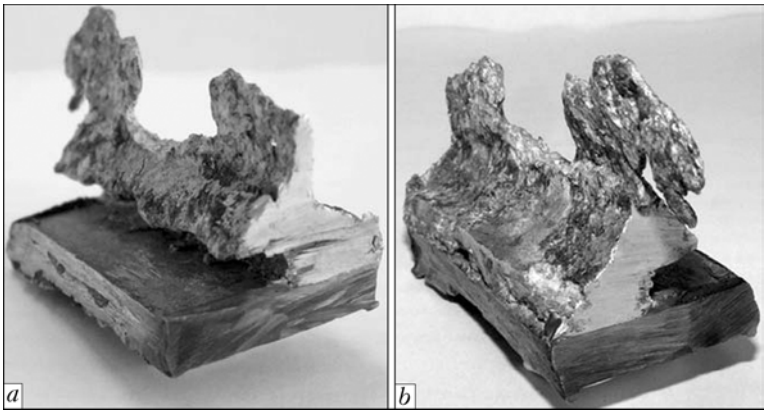

Figure 2. Appearance of fragment of bimetal joint on the side of the surface being in contact with sea environment (*a*), and on the opposite (inner) side (*b*)

The existing methods of fusion welding of structures of steel and aluminium alloys with application of bimetal transition pieces along with the overlapped ones foresee the performance of T- (cruciform) assemblies (Figure 4). The joints are produced using welding of steel and aluminium elements with appropriate layers of bimetal in T-joint position by fillet welds.

The analysis of damages at the fatigue tests of T-joints of large-sized steel-aluminium structure showed that the most weak places are the butt welds of bimetal transition pieces (Figure 5).

The fatigue cracks under the conditions of pure bending in bimetal butt joint, performed using earlier existing technology, were initiated already at 10,000 loading cycles which was a result of lack of penetration in the central part of the bimetal weld.

It is evident from above-mentioned that existing technical level of welding production of steel-aluminium joints and composition of bimetal transition pieces required design and technological improvements to provide quality, reliability, corrosion resistance and operational strength of loaded shipbuilding structures [2].

Development of new shipbuilding bimetal material. To increase reliability and service life of welded bimetal assemblies in the composition of ship hull structures of surface vessels with the developed aluminium multi-tiers superstructure, the complex of works was performed by our Institute on the creation of new shipbuilding bimetal and development of new design and technological solutions connected with making welded steel-aluminium joints.

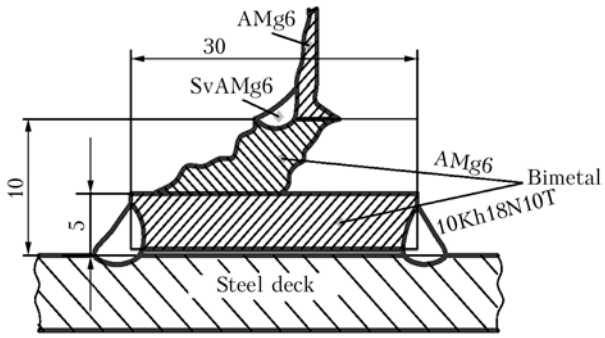

Figure 3. Sketch of welded bimetal joint after the effect of sea environment

In the CR&DI of Structural Materials «Prometej» the shipbuilding bimetal on the base of low-alloyed steel D40 and aluminium alloy 1561 was developed where commercially pure aluminium (alloy AD1) is used as a technological interlayer [3], that allows obtaining of reliable adhesion of aluminium with steel and the high level of strength and manufacturability of bimetal (Figure 6).

To produce bimetal the method of joint rolling of steel and aluminium billets with a single-component deformation of heated aluminium alloy is used. In the process of rolling the steel layer is not almost deformed.

The main difficulties in producing the quality composite material is its considerable difference in deformation resistance of steel and aluminium layer during rolling, high tendency of low-alloyed carbon steel to oxidation during heating impeding the formation of steel-aluminium joint, and also the possibility of formation of brittle intermetallic compounds at the interface of bimetal layers.

The technology of producing the steel-aluminium bimetallic material using the method of combined hot rolling with a single-component deformation of aluminium layer is consisted in the following. After cleaning of contact surfaces of a billet of aluminium alloy it is subjected to heating in electric furnaces up to the

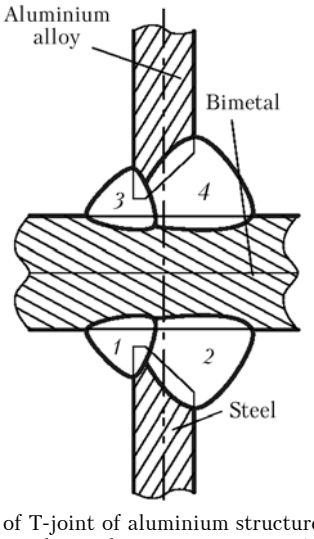

Figure 4. Scheme of T-joint of aluminium structure with the steel one produced using a bimetal transition pieces: *1–4* ---- passes in weld making

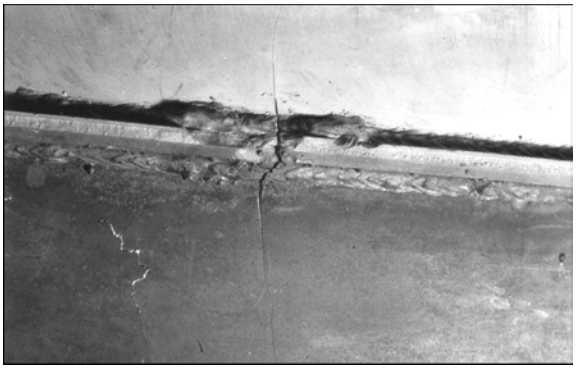

Figure 5. Type of damage of butt bimetal weld at fatigue tests of large-sized steel-aluminium structure

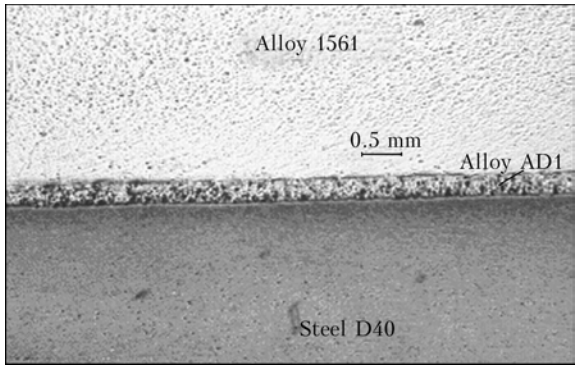

Figure 6. Macrostructure (×10) of laminated composite material of steel D40--AD1 and 1561 alloys

temperature of 430--480 °C. The heated aluminium billets are overlapped on the cleaned cold steel strips, and assembled package is set to the mill rolls, the gap between them is adjusted equal to the final thickness of bimetal. The rolling of the package is performed for one pass with 50--80 % reduction. At such level of deformation of aluminium alloy the reliable adhesion of joined metals is provided. The thickness of a billet of aluminium alloy is accepted from the conditions of providing a single-component deformation, gripping of metal by the rolls, power capabilities of rolling equipment and necessary level of deformation for reliable adhesion.

The developed shipbuilding bimetal on the base of aluminium alloy 1561 and low-alloyed steel D40 is produced in the form of strips of conventional production of KBM-1T grade (aluminium alloy is located along the entire surface of steel layer) and coaming production of KBM-1K grade (aluminium alloy is located in the form of a strip 'of width of not less than 55 mm along the edge on the surface of steel layer).

The thickness of bimetal part is equal to 100--130 mm, 8--12 mm (4--5 mm is steel layer, 4--7 mm is aluminium alloy layer), length is (1800 ± 200) mm, width of strips of KBM-1T is (165 ± 10) mm. Coaming bimetal (bimetal transition piece with a projected steel layer) represents an almost ready structural element with optimal ratio of thickness of steel and aluminium layers depending on the thickness of steel coaming and wall of aluminium superstructure. The produced bimetal was approved by Russian Maritime Register of Shipping. The adhesion strength of steel and aluminium bimetal layers is 100 MPa; the shear strength is not less than 55 MPa.

The industrial manufacturing of bimetal KBM-1 is mastered in the industrial equipment of «Prometej» and examined by Russian Maritime Register of Shipping.

Weldability of shipbuilding bimetal on the base of low-alloyed steel and aluminium alloy. It is known that during heating above the critical temperatures, intermediate intermetallic precipitates are formed at the boundary of contact of aluminium with steel, the composition, shape and sizes of which are defined by chemical composition of initial components and temperature-time conditions of their interaction. Depending on these factors different diffusion processes can occur near the contact of laminated composition, such as a self-diffusion of elements, atomic heterodiffusion and reactive diffusion with formation of new phases. The result of diffusive interaction is closely connected with strength properties of the composition.

The adhesion strength of layers of different metals with a different character of physical-mechanical interaction under the conditions of effect of plastic deformation depends greatly on the processes of mass transfer and formation of chemical compounds and also on clustering the structural defects at the near-boundary zone.

The experimental studies [4] showed that adhesion strength of layers of steel-aluminium joint after heating in solid state above 500--250 °C (depending on temperature and durability of interaction under the conditions of welding heating) can considerably decrease in result of interphase interaction of components and formation at the interface of intermetallic compounds of variable composition of the type AlmFen, solid interlayer of which results in sharp decrease of strength at reaching the critical thickness (Figure 7).

The obtained experimental results were used as a basis in the development of a rational technological process of fusion welding of bimetal materials on the base of low-alloyed steel and aluminium-magnesium alloy as applied to the shipbuilding hull structures.

Design-technological variants of welding of bimetal joints. The increase of service properties of welded bimetal joints, their reliability, life, and also decrease of labour intensiveness of manufacturing are closely connected with improvement of design solutions of steel-aluminium assemblies and technology of their performance. The improvement of assemblies of steel-aluminium joints became possible with the application of a transition piece in a coaming performance. In this case the projected steel bimetal layer

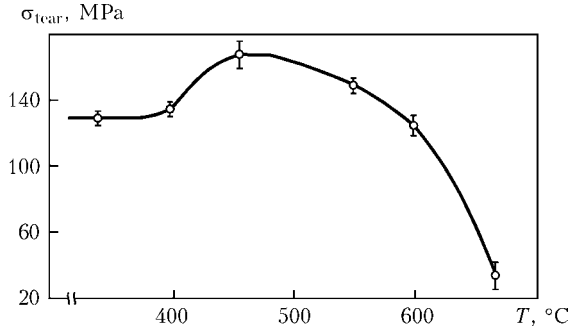

Figure 7. Dependence of tearing strength σ_{tear} of bimetal layers on heating temperature

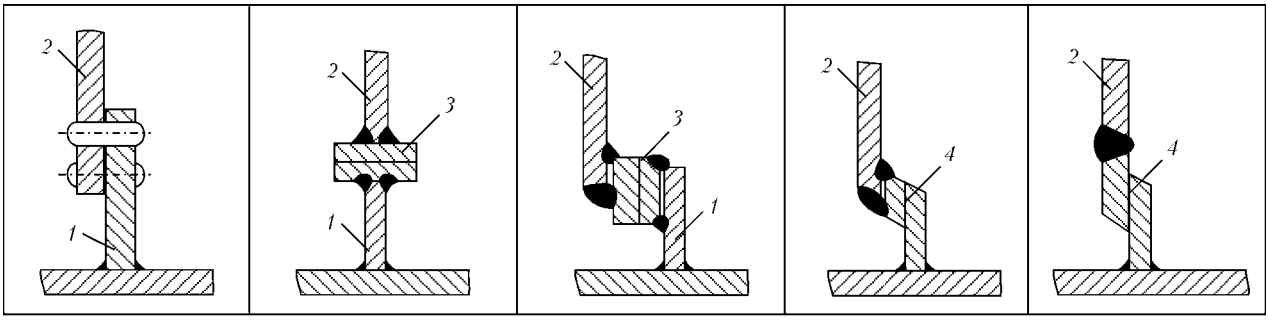

Figure 8. Variants of typical assemblies of joining of aluminium superstructures with steel ship hull: *I* ---- riveted assemblies; *II–V* ---- welded assemblies with application of bimetal (*II* ---- T-; *III, IV* ---- overlapped; *V* ---- butt); *1* ---- steel coaming; *2* ---- aluminium superstructure; *3* ---- conventional bimetal; *4* ---- coaming bimetal

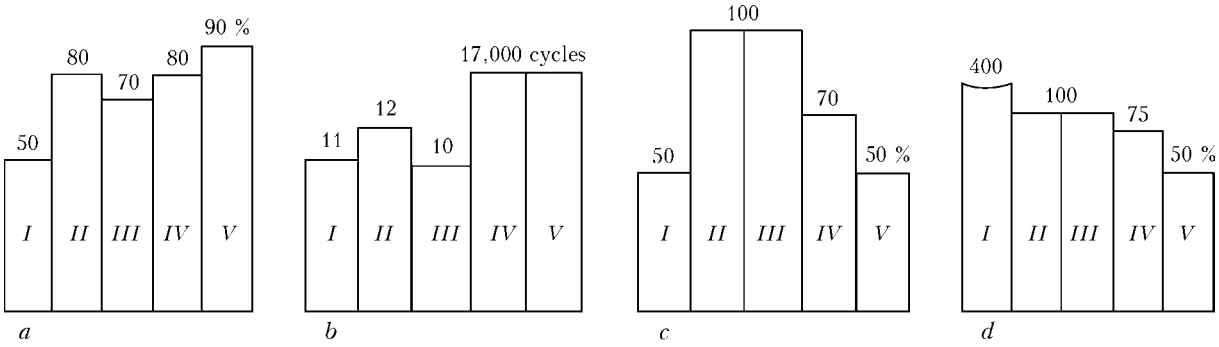

Figure 9. Comparative technical-economical characteristics of typical welded steel-aluminium assemblies: *a* ---- relative static strength $\sigma_{st}^{w.j}/\sigma_t^{Al}$; *b* ---- fatigue strength ($\sigma_{max} = 0{,}5\sigma_{st}^{Al}$; $\rho = 0.3$; $\nu = 0.1$ Hz); *c* ---- relative metal consumption per 1 run. m; *d* ---- relative labour intensiveness of manufacture per 1 run. m; *I–V* ---- the same as in Figure 8

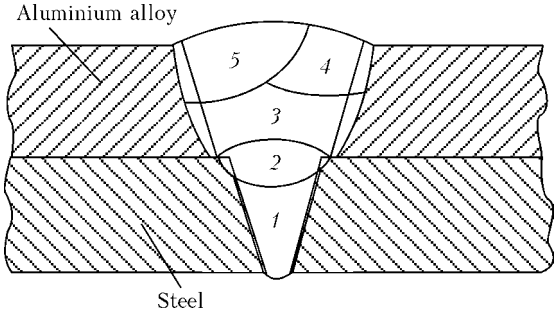

Figure 10. Scheme of filling the groove being welded of bimetallic butt joint: *1, 2* and *3–5* ---- passes in making, respectively, steel and aluminium weld

performing the role of a coaming, is joined directly to a steel hull and aluminium bimetal layer is joined to the aluminium wall of superstructure using overlapped or butt joints. The variants of typical assemblies of joints of aluminium superstructures with steel hull of the ship are shown in Figure 8.

The comparative technical characteristics of considered welded bimetallic assemblies (Figure 9) show that application of bimetal in a coaming performance allows realization of high values of static and fatigue strength at the lowest values of metal consumption in steel-aluminium joints and labour intensiveness of their manufacturing.

To solve the problem of increase of fatigue strength of welded long-sized bimetal transition pieces the welding technology and design of butt bimetal joint with complete penetration of each layer eliminating inner lack of penetration and, consequently, stress concentrators (Figure 10) were developed to increase their labour capacity to a maximum level, limited by the life of welded aluminium assemblies [5].

The fatigue strength of bimetal butt joints with V-groove edge preparation (the coefficient of cycle asymmetry $\rho = P_{min}/P_{max} = 0.33$, where P_{min}, P_{max} is, respectively, the minimum and maximum loading; loading frequency $\nu = 10$ Hz on the base of $2 \cdot 10^6$ loading cycle is not less than 100 MPa).

Thus, on the basis of new technological solutions and design of steel-aluminium joints the technology of welding of butt, T- and overlapped joints using bimetal was developed which allowed us to manufacture of reliable shipbuilding structures, to increase fatigue strength of steel-aluminium assemblies by 15–20 %, to eliminate the use of deficit austenite welding consumables, to provide tightness of bimetal butt joints and corrosion resistance of steel-aluminium joints on the level of requirements specified to the ship hull materials.

The developed bimetal aluminium-steel joints are used to manufacture steel-aluminium structures as transition elements in joining of steel deck and superstructures of aluminium alloys at the stages of designing, manufacturing, repair and modernization of surface vessels of different purpose and small displacement (yachts, cutters, boats, fishing trawlers).

1. Ryabov, V.R. (1975) *Application of bimetallic and armor steel-aluminium joints*. Moscow: Metallurgiya.
2. Nikitin, V.A., Kalnin, V.I., Shcheblykin, V.G. (1991) Investigation of strength of hull structure welded assembly units made with bimetallic strips. *Sudostroenie*, **3**, 43–47.
3. *Method of production of bimetals*. Pat. 2061073 RF. Int. Cl. 6 C 22 F 1/00, B 32 B 15/18. Publ. 27.05.96.
4. Pavlova, V.I. (1998) Investigation of processes of interaction between steel and aluminium and their adhesion strength in lamellar material under action of welding thermal cycle. *Voprosy Materialovedeniya*, 15(**2**), 12–29.
5. *Method of fusion welding of bimetal butt joints on the base of layers from aluminium alloys and steel or titanium with one- and double-sided welds*. Pat. 2284252 RF. Int. Cl. B 23 K 9/23, B 23 K 33/00, B 23 K 103/16. Publ. 27.09.2006.

DEFORMATION CRITERION OF THE EFFICIENCY OF STRENGTHENING OF WELDED JOINTS BY HIGH-FREQUENCY MECHANICAL PEENING

V.A. DEGTYARYOV[1], **B.S. SHULGINOV**[1] and **V.V. KNYSH**[2]
[1]G.S. Pisarenko Institute for Problems of Strength, NASU, Kiev, Ukraine
[2]E.O. Paton Electric Welding Institute, NASU, Kiev, Ukraine

The paper gives the results of fatigue testing of butt welded joints after high-frequency mechanical peening, allowing for different preparation technologies. It is shown that measuring the depth of the peened zone groove is one of the objective methods for assessment of the efficiency of treatment of the welded joints.

Keywords: *arc welding, specimen preparation, welded joint, high-frequency mechanical peening, groove depth, residual stresses, fatigue curve, fatigue limit, service life*

The need to increase strength and reduce probability of failure of machines and structures promoted the development of a big number of methods for strengthening of welded joints [1, 2], such as weld dressing, argon-arc treatment, explosion treatment, vibration treatment, etc., the main goal of which is an increase in their fatigue strength. Some treatment methods are aimed at reduction of stress concentration [3], and others ---- reduction of residual tensile stresses [4]. However, complexity of prediction of cyclic fatigue life of structures due to the influence of different structural and technological factors requires development of the new methods for increasing strength of the welded joints. High-frequency mechanical peening (HFMP) along weld to base metal fusion line [5], which is characterized by a high efficiency of strengthening of different types of the welded joints, as well as low labor intensiveness, has been gaining an increasingly wider acceptance in the last decade. This treatment method has been thoroughly studied. The positive effect of using this method is achieved due to reduction of stress concentration in the weld to base metal transition zone, strain hardening of surface metal layers and inducing of residual compressive stresses in the stress raiser zone.

The topical problem now is control of the quality of peening, the efficiency of which depends in many respects on the chosen tools and speeds of treatment of the structures operating under the cyclic loading conditions.

In study [6], for example, the optimal travel speed of a work tool was evaluated from formation of maximal residual stresses in the surface layer of a workpiece at a treatment speed of 0.3–0.5 m/min.

In the investigations carried out by the E.O. Paton Electric Welding Institute, the efficiency of HFMP is evaluated by measuring hardness of the bottom of a peened layer [7]. It was determined that the maximum value of specified hardness can be achieved in four passes at a peening speed of 0.5 m/min, i.e. at HFMP speed v = 0.125 m/min, which is determined as a ratio of the length of a peened weld to the time of peening. The efficiency of HFMP at the specified speed was proved by comparative fatigue tests of different types of the welded joints conducted under the loading asymmetry conditions [8, 9]. Study [10] suggests using the 0.3–0.5 m/min treatment speed with visual inspection of the treatment quality. In this case, the up to 0.5 mm deep groove providing removal of sharp undercuts is formed in quality HFMP.

At present, HFMP is performed manually by means of a special tool. The low-quality treatment may not provide the expected effect, as everything depends on the experience of operating the tool and proper choice of the peening speed.

The aim of the investigations lies in finding a simple and reliable criterion for evaluation of the efficiency of HFMP, particularly, at a stage of service of welded structures.

In this study the effect of HFMP was evaluated by the results of fatigue tests of the butt joints on low-carbon steel St3sp (killed) at a zero-to-compression harmonic loading cycle under bending conditions, by using the DSO-2 testing machine [11]. Test specimens were made from the 14 mm thick steel plates measuring 40 × 400 mm. Treatment of the weld to base metal fusion zone was performed at the E.O. Paton Electric Welding Institute by using the USP-300 ultrasonic piezoelectric tool [12] with an oscillation frequency of 22 kHz, waveguide tip oscillation amplitude of 19 μm and consumed power of 0.3 kW. The deformation tool was a special head with four built-in aligned steel rods 3 mm in diameter. A groove 3.0–3.5 mm wide with variable depth h, depending on the treatment time, i.e. speed of travel of the tool along the weld, is formed in HFMP if the tool is moved along the weld to base metal fusion line. The results of testing the specimens at external load stress σ_{max} = 375 MPa showed that their fatigue life increased with increase in the groove depth (Figure 1). Besides, there is a satisfactory correlation between the depth and fatigue life. Starting from depth h = 0.14 mm produced at a treatment speed of 0.065 m/min, no

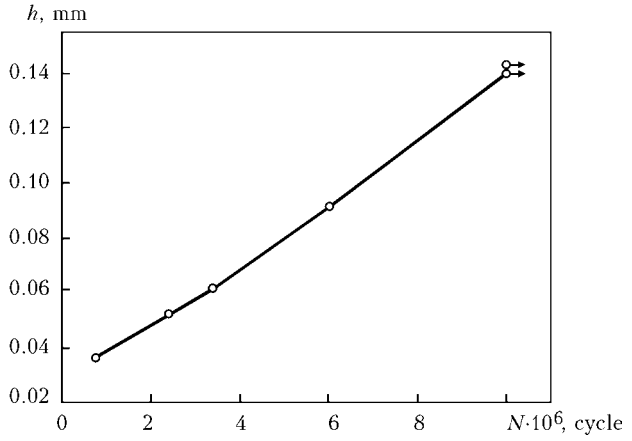

Figure 1. Dependence of fatigue life of St3sp steel specimen with a butt weld on groove depth in peened zone

fatigue cracks were formed in the welded specimens tested at N = 10 million cycles. Therefore, it can be concluded from the investigation results that, based on the fatigue life criterion, the optimal mode of treatment of the St3sp steel butt joints is that providing the groove not less than 0.14 mm deep. As reported in studies [7, 10], quality strengthening by HFMP does not lead to repeated strain hardening of metal at groove depth h = 0.2–0.5 mm. These data, however, are of a reference character and cannot serve as a basis to select an evaluation criterion for increasing strength of a welded joint.

Comparative tests of three series of specimens were carried out to evaluate the efficiency of HFMP, allowing for different technologies used for specimen preparation and skills in using a tool.

Specimens of the first series were not subjected to HFMP, i.e. the specimens were in as-welded state. The tests were conducted on several specimens at a time, mostly at four stress levels. If the fatigue crack reached a length of 10 mm, a specimen was considered to be fractured. The specimen test results (light circles) processed by the least-squares method, are shown in Figure 2 (curve *1*). Here the fatigue limit was 200 MPa.

Specimens of the second series were made from a welded plate 1000 mm long and 400 mm wide, comprising the preliminarily peened weld. HFMP of the

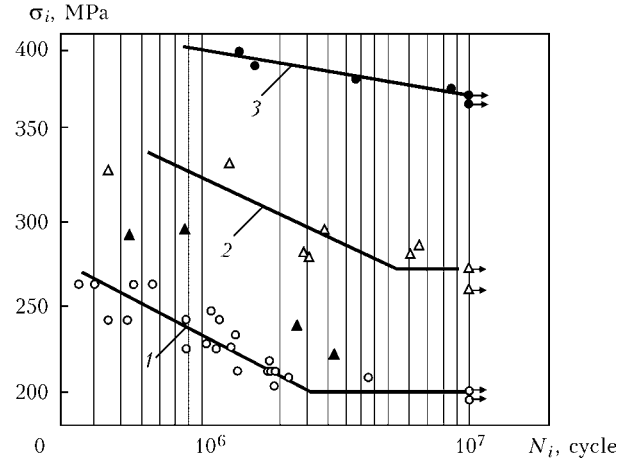

Figure 2. Fatigue curves for the first (*1*), second (*2*) and third (*3*) series of St3sp steel butt welded joint specimens

weld was deliberately entrusted to an untrained operator, having no experience in operation of the tool. This was done in order to check how HFMP of welded joints performed by an unskilled operator could influence the fatigue life of structures under cyclic loading. After the treatment the plate was cut into specimens of preset sizes (40 × 400 mm). The results of testing of such specimens are shown in Figure 2 by light and dark triangles. As seen from the Figure, the values of the fatigue life are characterized by a substantial scatter. It was determined by visual examination that the peened zone of some specimens of the second series contained the unsmoothed marks left from the strikers. Metal rolls were also detected. Photos of the fracture zones were made to analyze the causes of scatter of the test results. It can be seen from these photos that in some specimens the fatigue crack propagated along the peened bottom (Figure 3) to the end and center of a specimen. The crack initiated at a 5–7 mm distance from the specimen end. The tests were stopped after crack escaped to the specimen end. Analysis of the tests results for such specimens (light triangles), processed by the least-squares method (see curve *2* in Figure 2), showed that HFMP increased their fatigue limit by 36 %. Configuration of the groove was non-smooth, and characteristic metal rolls (collars) (Figure 4) formed as a result of low-quality peening of the weld to base metal fusion line were detected in some specimens. In this case, the fatigue crack started propagating not on the peened bottom, but from the collars acting as sources of stresses concentration. It can be seen from Figure 2 that the fatigue life of welded specimens with such defects is 3–4 times shorter (dark triangles). As a result, the fatigue limit increased by 11 %. The results obtained are indicative of the fact that deviation from the optimal treatment modes and insufficient skill of an operator may lead to deterioration of the quality of peening and, hence, to a substantial decrease in the efficiency of peening.

Specimens of the third series differed from those of the second series in a preparation sequence. A welded plate was preliminarily cut into specimens. Then each specimen was treated at a speed of 0.065 m/min by keeping to all HFMP technology specification requirements. The amplitude of oscillation of the work tool waveguide tip was 19 μm. This sequence of preparation of specimens allowed inducing and maintaining the residual compressive stresses. Measured depth of the peened zone groove varied from 0.14 to 0.16 mm, and its width was approximately 3.0–3.5 mm The tests results are shown in Figure 2 (curve *3*, dark circles). After this treatment the fatigue limit of the welded specimens amounted to 375 MPa, which was 87 % higher than that of the same specimens in the initial state. Peculiarity of the tests is that the fatigue cracks in specimens of the first and the second series initiated at a distance of 5–7 mm from the end of a specimen and propagated simultaneously to its end and center, whereas in specimens

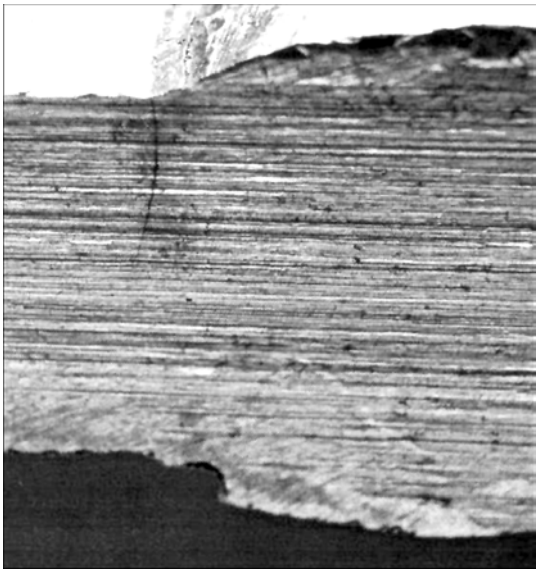

Figure 3. Side view of a specimen with fatigue crack

of the third series the fatigue cracks initiated at the same distance from the end of the specimen and propagated always to its end. In specimens of the first series the fatigue cracks also initiated at the center. This confirms the earlier obtained experimental data [7] that after HFMP the residual compressive stresses in the weld zone increase in a direction to the specimen center, and that their values considerably decrease at the specimen ends. Apparently, the compressive stress diagram is similar in specimens of the third series. This explains the observed regularity of the fatigue crack propagation. The difference between fatigue limits of the second and third series specimens can be explained, firstly, by the quality of peening and, secondly, by the specimen preparation sequence: cutting of the plate into specimens in the first case was done after peening, which resulted in relaxation of the residual compressive stresses.

As shown by the test results, the speed of HFMP cannot serve as a satisfactory criterion of the quality of treatment. Moreover, it is very difficult to control it under industrial conditions. As the groove is formed after HFMP of a welded joint, depending on the speed of travel of the work tool along the weld, it can be assumed that its depth, together with a measured value of hardness on the groove bottom, rather than the treatment speed, could serve as a more objective criterion of the efficiency of HFMP of welded structures at a stage of their running or fabrication.

CONCLUSIONS

1. Service life of a welded joint strengthened by the HFMP technology depends on the depth of the groove formed in the peened zone. Therefore, one of the objective criterions for evaluation of the efficiency of strengthening of the welded joints by the HFMP technology (if it cannot be evaluated with the help of direct fatigue tests) is measurement of the groove depth.

2. Fatigue limit of the St3sp steel butt welded joints after HFMP at a recommended speed of

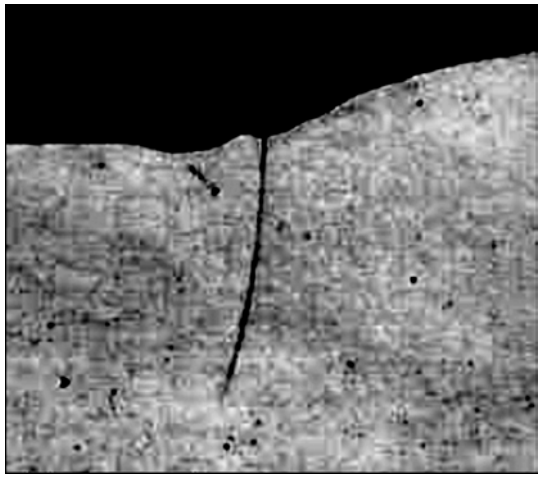

Figure 4. Side view of a specimen with fatigue crack formed in metal roll zone as a result of deviation from the weld peening technology

0.065 m/min with formation of the 0.14–0.16 mm deep groove in the peened zone increases by 87 %. Violation of the treatment technology may significantly reduce its efficiency for the welded joints operating under bending conditions, where maximal stresses act on the surface in a zone of location of characteristic metal rolls along the groove end. In test specimens this led to no more than 11 % increase in fatigue limit of the welded joints.

3. The efficiency of increase in fatigue resistance the welded joints depends both on the chosen HFMP mode and on the skills of an operator performing treatment of the joint. In this connection, HFMP of the welded joints should be performed by specially trained operators.

1. Trufyakov, V.I. (1973) *Fatigue of welded joints*. Kiev: Naukova Dumka.
2. Asnis, A.E., Ivashchenko, G.A. (1978) *Increase of strength of welded structures*. Kiev: Naukova Dumka.
3. Lobanov, L.M., Kirian, V.I., Knysh, V.V. (2006) Increase of service life of welded metal structures by high frequency mechanical peening. *Fizyko-Khim. Mekhanika Materialiv*, **1**, 56–61.
4. Polotsky, I.G., Nedoseka, A.Ya., Prokopenko, G.I. et al. (1974) Decrease of residual welded stresses by ultrasonic treatment. *Avtomatich. Svarka*, **5**, 74–75.
5. Lobanov, L.M., Kirian, V.I., Knysh, V.V. et al. (2006) Improvement of fatigue resistance of welded joints in metal structures by high-frequency mechanical peening (Review). *The Paton Welding J.*, **9**, 2–8.
6. Stepanov, V.G., Statnikov, E.Sh., Klestov, M.I. et al. (1974) Residual stresses during reinforcement of UZ steel welded joints by ultrasonic peening tool. *Tekhnologiya Sudostroeniya*, **7**, 32–34.
7. Knysh, V.V., Kuzmenko, A.Z., Vojtenko, O.V. (2006) Increasing fatigue resistance of welded joints by high-frequency mechanical peening. *The Paton Welding J.*, **1**, 30–33.
8. Mikheev, P.P., Garf, E.F., Kuzmenko, A.Z. et al. (1990) Increase in fatigue resistance of structure welded joints by ultrasonic peening. In: *Problems of welding and special electrometallurgy*. Kiev: Naukova Dumka.
9. Kudryavtsev, Yu.F., Korshun, V.F., Kuzmenko, A.Z. (1989) Increase in cyclic service life of welded joints by ultrasonic peening. *Avtomatich. Svarka*, **7**, 24–28.
10. *TsP-0176*: Recommendations for inspection, improvement and increase of service life of solid-stage welded spans. Kiev: Ukrzaliznytsya.
11. Degtyaryov, V.A. (1982) Unit of DSO type for fatigue tests at impact reloading with various cycle asymmetry. *Problemy Prochnosti*, **10**, 110–113.
12. Prokopenko, G.I., Klejman, Ya.I., Kozlov, O.V. et al. *Device for ultrasonic peening of metals*. Pat. 47536 Ukraine. Publ. 15.07.2002.

THEORETICAL PREDICTION OF FATIGUE LIFE OF WELDED STRUCTURES AT BIFREQUENCY SPECTRUM OF CYCLIC LOADING

V.I. MAKHNENKO and **I.Yu. ROMANOVA**
E.O. Paton Electric Welding Institute, NASU, Kiev, Ukraine

The method for theoretical prediction of service life of welded joints under bifrequency cyclic loading using Palmgren--Meier's hypothesis of linear summation of fatigue damage is considered. It is shown that this calculation procedure makes it possible to obtain appropriate estimates of service life of the joints requiring no additional experimental studies.

Keywords: *cyclic loading, bifrequency loading, theoretical prediction of fatigue life, Palmgren–Meier's hypothesis of linear summation of damage*

Modern welded structures are operating under diverse conditions. The force loads found in them in the majority of the cases are the most critical in terms of safe operating life. Fatigue failures of welded structures, related to alternating loads, are the subject of investigations of many research teams all over the world [1, 2]. The best studied is regular loading, characterized by a periodical law of load variation with one maximum and one minimum during one period at constant parameters of the stress cycle during the entire time of operation (service).

There is a large scope of experimental data and respective generalizations as regards fatigue resistance of welded joints under the regular loading conditions [1, 2, etc.]. Particularly interesting are the recommendations on the use of fatigue resistance parameters at regular loading by an arbitrarily assigned spectrum (Figure 1) based on application of Palmgren--Meier's hypothesis of linear summation of damage.

In keeping with this hypothesis the fraction of damage at any level of loading amplitude is proportional to the ratio of the number of cycles of its action n_i to the limit number of cycles $[N_{fi}]$, which would lead to fracture, i.e. $D_i = n_i/[N_{fi}]$, where D_i is the damage accumulation in the i-th mode. Then, in keeping with Palmgren--Meier's hypothesis this ratio for the spectrum given in Figure 1, can be expressed as

$$D = \sum_{i=1}^{k} \frac{n_i}{[N_{fi}]}, \qquad (1)$$

where k is the number of the loading modes.

Let us consider the application of this hypothesis to the case of bifrequency loading (Figure 2). Investigations showed that at such loading fatigue resistance lowering is much more pronounced than at unifrequency loading with the maximum amplitude, equal to the summary value of amplitudes of both the cycle components [1].

In work [1] fatigue life under bifrequency loading is assessed using empirical relationships connecting the amplitudes of stresses σ_{a1}, σ_{a2} and fatigue lives $[N_1]$, $[N_2]$, where $[N_1]$, $[N_2]$ is the low- and high-frequency loading, respectively. Such dependencies are most often derived from experimental data.

This work deals with the possibility of deriving the above dependencies based on Palmgren--Meier's hypothesis.

Let us assume that bifrequency cyclic loading conditionally consists of two sinusoidal, periodically changing in time t stresses σ_1 and σ_2, which can be presented by the following equations:

$$\sigma_1 = \sigma_0 + \sigma_{a1} \sin \omega_1 t \quad \text{at} \quad 0 \le \omega_1 t \le 2\pi, \qquad (2)$$

where $\omega_1 t = 2\pi \dfrac{m}{M}$ $(0 \le m \le M)$; and

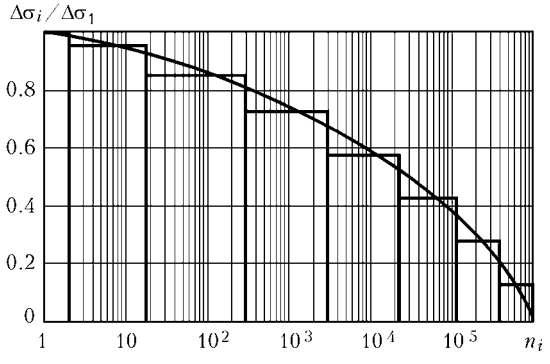

Figure 1. Example of the set cycle of cyclic loading $\Delta\sigma_i/\Delta\sigma_1$ -- n_i

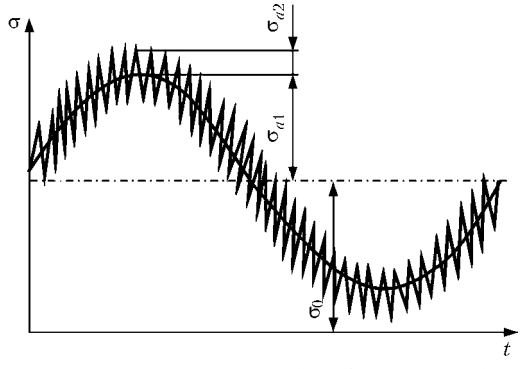

Figure 2. Stress variation under bifrequency loading

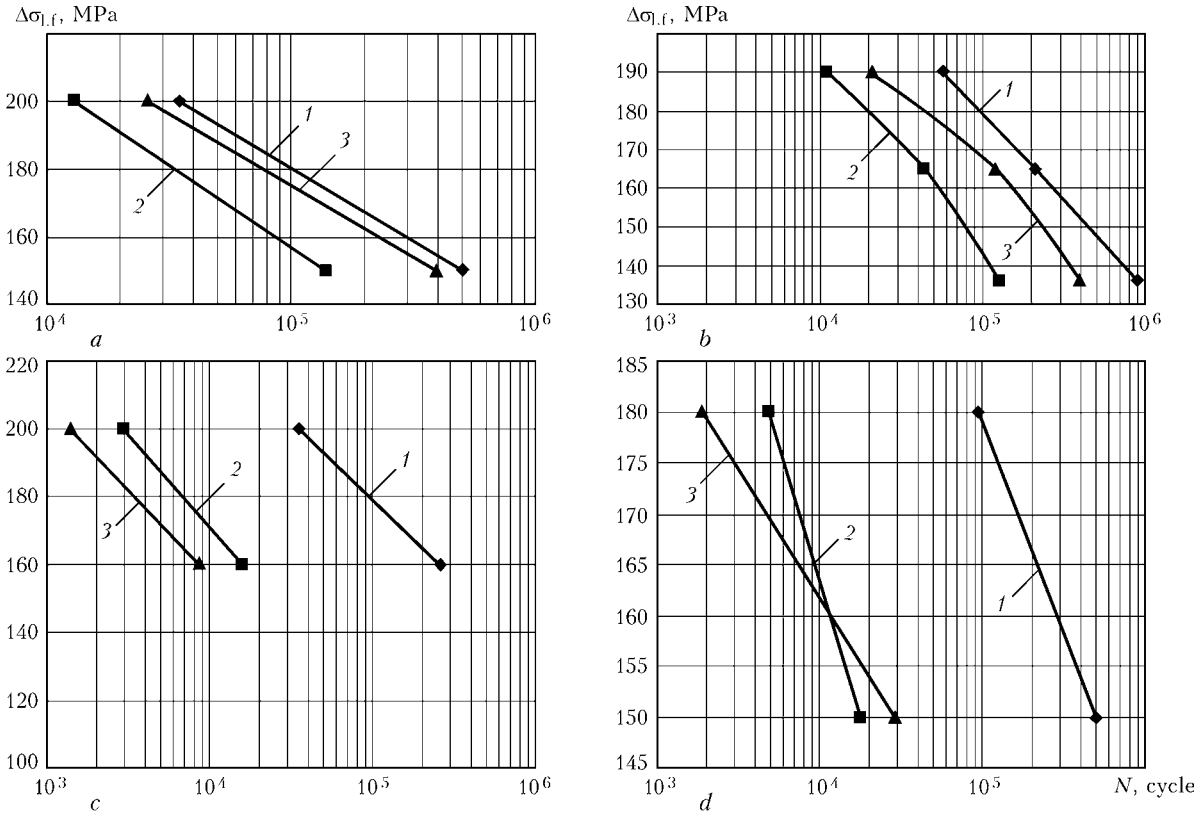

Figure 3. Fatigue life variation at loading of samples from 22K steel at M = 100 (*a*, *b*) and 1000 (*c*, *d*): *a* ---- σ_{a2}/σ_{a1} = 0.2; *b*, *c* ---- 0.3; *d* ---- 0.4; *1*, *2* ---- uni- and bifrequency loading by [1], respectively; *3* ---- calculated data obtained on the basis of Palmgren--Meier's hypothesis

$$\sigma_2 = \begin{cases} \sigma_{a2}, \\ 0 \text{ in section } m, \ldots, m+1, \\ -\sigma_a, \end{cases} \tag{3}$$

where σ_0 is the average value of low-frequency cycle stress; M is the number of intervals, within which expressions (3) are valid.

Thus, for the high-frequency cycle for m-th interval we have

$$\sigma_{\max}^{(m)} = \sigma_0 + \sigma_{a2} + \sigma_{a1} \sin 2\pi \frac{m}{M};$$
$$\sigma_{\min}^{(m)} = \sigma_0 - \sigma_{a2} + \sigma_{a1} \sin 2\pi \frac{m}{M}. \tag{4}$$

Accordingly,

$$R_m^{\text{h.f}} = \frac{\sigma_{\min}^{(m)}}{\sigma_{\max}^{(m)}}; \quad \Delta\sigma_m = \sigma_{\max}^{(m)} - \sigma_{\min}^{(m)} = 2\sigma_{a2}.$$

Moreover, superposed on the high-frequency loading cycle $\sigma_{\text{h.f}}$, is the low-frequency $\sigma_{\text{l.f}}$ cycle, in which

$$\Delta\sigma_{\text{l.f}} = 2\sigma_{a2}; \quad R_{\text{l.f}} = \frac{\sigma_0 - \sigma_{a1}}{\sigma_0 + \sigma_{a1}}. \tag{6}$$

During calculations based on fatigue life N, corresponding to the number of low-frequency cycles, we obtain MN cycles. Loading spectrum consists of M + + 1 elements. The allowable number of cycles for low- and high-frequency components is found from the following relationship:

$$[N] = 5 \cdot 10^6 \left(\frac{\Delta\sigma}{FAT f(R_m)} \right)^{-5} \text{ at } [N] > 5 \cdot 10^6 \text{ cycle};$$
$$[N] = 2 \cdot 10^6 \left(\frac{\Delta\sigma}{FAT f(R_m)} \right)^{-3} \text{ at } [N] < 5 \cdot 10^6 \text{ cycle}, \tag{7}$$

where $f(R_m)$ is given by the following relationships:

$$f(R_m) = 1.6 \text{ at } R_m \le -1.0,$$
$$f(R_m) = -0.4R_m + 1.2 \text{ at } -1.0 < R_m \le -0.05,$$
$$f(R_m) = 1.0 \text{ at } R_m > 0.5,$$
$$m = \overline{1, M};$$

FAT is the characteristic for the high- and low-frequency components, respectively, determined for the given welded joint by [2] on the base of $N = 2 \cdot 10^6$ cycles, or from equation (7) at the set value of fatigue life under unifrequency loading [1].

Hence, the fatigue life at bifrequency loading is equal to

$$N = \frac{1}{\left(\frac{1}{[N_1]} + \sum\limits_{m=1}^{M} \frac{1}{[N_{2m}]} \right)}. \tag{8}$$

Work [1] gives the results of testing specimens with a geometrical stress raiser from 22K steel under bifrequency loading. Figure 3, *a*, *b* gives the respective curves of fatigue life variation at uni- and bifrequency loading of samples from steel 22K with a stress raiser

at M = 100, where the low-frequency component of bifrequency loading corresponds to zero-to-tension cycle, Figure 3, *c, d* is the same, but at M = 1000.

As is seen from Figure 3, S–N curves characterizing the influence of bifrequency loading at different fixed values of amplitude and frequency relationships, are parallel to the initial curve, corresponding to unifrequency loading. Increase of amplitude and frequency ratios often leads to shifting of the curves to a lower fatigue life region. Figure 3 also shows a good correlation of the experimental and calculated data.

Thus, application of the hypothesis of linear summation of fatigue damage of welded joints for the case of bifrequency loading allows using the recommendations of [2] and deriving the respective fatigue life estimates for different joint types (at different *FAT*) without the need for any additional experimental investigations.

1. (1990) *Strength of welded joints at alternative loads*. Ed. by V.I. Trufyakov. Kiev: Naukova Dumka.
2. (1996) Recommendation for fatigue design of welded joints and components. *IIW Doc. XIII-1539–96/XV-845–96*.

NEWS

ELECTROSLAG WELDING OF HYDRAULIC PRESSES

Novokramatorsk Machine-Building Works (NKMZ Company) is one of the largest heavy mechanical engineering plants in the CIS and has unique capabilities of manufacturing various-purpose equipment due to continuous technical re-equipment (mastering advanced processes in steel-making and welding fabrication, fitting with modern machine tools with high-precision machining capability). Here the technology of electroslag welding (ESW) has the determinant role in widening the technological capabilities in fabrication of large-sized base members of up to 300 t weight for forge-pressing, rolling, power generation and other equipment. Introduced and mastered in NKMZ (for the first time in heavy mechanical engineering) the ESW technology and equipment in fruitful co-operation with PWI, is continuously developed and improved.

A new achievement in ESW application in the plant is mastering the welding of hydraulic press items, in the fabrication of which an electroslag joint with 3420 mm thickness of the welded section was produced for the first time in the world practice (previous limit of the maximum welded thickness was equal to 2650 mm in ESW of parts of a press with the force of 650 MN, made in the plant in the middle of the 70ties of the previous century for France, city of Issouar).

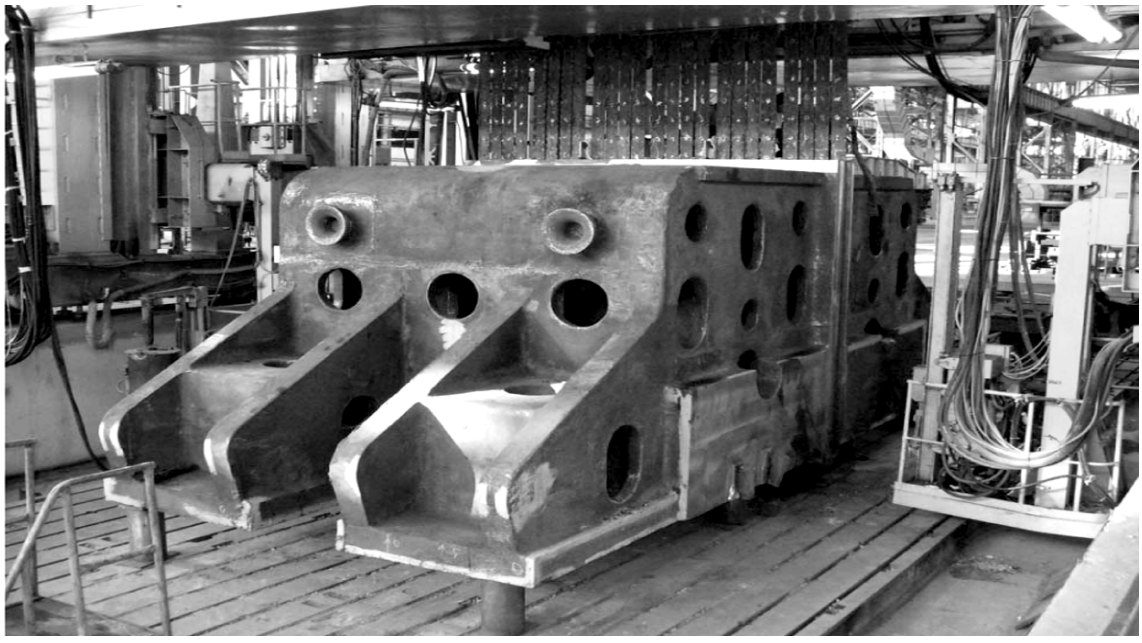

Welding of the base plates was performed in the unit for ESW of thick metal fitted with ASh-110 welding machines of PWI design. During ESW the appropriate technological measures were taken, providing the required precision of the dimensions, quality and properties of the welded joint.

NOVOKRAMATORSK MACHINE-BUILDING WORKS IS 75

Closed Joint Stock Company «Novokramatorsk Machine-Building Works» (NKMZ Company) over the period of 75 years has become the biggest enterprise of heavy machine-building in the world. It can provide almost any industry with high-performance equipment for the entire production cycle: design, manufacture, delivery, setup, and specialty maintenance of the produced units. The enterprise increases its production volumes annually, and continuously widens markets of its products, which are successfully used in many countries on all continents of the globe.

It is a pleasure to note that almost all stages of development of the Plant are based on the modern strategy of meeting the needs of the world market as a leading manufacturer of unique equipment through efficient utilization of intellectual and technical capabilities. It showed up most clearly in difficult postwar years, when the Plant headed the all-union movement for transition from heavy cast sections to welded ones. Resolving this problem at the Plant implied a 50 % decrease in labor expenditures, two-times reduction of duration of the production cycle, and up to 30 % decrease in metal consumption at lower production costs.

The success was achieved owing to a well-coordinated and self-denying work of staff of the Plant and wide involvement of scientists. The Plant increased its output of welded metal structures three times only over the period from 1951 to 1953 due to creative application of new high-efficiency methods and equipment for mechanized arc welding, resistance and electroslag welding (ESW).

It is encouraging to realize that the E.O. Paton Electric Welding Institute of the NAS of Ukraine made a significant contribution to the achievements of the enterprise:

- one-run ESW of 200 mm thick metal was successfully applied in 1951 for the first time in the world to manufacture stators of water turbines. Utilization of different ESW methods and specialized welding equipment ensured building of a wide range of unique units ---- rolling mills, hydraulic stamping presses with a load of up to 75,000 t, horizontal forging machines, hammers etc. At present, the Plant makes the unique longitudinal welds on billets 3500 mm thick and circumferential welds on hydro-press cylinders with outer diameter of up to 3000 mm and thickness of 430 mm. And this is not a limit;
- wide implementation of CO_2 welding provided a high level of mechanization of welding operations (up to 60 %).
- hard-facing of bells and cups of blast furnace charging devices, as well as other parts, found application in the Plant production cycle;
- technology and equipment for automatic narrow-gap submerged-arc welding was introduced to widen the capabilities of welding of large cylinder billets.

These and many other joint works allowed manufacturing products at a level of the best world stand-

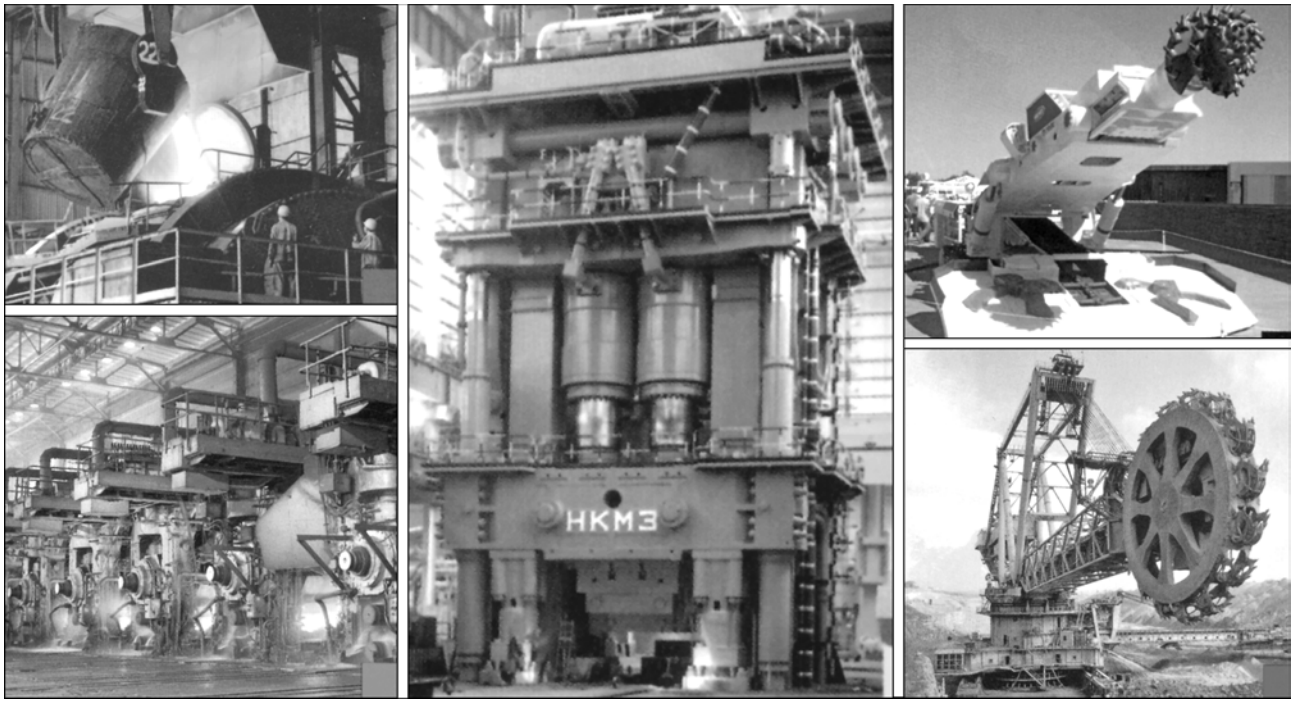

ards and successfully competing with leading foreign machine-building companies.

NKMZ was and still is the home enterprise for many employees of the E.O. Paton Electric Welding Institute, where the joint works on implementation of new welding methods and welding equipment were carried out, and where the business relationships and real friendship among people grew and became stronger.

The Chief Welding Engineering Department (CWED) of NKMZ also celebrates its 60th anniversary this year. Formation of this Department helped NKMZ to become a leader of the all-union machine building industry, which made much for successful recovery of the national economy after the Great Patriotic War. It was a timely and effective step in terms of improved management of the Plant welding production, as well as wide involvement, development and implementation of the latest achievements of science and technology, and mastering of the advanced technologies and welding equipment.

Over a period of 60 years of the CWED activity, good traditions of creative cooperation were set and constantly maintained between NKMZ and the Institute. Due to this, an important role of joint implementation and wide application of new mechanized welding and surfacing methods and equipment, many of which were developed for the first time in the world, is clearly seen in chronology of important events of Plant welding engineering activities. The bright example of this is a wide and successful implementation of the elecroslag technologies at the Plant, which was a pioneer of utilization, upgrading and further development of ESW.

Today CWED carries out the successful production and research activity, and train highly skilled specialists. Many remarkable organizers and managers of the machine-building industry, as well as many researches grew here. CWED continuously maintains a high production and scientific-technological potential, solves the most complex tasks at the sufficient professional level.

The E.O. Paton Electric Welding Institute
«The Paton Welding Journal»
Editorial Board

OPENING OF COMMEMORATIVE PLAQUES

Grand opening of commemorative plaques to Vradimir K. Lebedev and Daniil A. Dudko, famous scientists in the field of welding technology and equipment, honored workers of science and technology of Ukraine, permanent members of the editorial board of the «Avtomaticheskaya Svarka» journal, and academicians of the National Academy of Sciences of Ukraine, took place in September 28.

Numerous students, colleagues, as well as associates of the PWI, relatives and family members were present at the opening. Professor B.E. Paton, academicians of the NAS of Ukraine N.V. Novikov, I.K. Pokhodnya and B.A. Movchan spoke at the meeting. All speakers noted talent of the scientists, their remarkable innovative faculties, energy, care about growing generation, and selflessness in work.

B.E. Paton expressed the wish for the team-mates, students and representatives of a young generation of PWI to continue famous beginnings of V.K. Lebedev and D.A. Dudko, and multiply them by new achievements.

INTERNATIONAL EXHIBITION NEVA-2009

The 10th Jubilee International Exhibition and Conference on Shipbuilding, Shipping, Port Activities and Ocean and Offshore Development NEVA-2009 took place in St.-Petersburg at Open Joint Stock Company «LenExpo» in September 22--25, 2009. NEVA has been ranked among the four biggest world exhibitions since 1991. More than 600 companies and enterprises from 37 countries of the world participated in the Exhibition activities.

Representatives of the Russia state authorities set an optimistic fashion to the event. Thus, Igor Levitin, the Minister of Transport, while making a speech at the official Opening Ceremony of the Exhibition, noted the positive dynamics of growth of the total turnover of goods at Russian ports. The Governor of St.-Petersburg, Valentina Matvienko, also told the participant and guests of the Exhibition about achievements of the city in the field of marine activities. Among the biggest Petersburg projects, the Governor distinguished the «Morskoj Fasad» passenger port, which has started its active work in the current year.

A separate section of the Exhibition focused on welding. The ESAB Company presented its welding consumables: fluxes, wires, electrodes, ceramic backings and welding rods. Demonstration of the equipment was organized at the «Uraltermosvar» Company booth.

Attention of the visitors was attracted by import-substituting low-carbon electrodes of the LEZ LBgp grade produced by the Losinoostrovsky Plant and intended for oil and gas pipeline welding, which are not inferior in their welding-operational properties and mechanical characteristics to imported electrodes of the LB52U (Japan) and OK 53.70 (Sweden) grades widely applied in Russia.

The «Offshore» system developed for shipbuilding enterprises was demonstrated by the «Mir Svarki» Company. The system is a multi-station power source (the VDM-6303 and VDM-1202S type rectifiers of domestic production can be used) and low-voltage converter used instead of a ballast rheostat. The main advantages of the converter include the possibility of its location at a large distance from the power source (up to 200 m), absence of interferences of the welding stations, small weight and dimensions, and low power consumption. The «Severstalmetiz» Company presented welding consumables: rods, wires, stick electrodes, as well as their novelty ---- welding wire with a chemical coating. Interesting systems, combining a welding mask and a filter attached to the welder's belt, were demonstrated by the «Sizod» Company.

The Conference «Welding and Welding Technologies in Shipbuilding, Offshore Engineering and Construction of Coastal Facilities» took place in September 24. The Conference was organized by the Alliance of the St.-Petersburg and North-West Region Welders, and was held in two stages. The morning was dedicated to the papers presented in one of the halls of «LenExpo», and in the afternoon the Conference was moved to the Center for Shipbuilding and Ship Repair Technology (TsTSS), where the rest of the papers were presented to the participants, and where they took part in opening of the Joint Russian-Germany Laser Center at TsTSS, Ltd.

V.V. Kaprikov (OJSC «Severnaya Verf») in his paper «Training of Staff for Shipbuilding Industry» indicated the demand for establishing a training center in view of the shortage of qualified workers in the labor market. Welders are qualified in compliance with local standards for qualification of welders.

The report by V.V. Murzin (St.-Petersburg State Marine Technical University) was dedicated to the problems of organization of practical training of students. At the absence of financing, practical training causes an irresponsible attitude of both enterprises and institutions of higher education to its quality. As a result, the level of practical training of students is extremely low. H.-G. Gross (SLV, Rostok) made a presentation dedicated to the European and International system of welding certification. He noted that to promote any product, including welding processes, in Europe it requires certification acceptable for western customers. For Russian enterprises during the transition period, the joint certificates of NAKS (National

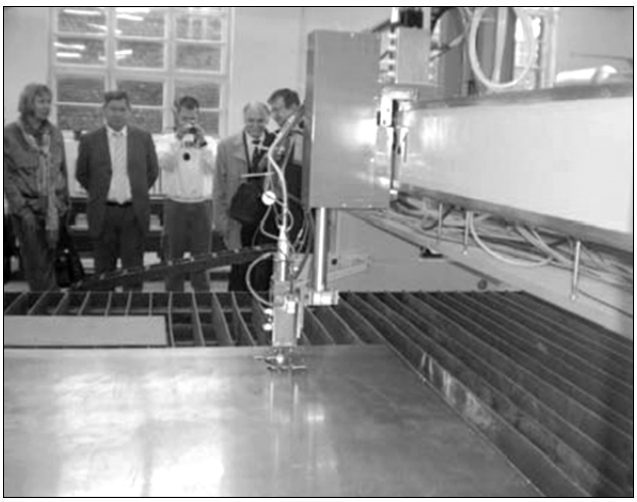

Association of NDT and Welding) and DVS can be used as such certificates. A transition from the GOST to ISO system is necessary for the future. The scale of such a transition is confirmed by the quantity of welders and enterprises certified each year in Germany ---- 10,000 and 380, respectively.

V. Helts (SLV, Hanover) covered the experience of training of welding divers in Germany in his paper «Qualification of Personnel for Underwater Welding in Accordance with International Standard ISO 15 618--1». Training is performed for three weeks if trainees have certificates of a diver and welder (arc welding). The cost of training is 5500 Euro.

A new approach to manufacture of welding equipment, based on a distinction in kind of a power (energy) component of the welding equipment, providing the arc process with energy, and an information (digital) component, providing the laws of current and voltage control during the welding process, was suggested in paper «Digital Synthesis ---- the Basis of Innovative Welding Technologies» by V.A. Khabuzov (Laboratory for Electron Technologies, Ltd). The proposed equipment manufacturing concept was tested at St.-Petersburg enterprises.

Review of the technologies used for welding titanium pipelines was made in paper «Peculiarities of Welding of Ship Pipings of Titanium Alloys» by V.A. Semyonov (FSUE CR&DISM «Prometej»). The main condition for producing sound welded joints in welding of titanium pipings is keeping exactly to all technological recommendations and requirements for shielding of the welding zone. It was noted that titanium pipings were in operation for 170,000 h at atomic submarines and icebreakers.

I.M. Lifshits (CJSC SVAMA) made presentation «Izhora Welding Consumables for Shipbuilding Industry», where he noted that at present the plant produces more than 70 grades of welding electrodes and 30 grades of fused fluxes, and continues mastering and implementing welding consumables developed by «Prometej». Welding consumables of the plant are certified according to the ISO-9000 quality system, BVQI. A certificate of approval by ABS (American Bureau of Shipping) has been received for some electrode grades. The largest Russian shipyards are customers of the SVAMA products. L.N. Orlov (TM.VELTEK, Ltd) noted in his paper «Advancement of Mechanized Gas-Shielded Small-Diameter Flux-Cored Wire Welding» that analysis of the status of welding in the world shipbuilding shows that around 80 % of the entire volume of welding operations is performed by mechanized CO_2 welding with 1.0--1.2 mm diameter solid or flux-cored wires. The current demand of Russian and Ukrainian shipbuilding industries is met due to import of flux-cored wires from world leading manufacturers: ESAB, Welding Alloys, Filarc, Cobelco, Hundai etc. At the same time, production capacities of Russian and Ukrainian manufacturers of flux-cored wires make it possible to meet in full the demand of shipbuilders for small-diameter flux-cored wires.

S.Yu. Maksimov (E.O. Paton Electric Welding Institute of the NAS of Ukraine) in his paper «Repair of Ships Afloat by Wet Underwater Welding» indicated that the Institute developed the specialized welding consumables (electrodes and flux-cores wires), technology and equipment for repair of ships afloat without docking by using wet underwater welding. He presented a retrospective review of more than 30 works completed on repair of ships in the Baltic and Murmansk basins.

V.V. Golikov (Spetspodvodremont, Ltd) in his paper «Underwater-Engineering Works for Repair of Defects in Pipes and Welded Joints at Spetspodvodremont, Ltd» reviewed the repair-and-renewal works carried out by dry hyperbaric welding using a special caisson in the largest Russian rivers, including the recovery works after the accident at the Sayano-Shushenskaya hydroelectric power station in August 2009.

P.I. Seyffarth (Ingenieurtechnik und Maschinenbau Gmbh) made, as usual, an interesting and informative presentation «Wide Application of Technological Lasers in German Shipbuilding». The speaker outlined the main advantages of laser welding in comparison with the arc one: absence of straightening and alignment, high precision (a premise for quick assembly and automation) and productivity, and reduction of the quantity of welders. Workshops of laser welding for enlargement of panels and welding of ribs at shipyards in Rostok (2004, Germany), Turku (Finland, 2006), Monfalcone (Italy, 2008) and at FSUE «Admiraltejskie Verfi» (2009) were launched under the Ingenieurtechnik und Maschinenbau Gmbh projects. The use of laser welding allowed a two times reduction of the production time. Appearance of high-power fiber lasers (5 kW or more) of the IPG Company on the market opens up new opportunities for wide application of laser welding in shipbuilding (the first 10 kW fiber laser was bought in 2004 by the Rostok shipyard).

In general the Conference provided a good exchange of useful information and promoted strengthening of scientific and business cooperation.

Dr. A.T. Zelnichenko, PWI

TECHNOPARK «THE E.O. PATON ELECTRIC WELDING INSTITUTE» TODAY

The technology park «The E.O. Paton Electric Welding Institute» was founded in accordance with the Law of Ukraine «On Special Policy of Innovation Activity of Technology Parks» № 9991-XIV of July 16, 1999 on the initiative of the National Academy of Sciences of Ukraine on the base of the E.O. Paton Electric Welding Institute, the leading welding research organization in the country. The priority directions of technopark activity include, respectively, both national innovation priorities and scientific specialization of the Institute.

The main function of technopark is the support of innovation activity of fundamental, field science and industrial enterprises; informational, organizational and scientific-methodological support of the processes of development and implementation of innovations. The real conditions of Ukrainian economy at the moment of establishment of Ukrainian technoparks excluded the possibility of receiving any initial investments and direct financial support during their activity from the budget. Therefore, the economic basis of the PWI Technopark is the special policy of innovation activity in the form of taxes and customs preferences, which are given to the participants of technopark in the fulfillment of innovation projects registered in accordance with the established procedure.

Legally, the PWI Technopark represents contractual (without creation of a legal person) association of participants, the part of which (bodies of management of Technopark, basic academician institute and other participants of Scientific-Technical Complex of the E.O. Paton Electric Welding Institute) are densely located in Kiev and the rest ones are located within the custom border of Ukraine. The similar decentralized location of participants of technoparks, allowing considerable decrease in primary investments, become recently ever more applicable in the world practice in the creation of so-called virtual technoparks or technoparks without walls.

The high cost-effectiveness of Ukrainian model allows providing the values exceeding the values of traditional technoparks. For example, in China it is considered normally when at governmental support of 1 yuan the technoparks release innovation products for the sum of 6 yuan. Over ten years the Ukrainian technoparks provided at the governmental support of 1 hryvnya the innovation products for the sum of 18.5 hryvnya.

For the past period the participants of the PWI Technopark fulfilled a number of innovation projects which were highly estimated by the specialists. There are some of them:

- machines for flash-butt welding of high-strength rails of high-speed railways, occupying the leading position at the world market of welding machinery. The work is protected by 48 patents of leading countries in the world. However, in the first years of technopark activity a new generation of equipment for rail welding protected by patents was developed and undertimely (1 year) manufactured. Except of Ukrainian enterprises (16 complexes were delivered) this equipment was successfully exported to Russia, USA, Canada, Austria, India, Taiwan. The tender was gained and a large batch of machines was delivered to China;
- the first high-frequency welding of soft tissues in the world. Today in Ukraine over 40,000 patients were operated without any serious post-surgical complications. The American specialists called this project as «the breakthrough in the surgery of the XXI century». The work is protected by the patents of Ukraine, USA, Germany, Australia, and awarded

Production of energy-saving glass units using technologies of magnetron sputtering

with the State prize of Ukraine (the E.O. Paton Electric Welding Institute);

• the duplex-process of melting of high-quality welding fluxes having no analogues in the world can replace 50 % of deficit raw materials by the slag wastes of domestic metallurgy. 70 % of production is exported (Zaporozhie plant of fused fluxes and glasswares, the E.O. Paton Electric Welding Institute);

• modern energy-saving equipment for arc welding, over 75 % of which is exported (Simferopol plant of welding equipment SELMA, Pilot plant of welding equipment of the E.O. Paton Electric Welding Institute).

In 2009 the project of the E.O. Paton Electric Welding Institute and Zaporozhstekloflyus was approved on the development and organization of production of synergetic agglomerated fluxes. The works on preparation of the project «The creation and providing the production of the complex of domestic railway machinery», which can provide conditions for accident-free railway transportations at the speed of up to 200 km/h, are carried out with Kakhovka plant of electric welding equipment. This is one of the requirements to create the transit passage way «East--West» in Ukraine.

The developments of the E.O. Paton Electric Welding Institute on the creation of new models of chambers for EBW, on application of modern methods for control of welds and prolongation of service life of the high-duty welded joints are challenging for the projects of Technopark.

There are developments in the prospects of the participants of the PWI Technopark, which allow the solution of the most important national economy tasks on the high level, including utilization of hazardous and high toxic wastes (medical as well), expanding of welding application in medicine; creation of challenging functional and structural nanomaterials and coatings, including aerospace engineering.

According to the evaluations of the experts the projects of the PWI Technopark are characterized by the highest level of innovations:

• 40 % of projects refer to the so-called pioneer projects, that means the line to achieve the world priority;

• 30 % ---- «follow up» projects aimed at approaching the world level;

• 30 % ---- «modification» projects connected with the improvement of existing processes of production and released products.

According to the technological categories the projects of the PWI Technopark refer to the III and IV category by 30 % and to the highest V and VI category ---- by 20 %.

According to the importance for the markets 40 % of the Technopark PWI projects are of international importance, 40 % are national and 20 % are field ones. To compare with Polish technoparks working according to the EC standards the projects of international importance are 1.9 % and national are 14 %. The majority of Polish projects are «follow up» or «modification» and correspond to the III and IV categories. The presence of economic studies department in the structure of the Institute and close cooperation with the services of technopark allows providing scientific-methodological support of research departments and other participants of technopark in the preparation and fulfilment of innovation projects.

The ten-year practical activity of Technopark «The E.O. Paton Electric Welding Institute» showed that governmental support of innovation projects in the frames of technopark which can amount to 5--15 % of all expenses for the project makes the performance of innovation activity at extremely limited financial possibilities of participants of technopark not only real, but also 2--3 times accelerates the fulfillment of projects.

Dr. A.A. Mazur, PWI

DOMESTIC AGGLOMERATED FLUXES FOR MULTI-ARC WELDING

For arc welding methods the fluxes are used produced according to two technologies having principal differences defining their characteristic peculiarities. Fused fluxes in the process of manufacturing are brought to condition of melting in gas-flame or electric arc furnaces with the heat and mechanical treatment of produced material. Non-fused (agglomerated or ceramic) fluxes in the process of manufacturing are not subjected to heat treatment at the temperatures equal or exceeding the temperature of melting the mixture of charge components.

In the field of manufacture of welded structures the process of constant growing of volume of application of low-alloyed steels of increased and high strength instead of carbon steels is observed. For example, the manufacturers of large-diameter pipes, designed for construction of main pipelines, mastered the welding of pipes of low-alloyed steels of X80 strength and currently perform works on preparation to manufacturing of pipes of steels of X100 strength category. The standard documentation on the large-diameter pipes regulates requirements to the mechanical properties of welded joints of not lower than level of base metal. If the properties of HAZ of welded joint can be regulated due to the control of thermal welding cycle, the quality of weld metal depends, first

Flux ANKS-199

DSTU/ISO 14171-A-S-46 3 AR S2Mo

Basicity: BI = 1.4; bulk weight: 0.8–1.2 g/cm^3; granulometric composition: 0.4–1.6 mm

Chemical composition of flux, %

SiO_2 + MnO	CaO + MgO	Al_2O_3 + TiO_2	CaF_2
23–30	18–28	28–32	15–20

Chemical composition of deposited metal, wt.%

Wire	Si	Mn	S
	Not more than		
Sv-08G1NMA	0.40	1.75	0.025

Mechanical properties of deposited metal

Wire	Impact toughness *KCV*, J/cm^2, at *T*, °C			
	–60	–40	–20	0
Sv-08G1NMA	48	75	101	129

Flux ANKS-28

TU U 24.6-00293255-003:2007, DSTU/ISO 14171-A-S 50 4 AB S2Mo

Basicity: BI = 1.5; bulk weight: 0.8–1.2 g/cm^3; granulometric composition: 0.4–1.6 mm

Chemical composition of flux, %

SiO_2 + ZrO_2	CaO + MgO	TiO_2 + Al_2O_3	CaF_2
15–25	25–30	20–30	13–18

Chemical composition of deposited metal, wt.%

Wire	Si	Mn	Mo	C	S	P
	Not more than					
Sv-08G1NMA	0.45	1.90	0.55	0.12	0.015	0.025

Mechanical properties of deposited metal

Wire	Tensile strength, MPa	Elongation, %	Impact toughness *KCV*, J/cm, at *T*, °C			
			–60	–40	–20	0
Sv-08G1NMA	680	27	48	82	98	135

of all, on the combination of used welding consumables. In this situation the use of agglomerated fluxes able to exert active metallurgical effect on solidifying metal of weld pool does not have an alternative. Therefore, the largest pipe-welding plants of Ukraine and Russia, mastering the pipes production of low-alloyed high strength steels, preferred welding technology under agglomerated fluxes.

Up to the recent time the domestic enterprises produced exceptionally fused fluxes, the technology

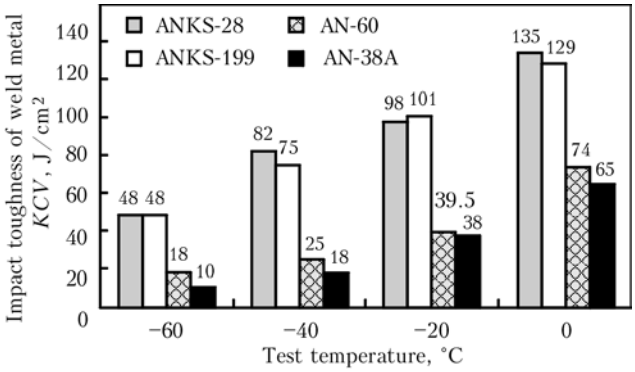

Impact toughness *KCV* of weld metal. Base metal ---- steel 10G2FB + wire Sv-08G1NMA

of production of agglomerated fluxes was mastered only in limited volumes at the Pilot Plant of Welding Materials of the E.O. Paton Electric Welding Institute. Therefore at the pipe-welding plants the agglomerated fluxes were applied only of foreign producers. Taking into consideration the problems and meeting the demand of the domestic consumers, OJSC «Zaporozhstekloflyus» together with specialists of the E.O. Paton Electric Welding Institute mastered the production of agglomerated fluxes in the shortest period of time. Here the many-year experience of developers in the field of development of welding fluxes and technologies of their production was used. Such combination of science and practice allowed creation of new technology of manufacturing the fluxes combining the advantages of fused and agglomerated fluxes. In 2008 the production line of agglomerated fluxes of the capacity of 5,000 t per year was put into operation at the Plant, the production of fluxes was mastered, designed for multi-arc welding of low-alloyed steels of strength category X70 and X80 for one- and multi-pass welding of carbon and low-alloyed steels with the yield strength of up to 420 MPa, and also for hardfacing the wear-resistant layer of hardness of up to *HB* 250. Some characteristics of fluxes, produced by the Plant, obtained during the tests in accordance with the requirements of DSTU/ISO 14171 are given in the Figure showing the weld metal toughness values obtained in multi-pass welding of low-alloyed steel of the strength category X70.

The considerable volumes of production of welding fluxes at the OJSC «Zaporozhstekloflyus», the optimized technology of their manufacturing with high level of energy saving, established production links allows the plant to manufacture the products with the quality equal to foreign analogues, however, with a lower release price.

O.Ya. Osipov,
Director of OJSC «Zaporozhstekloflyus»